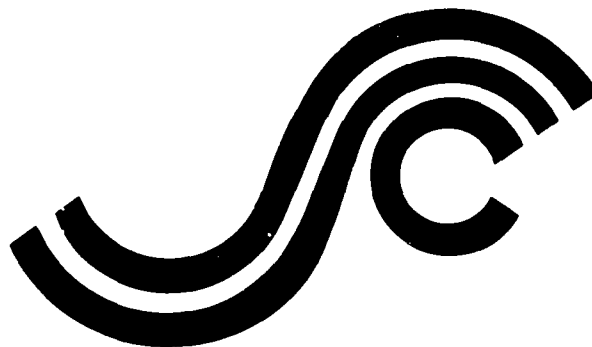# SSC-303

# FATIGUE AND FRACTURE-TOUGHNESS CHARACTERIZATION OF SAW AND SMA A537 CLASS I SHIP-STEEL WELDMENTS



DTIC
ELECTE
JUL 20 1982
S         D
F

## SHIP STRUCTURE COMMITTEE

1981

82 07 19 173

# SHIP STRUCTURE COMMITTEE

The SHIP STRUCTURE COMMITTEE is constituted to prosecute a research program to improve the hull structures of ships and other marine structures by an extension of knowledge pertaining to design, materials and methods of construction.

RAdm Clyde T. Lusk, Jr. (Chairman)
Chief, Office of Merchant Marine
  Safety
U. S. Coast Guard Headquarters

Mr. P. M. Palermo
Executive Director
Ship Design & Integration
  Directorate
Naval Sea Systems Command

Mr. W. N. Hannan
Vice President
American Bureau of Shipping

Mr. J. Gross
Deputy Assistant Administrator for
  Commercial Development
Maritime Administration

Mr. J. B. Gregory
Chief, Research & Development Staff
  of Planning & Assessment
U.S. Geological Survey

Mr. Thomas W. Allen
Chief Engineering Officer
Military Sealift Command

LCdr D. B. Anderson, U.S. Coast Guard (Secretary)

## SHIP STRUCTURE SUBCOMMITTEE

The SHIP STRUCTURE SUBCOMMITTEE acts for the Ship Structure Committee on technical matters by providing technical coordination for the determination of goals and objectives of the program, and by evaluating and interpreting the results in terms of structural design, construction and operation.

U. S. COAST GUARD

Capt. R. L. Brown
Cdr. J. C. Card
Mr. R. E. Williams
Cdr. J. A. Sanial

NAVAL SEA SYSTEMS COMMAND

Mr. R. Chiu
Mr. J. B. O'Brien
Mr. W. C. Sandberg
Lcdr D. W. Whiddon
Mr. T. Nomura (Contracts Admin.)

MARITIME ADMINISTRATION

Mr. N. O. Hammer
Dr. W. M. Maclean
Mr. F. Seibold
Mr. M. Touma

NATIONAL ACADEMY OF SCIENCES
  SHIP RESEARCH COMMITTEE

Mr. A. Dudley Haff - Liaison
Mr. R. W. Rumke - Liaison

SOCIETY OF NAVAL ARCHITECTS &
  MARINE ENGINEERS

Mr. A. B. Stavovy - Liaison

WELDING RESEARCH COUNCIL

Mr. K. H. Koopman - Liaison

MILTARY SEALIFT COMMAND

Mr. Albert Attermeyer
Mr. T. W. Chapman
Mr. A. B. Stavovy
Mr. D. Stein

AMERICAN BUREAU OF SHIPPING

Dr. D. Liu
Mr. I. L. Stern

U. S. GEOLOGICAL SURVEY

Mr. R. Giangerelli
Mr. Charles Smith

INTERNATIONAL SHIP STRUCTURES CONGRESS

Mr. S. G. Stiansen - Liaison

AMERICAN IRON & STEEL INSTITUTE

Mr. R. H. Sterne - Liaison

STATE UNIV. OF NEW YORK MARITIME COLLEGE

Dr. W. R. Porter - Liaison

U. S. COAST GUARD ACADEMY

LCdr R. G. Vorthman - Liaison

U. S. NAVAL ACADEMY

Dr. R. Battacharyya - Liaison

U. S. MERCHANT MARINE ACADEMY

Dr. Chin-Bea Kin - Liaison

**Ship
Structure
Committee**

An Interagency Advisory Committee
Dedicated to Improving the Structure of Ships

SR-1238

1981

Low temperature applications (below 32F) for marine
structures have grown over recent years. The need to assess
various notch toughness tests and criteria to determine the
low temperature capabilities of each, when used on welded
structures having low toughness in the heat affected zone
(HAZ), became apparent.

Fracture toughness was characterized by using the
Charpy test, nil-ductility transition (NDT), 5/8 inch dynamic
tear (DT), plane-strain fracture toughness ($K_{Ic}$) and crack
opening displacement (COD) tests on shielded metal arc (SMA)
and submerged arc welded (SAW) A537 Class 1 sulphide-shape-
controlled steel.

The Ship Structure Committee undertook this effort
as a portion of its continuing program to enhance the rational
use of material selection, fabrication and design analysis.

Clyde T. Lusk, Jr.
Rear Admiral, U.S. Coast Guard
Chairman, Ship Structure Committee

Accession For

NTIS CRA&I
DTIC TAB
Unannounced
Justification

By
Distribution/
Availability Codes

Dist    Avail and/or
        Special

A

DTIC
COPY
INSPECTED
2

| 1. Report No. SSC-303 | 2. Government Accession N. AD-A117057 | 3. Recipient's Catalog No. |
|---|---|---|
| 4. Title and Subtitle FATIGUE AND FRACTURE TOUGHNESS CHARACTERIZATION OF SAW AND SMA A537 CLASS I SHIP STEEL WELDMENTS | | 5. Report Date DECEMBER 1981 |
| | | 6. Performing Organization Code |
| 7. Author's) J.F. Sovak, J.W. Caldwell, and A.K. Shoemaker | | 8. Performing Organization Report No. SR-1238 |
| 9. Performing Organization Name and Address U.S. Steel Research Laboratory 125 Jamison Lane Monroeville, PA 15146 | | 10. Work Unit No. (TRAIS) |
| | | 11. Contract or Grant No. DOT-CG-63116-A |
| 12. Sponsoring Agency Name and Address U.S. Coast Guard Office of Merchant Marine Safety Washington, D.C. 20593 | | 13. Type of Report and Period Covered Final Report |
| | | 14. Sponsoring Agency Code G-M |

15. Supplementary Notes

Performed under CG contract for the interagency Ship Structure Committee

16. Abstract

A study was conducted to assess the use of various toughness tests and criteria to predict the fracture behavior of weldments containing a low-toughness heat affected zone. Natural fatigue cracks were initiated and propagated to various sizes in 1-inch A537 Class I steel submerged-arc-welded (SAW) and shielded-metal-arc (SMA) butt-welded Tee joints having various weld reinforcement heights (surface cracked specimens). The most severe service temperature and loading rate of secondary containment shells for LNG ships was duplicated by testing the surface cracked specimens at -60°F at loading times of about a second. Fracture mechanics procedures and existing empirical correlations among tests were used to interpret the data.

The fatigue crack initiation and propagation behavior observed during preparation of these specimens was consistent with published data. Fatigue crack initiation data were obtained at -60°F. Elastic plastic behavior was observed in 15 out of 16 tests of the surface cracked weldments. The brittle fracture observed in the one test was analyzed and predicted from the lowest values of all the fracture toughness tests except for the $K_{Ic}$ (3 point bend) test. Discussions and recommendations are given for assessing toughness results of weldments having a low-toughness zone "masked" by adjacent high-toughness regions.

| 17. Key Words Fracture Fracture Mechanics Welds Fatigue Submerged Arc Welding Shielded Metal Arc Materials Low Temperature Heat Affected Zone | 18. Distribution Statement Document is available to the U.S. public through the National Technical Information Service, Springfield, VA 22161 | |
|---|---|---|
| 19. Security Classif. (of this report) Unclassified | 20. Security Classif. (of this page) Unclassified | 21. No. of Pages 145 | 22. Price |

Form DOT F 1700.7 (8-72)    Reproduction of completed page authorized

iii

# METRIC CONVERSION FACTORS

## Approximate Conversions to Metric Measures

| Symbol | When You Know | Multiply by | To Find | Symbol |
|---|---|---|---|---|
| | | **LENGTH** | | |
| in | inches | *2.5 | centimeters | cm |
| ft | feet | 30 | centimeters | cm |
| yd | yards | 0.9 | meters | m |
| mi | miles | 1.6 | kilometers | km |
| | | **AREA** | | |
| in² | square inches | 6.5 | square centimeters | cm² |
| ft² | square feet | 0.09 | square meters | m² |
| yd² | square yards | 0.8 | square meters | m² |
| mi² | square miles | 2.6 | square kilometers | km² |
| | acres | 0.4 | hectares | ha |
| | | **MASS (weight)** | | |
| oz | ounces | 28 | grams | g |
| lb | pounds | 0.45 | kilograms | kg |
| | short tons (2000 lb) | 0.9 | tonnes | t |
| | | **VOLUME** | | |
| tsp | teaspoons | 5 | milliliters | ml |
| Tbsp | tablespoons | 15 | milliliters | ml |
| fl oz | fluid ounces | 30 | milliliters | ml |
| c | cups | 0.24 | liters | l |
| pt | pints | 0.47 | liters | l |
| qt | quarts | 0.95 | liters | l |
| gal | gallons | 3.8 | liters | l |
| ft³ | cubic feet | 0.03 | cubic meters | m³ |
| yd³ | cubic yards | 0.76 | cubic meters | m³ |
| | | **TEMPERATURE (exact)** | | |
| °F | Fahrenheit temperature | 5/9 (after subtracting 32) | Celsius temperature | °C |

*1 in = 2.54 (exactly). For other exact conversions and more detailed tables, see NBS Misc. Publ. 286, Units of Weights and Measures. Price $2.25. SD Catalog No. C13.10:286.

## Approximate Conversions from Metric Measures

| Symbol | When You Know | Multiply by | To Find | Symbol |
|---|---|---|---|---|
| | | **LENGTH** | | |
| mm | millimeters | 0.04 | inches | in |
| cm | centimeters | 0.4 | inches | in |
| m | meters | 3.3 | feet | ft |
| m | meters | 1.1 | yards | yd |
| km | kilometers | 0.6 | miles | mi |
| | | **AREA** | | |
| cm² | square centimeters | 0.16 | square inches | in² |
| m² | square meters | 1.2 | square yards | yd² |
| km² | square kilometers | 0.4 | square miles | mi² |
| ha | hectares (10,000 m²) | 2.5 | acres | |
| | | **MASS (weight)** | | |
| g | grams | 0.035 | ounces | oz |
| kg | kilograms | 2.2 | pounds | lb |
| t | tonnes (1000 kg) | 1.1 | short tons | |
| | | **VOLUME** | | |
| ml | milliliters | 0.03 | fluid ounces | fl oz |
| l | liters | 2.1 | pints | pt |
| l | liters | 1.06 | quarts | qt |
| l | liters | 0.26 | gallons | gal |
| m³ | cubic meters | 35 | cubic feet | ft³ |
| m³ | cubic meters | 1.3 | cubic yards | yd³ |
| | | **TEMPERATURE (exact)** | | |
| °C | Celsius temperature | 9/5 (then add 32) | Fahrenheit temperature | °F |
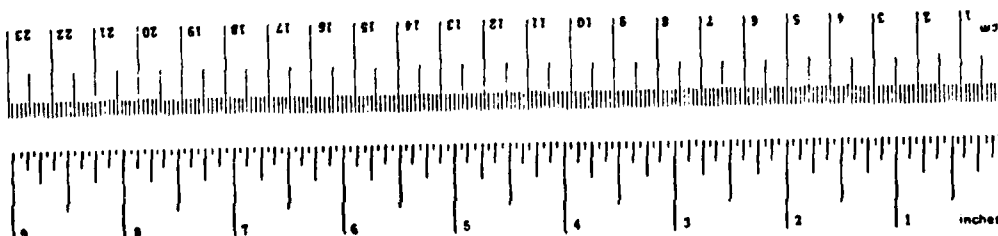
°F    -40    0    32    98.6    160    212
°C    -40    -20    0    20    37    40    60    80    100

iv

# 1.0  PREFACE

The present study was conducted under contract to the U. S. Coast Guard to compare test methods that can be used to characterize the fracture toughness of a ship-steel weldment having a low-toughness region in the heat-affected zone (HAZ) and to determine which of the methods correctly predicts the effect of a low-toughness HAZ on structural performance. The material chosen for this investigation was an A537 Class 1 sulphide-shape-controlled steel welded by the shielded-metal-arc (SMA) and submerged-arc (SA) processes commonly used in shipbuilding. The welding parameters and steel plate were the same as those used in a previous program conducted by MARAD/NBS to produce a low-toughness HAZ.

The fracture toughness was characterized by using the Charpy test specified by the American Bureau of Shipping (ABS) as well as the nil-ductility-transition (NDT), 5/8-inch dynamic-tear (DT), plane-strain fracture-toughness ($K_{Ic}$) and crack-opening-displacement (COD) tests. To compare these test results with service performance, full-thickness surface-cracked strap-tensile (SCT) specimens containing Tee butt welds were prepared by precracking at various stress levels with fully reversed loading (R=-1) without the use of artificial starter notches. Both fatigue-crack-initiation and propagation data were obtained during specimen preparation. Several specimens were also used to assess the effect of a low service temperature (-60°F or -51°C) on the fatigue-crack-initiation behavior of the weldments. The surface-cracked specimens were then tested to failure at -60°F at an initial loading rate of about one second to maximum load, which approximates the maximum rate measured during "slamming" conditions of a ship.

The fatigue-crack-initiation sites, fatigue-crack path, and fatigue strength at $10^6$ cycles were determined for weldments both with and without the full weld reinforcement and with and without the original mill plate surface. Fracture-mechanics procedures were used to compare the service behavior under severe operating conditions, as estimated from results of the surface-cracked-weldment test, with the behavior predicted from the various fracture-toughness tests and with the behavior expected for weldments meeting the toughness requirements of the current ABS Charpy criterion and proposed NDT-DT criterion of Rolfe. Recommendations are made and further research is suggested to help clarify the assessment of weldments containing a very-low-toughness HAZ.

## 2.0 TABLE OF CONTENTS AND TERMINOLOGY

### 2.1 Table of Contents

## Table of Contents
### (Continued)

## Table of Contents
### (Continued)

## 2.2 List of Abbreviations and Symbols

$a_{cct}$     Half crack length for a center-cracked-tension (CCT) specimen.

a/c     Crack depth to half surface crack length ratio for a semi-elliptical surface crack.

BM     Base metal.

c     As a subscript, denotes the critical value of $K_I$ corresponding to a valid test.

CCT     Center-cracked-tension (specimen).

COD     Crack opening displacement at the tip of a crack.

COS     Crack opening stretch--the critical value of the COD at the tip of a crack.

CVN     Charpy V-Notch (specimen).

da/dN     Fatigue-crack advance per cycle.

d,D     As a subscript, denotes dynamic loading conditions.

DPH     Diamond Pyramid Hardness.

DT     Dynamic tear (specimen).

G     As a subscript, denotes a gross-section parameter.

HAZ     Heat-affected zone (in the base plate of a weldment).

ι     As a subscript, denotes that the parameter refers to an internal crack.

$K, K_I$     The plane-strain stress-intensity factor. The subscript, I, denoting tensile loading of a cracked structure, is sometimes omitted when only tensile loading occurs.

$K_f(max)$     The maximum value of K applied during fatigue cracking.

LNG     Liquified natural gas.

N     As a subscript, denotes a net-section parameter.

NDT     Nil ductility transition (temperature).

## List of Abbreviations and Symbols
### (Continued)

P   The load applied to a specimen.

PTC  Part-through-crack (specimen).

Q   As a subscript, indicates that the value of the parameter may not correspond to a valid result.

R   Ratio of minimum to maximum fatigue stress.

s   As a subscript, denotes that the parameter refers to a surface crack.

SAW  Submerged arc weld.

SMA  Shielded metal arc (weld).

S-N  Stress versus number of cycles (graph).

SSC  Sulfide shape control.

T   COD specimen thickness.

WOL  Wedge opening loading (specimen).

y,ys  As a subscript, value corresponding to the yield strength.

$\Delta$   Indicates fluctuation of a parameter.

$\delta$   Symbol sometimes used for COD or COS.

$\rho$   Notch-tip radius.

$\sigma$   Stress.

$\Phi$   A crack-shape factor derived from an elliptical integral used when calculating K values for elliptical internal or semi-elliptical surface cracks.

$\emptyset$   An integration parameter.

## 3.0  SUMMARY OF FINDINGS

A study was conducted to assess the use of various toughness tests and criteria to predict the fracture behavior of weldments containing a low-toughness heat-affected zone. The material is believed to be atypical of steels used in ships. Natural fatigue cracks were initiated and propagated to various sizes in 1-inch-thick A537 Class I steel submerged-arc-welded (SAW) and shielded-metal-arc (SMA) butt-welded Tee joints having various weld-reinforcement heights. Thus, the crack fronts of these surface-cracked specimens resided in the various regions of the weldments. The most severe loading rate and temperature of the secondary containment shell of an LNG ship were simulated by loading the fatigue-cracked (surface-cracked) specimen to failure at an intermediate loading rate (about 1 second loading time) at a temperature of -60°F (-51°C). However, the specific relationship between tests used in this investigation and service performance was not studied. The results from the fatigue-crack-initiation, fatigue-crack-propagation, and fracture-toughness-behavior tests can be summarized as follows:

### 3.1  Fatigue-Crack-Initiation Behavior

1) The fatigue behavior observed for all the SMA and SAW weldments was conservative compared with the American Association of State Highway and Transportation Officials (AASHTO) fatigue design specifications for weldments. The fatigue behavior was compared with the AASHTO specifications because they represent one of the most complete and recent studies of the fatigue behavior of welded structural components.

2) Both the SMA and SAW weldments had approximately the same fatigue strength for a life of $10^6$ cycles when the full weld reinforcement or any portion of the reinforcement was left in place.

3) When the weld reinforcement and a portion of the undercut region were removed, the fatigue strength of the SAW weldments was doubled, whereas the fatigue behavior of the SMA weldments remained approximately the same. This difference in behavior occurred even though, for both types of weldments, fatigue cracks no longer initiated on the specimen surface but internally from slag or porosity near the bond line of the welds.

4) Analysis of the fatigue data showed that the imperfections causing fatigue-crack initiation had initiation lives similar to calculations for a sharp notch rather than a crack; thus, the fatigue life of a specimen consists of the number of cycles necessary to sharpen an imperfection and propagate the crack to failure.

5) The incidence of fatigue-crack initiation at the weld toe on the specimen surface was neither increased nor decreased near the Tee intersection of the longitudinal and transverse butt welds.

6) Fatigue cracks initiating internally in smooth specimens taken from the SAW weldments made it difficult to discontinue cyclic loading before the specimen had completely fractured. This behavior was caused by the rapid increase in growth rate as the crack size increased and by the rapid increase in $\Delta K$ when a buried fatigue crack becomes a surface crack.

7) At -60°F, the fatigue-crack-initiation performance of SAW weldments with reinforcements was better than that at room temperature. The improvement was greater than would be predicted from the increase in yield strength at the reduced temperature.

### 3.2 Fatigue-Crack-Propagation Behavior

1) Once fatigue cracks initiated and grew a short distance in both the SMA and SAW weldments, they tended to propagate perpendicular to the direction of applied stress rather than remain in a particular region of the HAZ.

2) Measured crack-growth rates were consistent both with estimates made by using fracture-mechanics procedures and with published data available for ferrite-pearlite steels.

### 3.3 Fracture Behavior

1) Of the 15 surface-cracked specimens tested at -60°F and an intermediate strain rate to simulate service conditions, one near-plane-strain brittle fracture occurred. This fracture was classified as brittle because the net-section failure stress was less than the yield strength, the fracture toughness

2

was a "nearly valid" plane-strain $K_{IC}$ value, and the calculated crack-opening-displacement (COD) value was very small. Stable crack extension before final fracture (indicating ductile fracture behavior) occurred in only four tests. The remaining specimens exhibited various degrees at elastic-plastic behavior. Thus the results from the service-simulated tests confirmed that these low-toughness heat-affected-zone (HAZ) weldments could occasionally fail in an unacceptable brittle manner.

2) Some of the results from Charpy V-notch tests of the various regions of the weldments marginally did not meet the current American Bureau of Shipping (ABS) specifications for this service application. A great deal of data scatter was obtained for the weldments tested. As long as attention was focused on the poorest performance of the sets of weldments investigated, it could be concluded that the Charpy toughness in the 3-mm position of the HAZ did not meet the ABS specification. Therefore, the brittle-fracture behavior of the one service-simulated specimen gives credence to the existing ABS criteria and procedures.

3) Because of the "masking" of the low-toughness region (3- to 5-mm position) by the adjacent high-toughness region (weld metal and base plate), attention must be focused on the minimum rather than the average of the toughness values measured for the weldment.

4) The lowest toughness region in the HAZ of the 1-inch-thick SMA weldments was also observed at the 3-mm position when surface-notched, rather than edge-notched. Charpy specimens were tested with the entire notch located in a particular region of the HAZ. Moreover, both the average and minimum energy absorption were reduced by one third or more. Thus, a change in specimen orientation reduced the "masking" effect of the adjacent higher toughness regions and verified that a small region in the HAZ showed brittle rather than the desired elastic-plastic behavior.

5) If it is assumed that the NDT temperature is the limit of dynamic brittle fracture and the measured NDT results are adjusted for an intermediate rate of loading, the NDT results predict marginal elastic-plastic behavior. Thus, the NDT results were consistent with the results from the tests simulating the

service application. However, the NDT specimen is not recommended as a quality-control test for ship-steel weldments because the location of the crack initiating from the hard-X bead is unpredictable and can lead to incorrect interpretation of the test results.

6) Application of the present ABS rules to the results from the CVN tests of the weldments indicated somewhat less than acceptable performance at -60°F. Likewise, at -60°F the NDT and DT data for these weldments marginally exceed the criteria proposed by Rolfe when the criteria are adjusted for intermediate loading rates. However, for both dynamic and intermediate loading rates, the CVN values for these weldments exceed the CVN values equivalent to the 5/8 DT values required by Rolfe. The 5/8-inch dynamic-tear specimen is not recommended as a quality-control test for weldments because it is too thick to assess small regions of low toughness in a HAZ that are "masked" by adjacent material of greater toughness.

7) Although full-plate-thickness three-point-bend fracture-mechanics specimens that sampled the lowest toughness HAZ were tested at -60°F at an intermediate strain rate, the fracture-toughness ($K_Q$) results did not indicate valid plane-strain $K_{IC}$ behavior. Thus, this test could not be used to properly assess the marginal toughness performance of the weldments. However, the lower bound of the COS (crack-opening-stretch) values (approximately 0.001 inch) obtained from these same specimens is considered to represent inadequate elastic-plastic fracture toughness and thus confirmed the marginal toughness of the weldments.

8) The three surface-cracked specimens that contained internally initiated fatigue cracks were tested at -60°F at an intermediate loading rate and fractured only after stable crack extension had occurred. Because the fatigue-crack front of these specimens was in the weld metal as well as the HAZ and base plate, a smaller portion of the HAZ was sampled in these tests. Although limited, these results are consistent with the elastic-plastic behavior predicted from the results for the CVN, NDT, 5/8 DT, and three-point-bend plane-strain fracture-toughness specimens which primarily sampled the weld metal and base plate.

9) At -60°F, the toughness at the 3- to 5-mm position in these weldments was very low compared with that of the adjacent base plate and weld metal and may not be typical of other ship-steel weldments. Extensive searching was done before such a weldment system could be identified for this program.

## 4.0  BACKGROUND AND INTRODUCTION

Increased attention to notch toughness as a material parameter in ship construction for low-temperature service has focused on the inability to economically produce weldments that satisfy current Charpy V-notch (CVN) energy requirements and on the multiplicity of test specimens and notch locations required for the variety of plate thicknesses used for applications where the temperature can fall below +32°F (0°C).  At present, CVN notch locations are prescribed to be at the weld center line, fusion line, in the heat-affected zone (HAZ) 1 mm, 3 mm, and 5 mm from the fusion line, and in the base plate.

Metallurgical studies are currently under way to determine whether economical steels are available that will have adequate HAZ toughness for low-temperature applications when used with high-deposition-rate welding procedures in shipyard fabrication (for example, Ship Structure Committee sponsored research project SR-1256 entitled "Investigation of Steels for Improved Weldability").  The appropriateness of current Charpy energy requirements for both as-rolled and heat-treated ship steels is also being questioned.  In as-rolled plate, the HAZ toughness is usually improved near the fusion zone but may be impaired at the outer regions of the HAZ.  In contrast, the HAZ toughness of heat-treated steel plate is sometimes impaired near the fusion zone.

The primary purpose of this project was to assess the toughness of various regions of a weldment having a low-toughness HAZ by utilizing various quality-control fracture-toughness tests.  In addition, fracture-mechanics-type tests were used to assess the lowest toughness region of the weldment. The results from all these tests were then compared with results from tests of specimens (surface-cracked) in which natural fatigue cracks had been grown to various sizes and the specimens tested to failure at the lowest temperature and highest loading rate expected in actual service.  The quality-control tests used in this investigation were the Charpy V-Notch, 5/8-inch dynamic tear (DT), and the nil-ductility transition temperature (NDT).

Existing quantitative predictive equations relating the quality-control test results to quantitative fracture-mechanics-toughness values allowed the comparison of predicted fracture behavior with that obtained from tests of surface-cracked specimens simulating service at -50°F or -46°C and an intermediate rate of loading.  The surface-cracked specimens were obtained by cyclically loading submerged-arc-welded (SAW) and shielded-metal-arc (SMA) butt-welded Tee joints.  The crack

6

lengths were monitored during initiation and propagation and the results compared with data from the literature. Weldments with the reinforcement remaining and removed were examined.

The service performance of ship-steel weldments, like that of weldments for other structures, is best evaluated by examining the parameters that govern (1) the initiation of a crack, (2) the stable propagation of a crack, and (3) unstable extension of the crack. Thus, this report considers each of these three events separately and sequentially.

## 5.0 MATERIALS

### 5.1 Plate

The original contract for the present study specified the use of ABS-CS steel weldments. Because the 1-1/2-inch and 5/8-inch-thick (38 and 16 mm) ABS-CS plates of the original program did not clearly indicate a low-toughness heat-affected-zone (HAZ) when evaluated by the Charpy V-notch[1] (CVN) test (see Appendix Supplement), plates of A537 Class 1 (formerly Grade A) sulfide-shape-controlled steel which were found[2] to exhibit very low HAZ toughness at -60°F (-51°C) were substituted. The plates were 1- and 1/2-inch thick and had been used earlier in the MARAD[2] program as discussed in Section 8.1.

### 5.11 Chemical Composition

The composition of the 1- and the 1/2-inch (25.4 and 12.7 mm) A537 Class I plates was essentially the same and agreed closely with the composition reported in the MARAD[2] program, Table 1. The rare-earth additions used in steelmaking cause formation of globular rather than strung-out sulfides, thus increasing the fracture toughness of the plate.

### 5.12 Tensile Properties

Duplicate longitudinal and transverse standard[1] 0.252-inch-diameter (6.4 mm) tension specimens from the quarter-thickness of the 1-inch-thick plate and the mid-thickness of the 1/2-inch-thick plate were tested, Table 2. The transverse yield and tensile strengths for the 1-inch-thick plate are about 5 ksi (34 MPa) greater than those reported in the MARAD[2] program and those for the 1/2-inch plate are essentially identical.

### 5.2 Weldments

The weldments were made as large as practical, consistent with testing-machine capacity, both to provide constraint and to allow for heat dissipation during welding. The welding conditions used were similar to those that had produced a very

---

[1] "Mechanical Testing of Steel Products," ASTM Standards, Part 10, 1978, pp. 28-83.

[2] K. Willens, "Final Report of Phase I, MARAD/(NBS) General Dynamics Ship Steel Improvement Program," General Dynamics, Quincey Ship-Building Division, May 17, 1977.

Table 1

Chemical Composition of the 1/2-Inch- and 1-Inch-Thick A537 Class
Steel Plates Studied-Percent by Weight

| | C | Mn | P | S | Si | Cu | Ni | Cr | Mo | V | N | Nb | Zr | Ce |
|---|---|---|---|---|---|---|---|---|---|---|---|---|---|---|
| | | | | | | 1-Inch-Thick Plate | | | | | | | | |
| Present Results | 0.12 | 1.46 | 0.011 | 0.002 | 0.32 | 0.023 | 0.18 | 0.020 | 0.054 | 0.042 | 0.010 | <0.005 | <0.004 | 0.025 |
| Results from MARAD Program | 0.11 | 1.42 | 0.017 | 0.004 | 0.33 | 0.03 | 0.21 | 0.04 | 0.049 | 0.048 | ND* | ND | ND | 0.040 |
| | | | | | | 1/2-Inch-Thick Plate | | | | | | | | |
| Present Results | 0.11 | 1.43 | 0.011 | 0.003 | 0.32 | 0.022 | 0.18 | 0.020 | 0.055 | 0.042 | 0.007 | <0.005 | <0.004 | 0.40 |
| Results from MARAD Program | 0.11 | 1.42 | 0.017 | 0.004 | 0.33 | 0.03 | 0.21 | 0.04 | 0.049 | 0.048 | ND | ND | ND | 0.040 |

* Not determined.

9

Table 2

Tensile Properties of the 1/2-Inch- and 1-Inch-Thick A537 Class 1
Steel Plates and the SMA and SAW Weld Metals Studied

| 0.2% Yield Strength, ksi | Stress Values, ksi, @ Various Values of Elongation | | | | Tensile Strength, ksi | Elongation Values in 1 Inch, percent | | Reduction of Area Values, percent | |
|---|---|---|---|---|---|---|---|---|---|
| | 0.5% | 2% | 3% | 5% | | @ Maximum Load | @ Fracture | @ Maximum Load | @ Fracture |
| 1-Inch Base Plate (Longitudinal) | | | | | | | | | |
| 53.8 | 53.7 | - | 58.7 | 64.8 | 75.1 | 17.0 | 34.0 | 21.0 | 78.8 |
| 1-Inch Base Plate (Transverse) | | | | | | | | | |
| 57.0 | 57.0 | - | 60.7 | 66.7 | 76.2 | 15.0 | 33.0 | 15.4 | 75.7 |
| 1/2-Inch Base Plate (Longitudinal) | | | | | | | | | |
| 55.4 | 54.6 | - | 62.1 | 66.9 | 73.6 | 20.3 | 34.0 | 26.3 | 78.0 |
| 1/2-Inch Base Plate (Transverse) | | | | | | | | | |
| 57.3 | 55.7 | - | 62.4 | 66.8 | 73.6 | 18.0 | 34.0 | 20.0 | 76.7 |
| 1-Inch SMA Weld Metal | | | | | | | | | |
| 83.0 | 83.1 | - | 80.6 | 83.7 | 86.2 | 14.0 | 28.5 | 20.6 | 69.8 |
| 1-Inch SAW Weld Metal | | | | | | | | | |
| 75.6 | 74.2 | - | 89.5 | 92.4 | 94.4 | 12.0 | 26.0 | 17.0 | 26.0 |
| 1/2-Inch SMA Weld Metal | | | | | | | | | |
| 75.6 | - | 77.0 | 79.2 | 83.1 | 87.2 | 12.0 | 25.5 | 16.4 | 74.5 |
| 1/2-Inch SAW Weld Metal | | | | | | | | | |
| 62.5 | - | 68.1 | 72.1 | 76.8 | 84.4 | 14.0 | 31.0 | 21.6 | 75.4 |

low toughness HAZ in the 1-inch plate tested as part of the MARAD[2] program.

## 5.21  Consumables

The 1- and the 1/2-inch plates were welded by using two welding processes.  The shielded-metal-arc (SMA) process incorporated an E8018-C1 electrode for both plate thicknesses. For the 1-inch-thick plate, the electrode diameters were 5/32- and 1/8-inch (4 and 3 mm) for the first and second root passes, respectively, and a combination of 5/32- and 3/16-inch (4 and 5 mm) for all remaining weld passes.  For the 1/2-inch-thick plate, the electrode diameter was 1/8-inch for the root pass and a combination of 5/32 and 3/16-inch for the remaining passes. The SAW process incorporated 5/32-inch ARMCO W18 wire and Lincoln 880 flux.

The chemical compositions of the electrodes are shown in Table 3.  A typical photomicrograph of each type of weldment is shown in Figures 1-1 and 1-2.  The base-metal microstructure was ASTM grain size 8, consistent with the MARAD[2] program value of 7 to 8.

## 5.22  Welding Procedures and Tension-Test Results

All the welds were butt joints.  The mating edges of the plates were machined to form Vee grooves having a 60-degree included angle.  For the 1-inch SMA weldments, a double Vee centered on the plate thickness was used with a zero land and a 1/8-inch root opening, whereas for the 1/2-inch SMA weldments a single-Vee groove was used with a 1/8-inch (3 mm) root gap and a backup bar.  For the 1-inch SAW weldments, a single Vee with a 1/2-inch land was used while welding the first side, then the opposite side was prepared in the same manner for the completion of welding.  The plates for the 1/2-inch SAW weldments were machined in a similar manner, except that a 1/8-inch land was used.

A typical weld-pass-sequence record for each weld type and plate thickness is listed in Table 4.  For the Tee weldments, the longitudinal welds were made first, then the ends were beveled and the transverse welds were completed.  All welds were radiographed according to UW51 of Section VIII, Division 1, 1977 ASME Boiler and Pressure Vessel Code.  For the 1-inch SMA weldments, the heat input was about 40 to 45 kJ/in. (1.57 to 1.77 kJ/mm) for all but one weldment for which the heat input was 35 kJ/in. (1.38 kJ/mm).  For the 1/2-inch SMA weldments, the heat input was about 40 kJ/in. (1.57 kJ/mm).  For both the 1-

LAST PASS GRAIN COARSENED ZONE

INTERCRITICAL ZONE

7X

CODE 1M3

REHEATED GRAIN COARSENED ZONE

LAST PASS WELD METAL ZONE

REHEATED WELD METAL ZONE
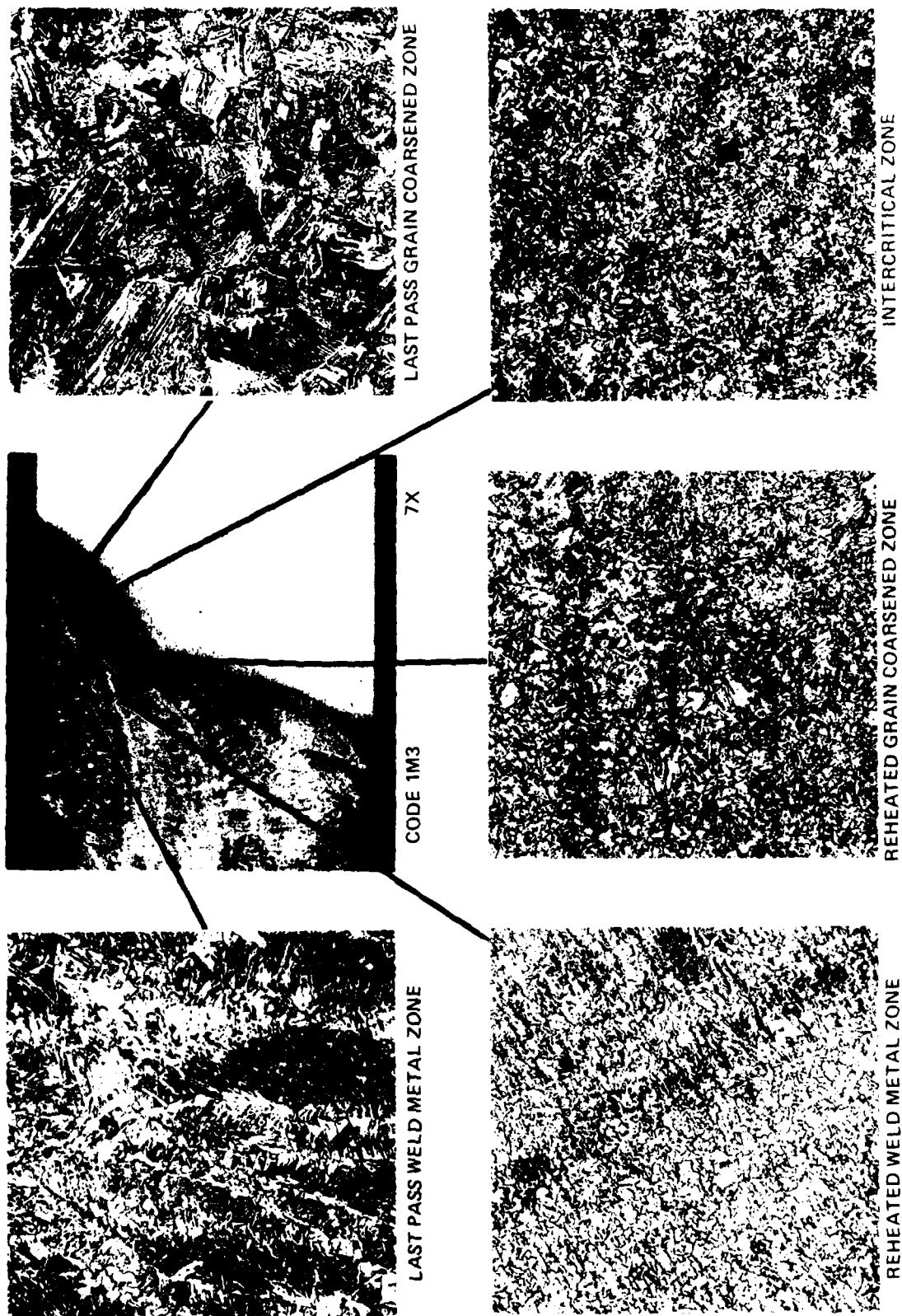
Figure 1-1) Typical Photomicrograph of SMA Weldments with Picral and Nital Etch - 200X Except as Noted

12

LAST PASS WELD METAL ZONE

REHEATED WELD METAL ZONE

CODE 1S3

7X

REHEATED GRAIN COARSENED ZONE

LAST PASS GRAIN COARSENED ZONE

INTERCRITICAL ZONE
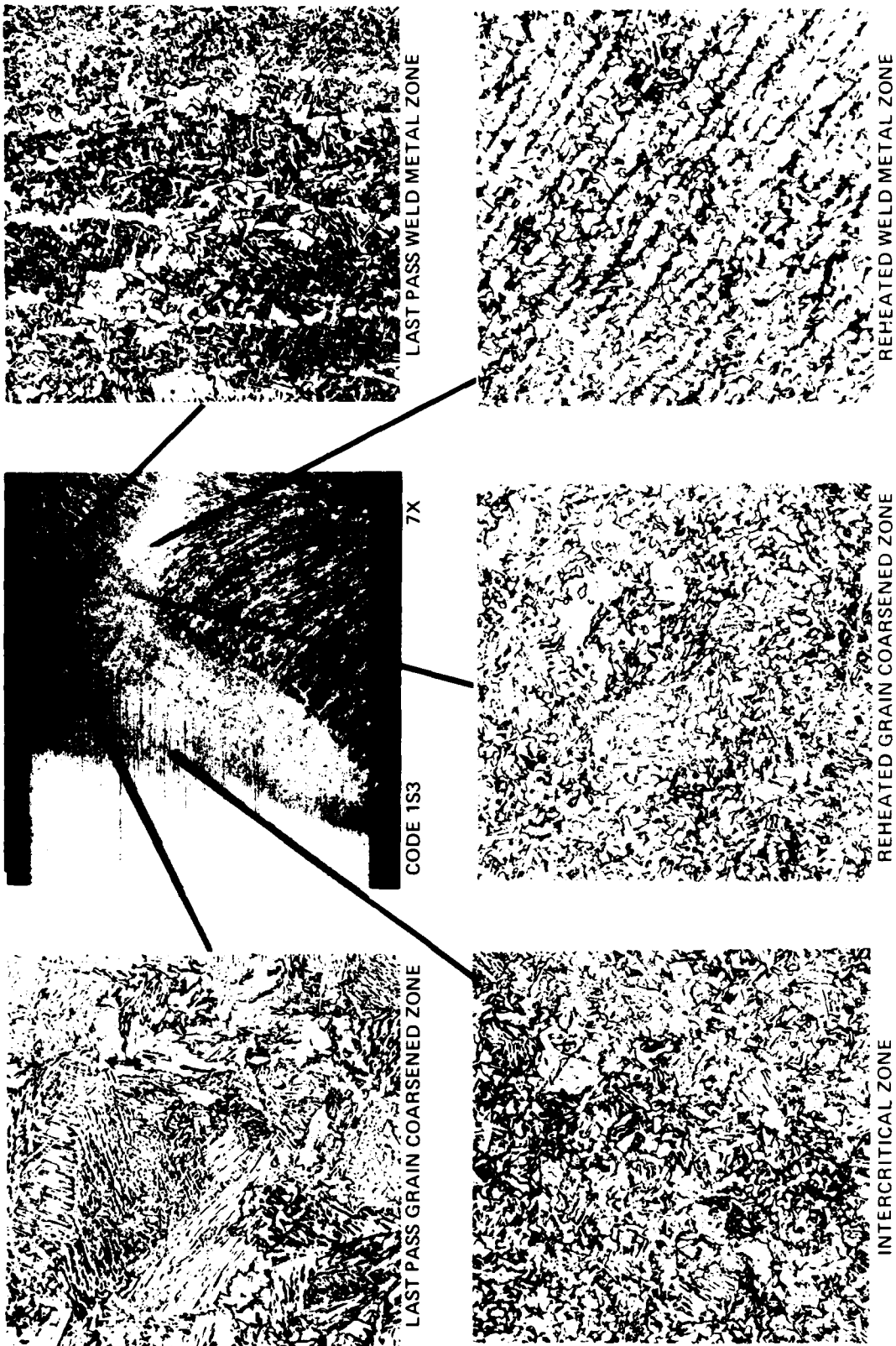
Figure 1-2  Typical Photomicrograph of SAW Weldments with Picral and Nital Etch – 200X Except as Noted

13

Table 3

Chemical Composition of SMA and SAW Welding Consumables-Percent by Weight

| | C | Mn | P | S | Si | Cu | Ni | Cr | Mo |
|---|---|---|---|---|---|---|---|---|---|
| SMA Welds—E8018-C1 Electrode | | | | | | | | | |
| Manufacturers | 0.039 | 1.18 | ND* | 0.018 | 0.45 | 0.017 | 2.25 | 0.024 | 0.007 |
| Nominal Composition | 0.05 | 0.80 | - | - | 0.45 | - | 2.30 | - | - |
| SAW Welds—W18 Electrode | | | | | | | | | |
| Manufacturers | 0.15 | 0.59 | 0.007 | 0.009 | 0.13 | 0.26 | 1.80 | 0.036 | 0.13 |
| Nominal Composition | 0.16 | 0.75 | 0.010 | 0.009 | 0.15 | 0.25 | 1.85 | 0.11 | 0.15 |

* ND - Not determined.

14

## Table 4

### Typical Weld-Pass Sequence Records for 1- and 1/2-Inch SMA and SAW Weldments

| Weld Pass No. | Side | Electrode or Wire Diameter, inch | Voltage | Amperage | Travel Speed, ipm |
|---|---|---|---|---|---|
| **1-Inch SMA (E8018-C1 Electrode)** | | | | | |
| 1 | 1 | 5/32 | 24 | 165 | 3 to 4 |
| 2 | 1 | 3/16 | 24 | 210 | 3 to 4 |
| 3 | 2 | 3/16 | 22 | 125 | 3 to 4 |
| 4 | 2 | 5/32 | 24 | 175 | 3 to 4 |
| 5 to 7 | 2 | 3/16 | 24 | 210 | 3 to 4 |
| 8 and 9 | 1 | 3/16 | 24 | 210 | 3 to 4 |
| 10 and 11 | 2 | 3/16 | 24 | 210 | 3 to 4 |
| 12 to 14 | 1 | 3/16 | 24 | 210 | 3 to 4 |
| 15 and 16 | 2 | 3/16 | 24 | 210 | 3 to 4 |
| **1/2-Inch SMA (E8018-C1 Electrode)** | | | | | |
| 1 | 1 | 1/8 | 22 | 130 | 3 to 4 |
| 2 to 6 | 1 | 5/32 | 24 | 175 | 3 to 4 |
| 7 and 8 | 1 | 3/16 | 24 | 210 | 3 to 4 |
| **1-Inch SAW (ARMCO W18 Wire and Lincoln 880 Flux)** | | | | | |
| 1 | 1 | 5/32 | 32 | 600 | 23 |
| 2 | 1 | 5/32 | 32 | 530 | 20 |
| 3 | 1 | 5/32 | 32 | 600 | 23 |
| 4 to 8 | 2 | 5/32 | 32 | 600 | 23 |
| 9 | 1 | 5/32 | 32 | 600 | 23 |
| 10 | 2 | 5/32 | 32 | 600 | 23 |
| 11 | 1 | 5/32 | 32 | 600 | 23 |
| 12 | 2 | 5/32 | 32 | 600 | 23 |
| **1/2-Inch SAW (ARMCO W18 Wire and Lincoln 880 Flux)** | | | | | |
| 1 | 1 | 5/32 | 32 | 600 | 23 |
| 2 | 1 | 5/32 | 32 | 600 | 23 |
| 3 | 2 | 5/32 | 32 | 600 | 25 |

15

and 1/2-inch SAW weldments, the heat input was 50 kJ/in. (1.99 kJ/mm).

Duplicate all-weld-metal standard[1]) 0.252-inch-diameter (6.4 mm) tension specimens were machined and tested from the quarter-thickness of the 1-inch and from near the surface of the 1/2-inch SMA and SAW weldments. The tensile properties are shown in Table 2. Samples were cut from the 1-inch SMA and SAW weldments, polished, and etched to obtain hardness surveys for the weld metal, HAZ, and base metal at various locations within the plate thickness. These locations corresponded to fracture-critical locations of the various specimens included in the test program. The locations were near the surface for the NDT specimens (0.050 in. or 1.27 mm below the plate surface), at the center of the CVN specimens (approximately 0.30 in. or 7.62 mm below the plate surface), and at the 1/3-thickness and mid-thickness of the $K_{IC}$ and DT specimens (0.30 and 0.40 in. or 7.62 and 10.16 mm below the plate surface for the 1/3-thickness locations and at the actual plate mid-thickness for the specimen mid-thickness locations).

The results of the hardness surveys are summarized in Figures 2-1 and 2-2. The SMA weld metal and HAZ were a maximum of about 99 and 104 Diamond Pyramid Hardness (DPH) points greater than the base plate, whereas the SAW weld metal and HAZ were a maximum of about 76 and 70 DPH points greater than the base plate, respectively.
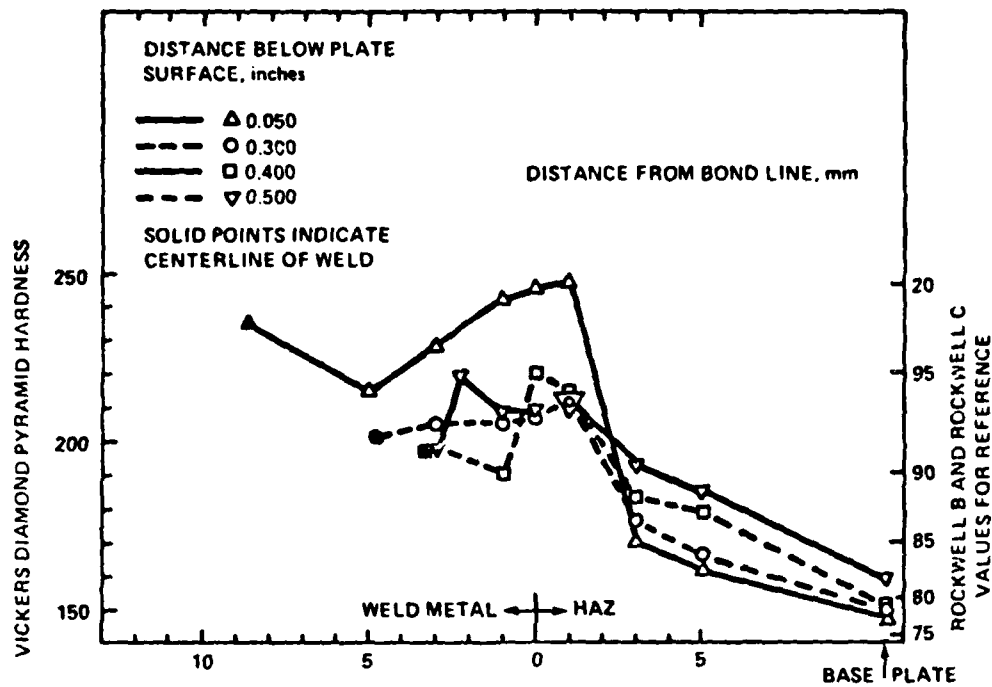
16

Figure 2-1    Hardness of A537 Class 1 1-Inch-Thick SMA Weldment
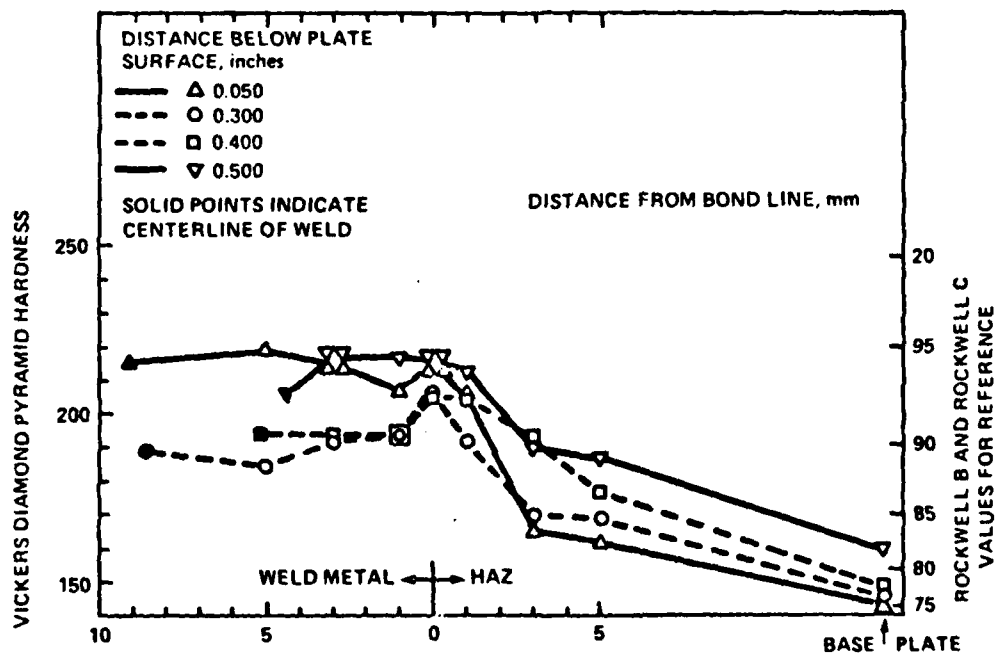


Figure 2-2    Hardness of A537 Class 1 1-Inch-Thick SAW Weldment

17

## 6.0 FATIGUE-CRACK-INITIATION BEHAVIOR

### 6.1 Background

Early analysis of the fatigue behavior of steels involved development of S-N curves for the particular steel of interest. Samples of the material were machined in the form of round bars or cantilever strips, and cyclically loaded to maximum-stress, S, levels until failure occurred after a number of cycles, N, or until some maximum number of cycles were applied with no failure, representing infinite life. For the finite-life data generated in this manner, the life of the specimen includes both the number of cycles that it takes to generate a crack on the surface of the specimen (fatigue-crack initiation) and the number of cycles that it takes to propagate the crack (fatigue-crack propagation) through the particular specimen geometry being tested.[3]

Fracture-mechanics analyses have shown a more quantitative means of evaluating both the initiation and the propagation behavior. For fatigue-crack initiation from notches in various steels subjected to different stress ratios (R = -1 to 0.5), the threshold value of the stress-intensity-factor range, $\Delta K$, can be estimated from the equation[4]

$$\left. \frac{\Delta K}{\sqrt{\rho}} \right)_{th} = 10 \sqrt{\sigma_{ys}}$$

where $\Delta K$ is the cyclic stress-intensity factor for a crack of equivalent length, $\rho$ is the notch-root radius, and $\sigma_{ys}$ is the yield strength. These data show that increasing the yield strength retards fatigue-crack initiation in steel plate.

Predicting fatigue-crack initiation in weldments is far more difficult than predicting behavior in base plate. When the weld reinforcement is not removed, the fatigue crack will initiate at the toe of the reinforcement because of the stress concentration. If weld porosity or crack-like discontinuities are present, the cycles (or life) required to initiate a fatigue crack may be shortened or eliminated.

---

[3] J. M. Barsom, "Fatigue Behavior of Pressure Vessel Steels," Welding Research Council Bulletin, No. 194, May, 1974.

[4] R. Roberts, J. M. Barsom, S. T. Rolfe, and J. W. Fisher, "Fracture Mechanics for Bridge Design," Report No. FHWA-RD-78-68, Federal Highway Administration, Department of Transportation, Washington, D.C., July, 1977.

Work at the British Welding Institute[5] suggests that crack-like discontinuities or actual microcracks of about 0.010 inch or less in depth are always present in the undercut area at the base (toe) of the weld. If this is true, the fatigue-crack-initiation life is limited to that necessary to sharpen these imperfections and is completely eliminated if microcracks are present. This viewpoint raises an interesting fundamental question: if the imperfections in the weld-undercut region significantly shorten or eliminate the fatigue-crack-initiation life, then all steel weldments, independent of yield strength, will have the same fatigue behavior (because the fatigue-crack-propagation behavior is the same for all steels, as discussed in the next section). In the present investigation, this question was examined by comparing fatigue-crack-initiation data for smooth weldment surfaces, where the weld reinforcement and the undercut regions were removed, with fatigue-crack-initiation data for weldment surfaces where the reinforcement had been removed but the undercut region was untouched.

## 6.2   Test Procedures and Results

### 6.21   Fatigue-Crack-Initiation Tests
at Room Temperature

Room-temperature fatigue-crack-initiation data were obtained for the 1-inch SMA and SAW weldments by using full-thickness specimens containing Tee welds, as shown in Figures 3 and 4, which simulate a weld-joint geometry frequently used for shipbuilding. To produce the most severe orientation for subsequent fracture tests, the rolling direction of the base plate was always perpendicular to the axis of the specimen and thus to the loading direction. If a fatigue crack initiated in a specimen, the number of cycles and crack length were recorded for crack-propagation analysis (Section 7). Selected cracked specimens were tested to failure by simulating the most severe service conditions (Section 8).

Four weldment surface conditions were tested: (1) SMA and SAW as welded, (2) SAW with both the weld reinforcement and the entire undercut region removed (smooth), (3) SMA and SAW

---

[5] B. A. Granville and F. Watkinson, "Research Programs to Investigate the Fatigue of High Strength Steels: Initiation in Fillet Welds," Fatigue Performance of Welded High Strength Steels," The Welding Institute, 1974.

1 inch = 25.4 mm
RD = ROLLING DIRECTION
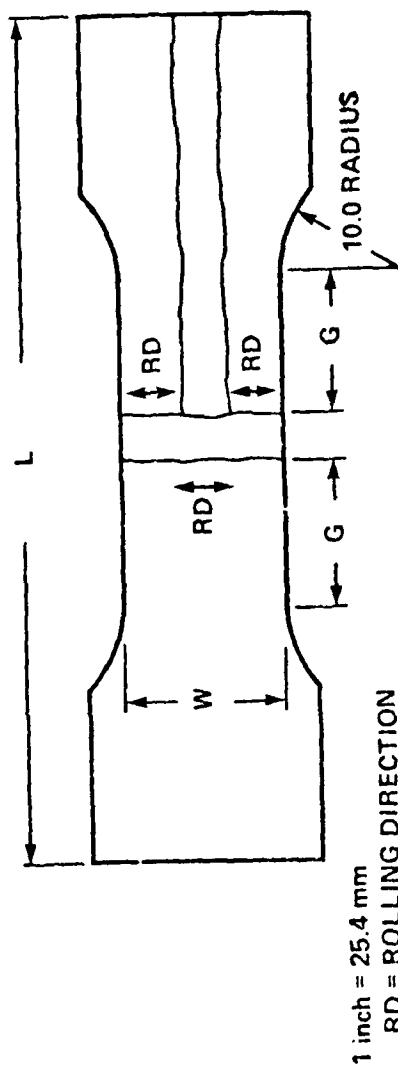
| | SPECIMEN TYPE | L, in. | W, in. | G, in. |
|---|---|---|---|---|
| 1 | SMA & SAW AS WELDED | 19.5 | 4.25 | 2.5 |
| | | 15.75 | 3.50 | 2.125 |
| 2 | SMA & SAW SMOOTH UNDERCUT | 19.5 | 4.25 | 2.5 |
| | | 15.75 | 3.50 | 2.125 |
| 3 | SMA & SAW ROUGH UNDERCUT | 15.75 | 3.50 | 2.125 |
| 4 | SAW SMOOTH | 24.0 | 4.25 | 5.0 |
| | | 19.5 | 4.25 | 2.5 |

Figure 3    Dimension of Tee-Weld Specimens Used for Fatigue Crack
Initiation, Fatigue Crack Propagation, and Fracture Tests

20

Figure 4    SAW As-Welded Tee-Weld Specimen Showing Terminal Strips
            Used to Detect Fatigue Crack Initiation (RD = Plate
            Rolling Direction)

21

with the weld reinforcement removed but the undercut region and the original plate surface retained (rough undercut), and (4) SMA and SAW with the weld reinforcement and a minimum amount of the original plate surface removed to produce a smooth finish away from the undercut region (smooth undercut).

In general, the as-welded and rough-undercut specimens were 3.5 inches (88.9 mm) wide and had a uniform section length of 4.25 inches (108 mm) plus t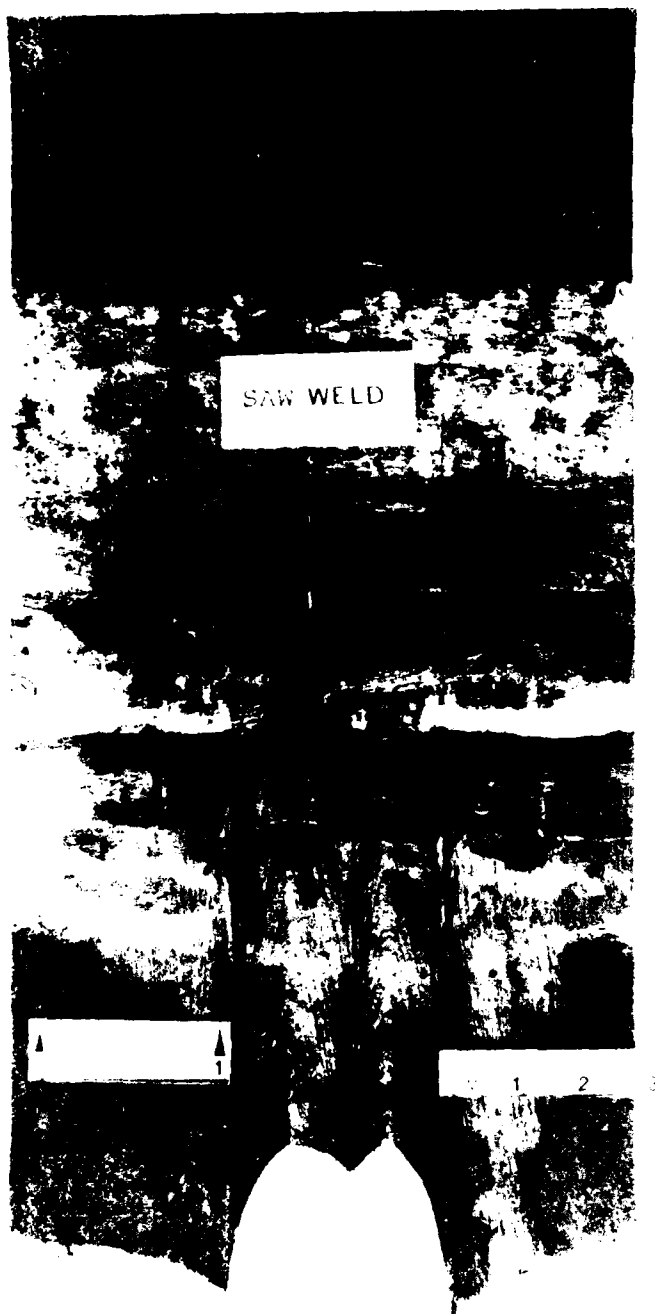he width of the weld, whereas, the smooth and smooth-undercut specimens were 4.25 inches (108 mm) wide and had a uniform section length of 5.0 inches (127 mm) plus the width of the weld.

Most of the fatigue-crack-initiation tests for the as-welded specimens and all of the fatigue-crack-initiation tests for the undercut specimens were conducted with a 300-kip (1.33 MN) closed-loop hydraulic machine cycled at 2.5 to 4.75 cycles per second (cps). All other tests (including all tests at -60°F) were conducted with a 150-kip (667 kN) resonant fatigue machine at 114 to 124 cps. The smooth specimens were all tested in the 300-kip closed-loop hydraulic machine at 0.5 to 6 cps. Because there were only limited comparative data, a firm conclusion cannot be drawn regarding the effect of test frequency. The tests were conducted at a minimum- to maximum-stress ratio (R ratio) of -1 except Specimen 3AM2, which had an R ratio of zero.

To determine when a crack had initiated without constant monitoring of the specimen, bondable terminal strips were mounted on most specimens with an epoxy adhesive. These terminal strips were mounted both at the center and quarter-width positions on both faces of the specimen such that they crossed both bond lines of the transverse weld or, in the case of the center strips, crossed one bond line and ran along the center of the longitudinal weld, as shown in Figure 4. The strips were connected in series to form an electrical circuit. When a crack initiated and broke one of the terminal strips, the electrical circuit was also broken, and a relay opened to shut off the testing machine. In this manner, fatigue cracks that ranged from about 0.010 to 2.707 inches (0.25 to 68.7 mm) in length were detected during the fatigue-crack-initiation tests. The weldment specimens were cyclically tested for a maximum of $10^6$ cycles.

The location and surface length of the first crack detected in each specimen, along with the corresponding number of fatigue cycles, are presented in Figures 5-1 to 5-9 and Appendix A. Cyclic stress amplitude and cycles to failure are

I = INITIAL CRACK LENGTH, in.
F = FINAL CRACK LENGTH, in.

±16 KSI INITIATION
9AM1 ±29 KSI PROPAGATION

I = 0.35   I* = 0.086
F = 1.972  F* = 0.428
• OPPOSITE FACE
• DISCONTINUOUS

8AM2 ±20 KSI

I & F = 0.876

I = 0.483
F = 0.497

5AM2 ±13 KSI

RUNOUT

7AM1 ±16 KSI

1 ksi = 6.895 MPa
1 in. = 25.4 mm

Figure 5-2   Location and Surface Length
of Fatigue Cracks in 1-Inch-
Thick A537 Class 1 As-Welded
SMA Tee Weldments

I = INITIAL CRACK LENGTH, in.
F = FINAL CRACK LENGTH, in.

3AM2 0-48 KSI

I = 1.156
F = 1.477

2AM1 ±29 KSI

I = 0.065  I** = 1.291
F* = 0.812 F*** = 1.490
• DISCONTINUOUS
** ON OPPOSITE FACE

I = 0.921
F = 0.845

9AM2 ±20 KSI

I = 0.917
F = 1.309
• CYCLED TO
  FAILURE LATER

4AM1 ±24 KSI

1 ksi = 6.895 MPa
1 in. = 25.4 mm

Figure 5-1   Location and Surface Length
of Fatigue Cracks in 1-Inch-
Thick A537 Class 1 As-Welded
SMA Tee Weldments

23

I = INITIAL CRACK LENGTH, in.
F = FINAL CRACK LENGTH, in.

9AS2 ±20 KSI

I = 1.685
F = 2.031

9AS3 ±19 KSI

RUNOUT

9AS4 ±20 KSI

I & F = 0.841

I & F

3AS2 ±20 KSI

I = 0.026
F = 0.949

F

Figure 5-4   Location and Surface Length of Fatigue Cracks in 1-Inch-Thick A537 Class 1 As-Welded SAW Tee Weldments

I = INITIAL CRACK LENGTH, in.
F = FINAL CRACK LENGTH, in.

9AS1 ±24 KSI

SAW

I = 1.497
F = 3.035

F

9AS3 ±21 KSI INITIATION & PROPAGATION
1.3-27.3 KSI PROPAGATION

SAW

I = 0.599
F = 0.638
F* = 1.151
* @ 1.3-27.3 KSI

F*
F

7AM2 ±13 KSI

RUNOUT

SMA

6AS2 ±23.6 KSI

I = 2.460
F = FULL WIDTH = 3.499

SAW

F

I

Figure 5-3   Location and Surface Length of Fatigue Cracks in 1-Inch-Thick A537 Class 1 As-Welded SMA and SAW Tee Weldments

24

I = INITIAL CRACK LENGTH, in.
F = FINAL CRACK LENGTH, in.

4AS2 ±13 KSI

I & F = 0.140

SAW AS-WELDED

I & F

8AS3 ±13 KSI

I & F = 1.241

SAW AS-WELDED

I & F

7AM2 ±20 KSI

I = 0.010
F* = 0.143
• DISCONTINUOUS
SMA ROUGH-UNDERCUT

F

7AM1 ±21 KSI INITIATION
1.1-22.1 KSI PROPAGATION

I = 0.223
F = 1.154
F* = 0.223
SMA ROUGH-UNDERCUT

F

F*

1 in. = 25.4 mm
1 ksi = 6.895 MPa

Figure 5-6   Location and Surface Length of
Fatigue Cracks in 1-Inch-Thick
A537 Class 1 As-Welded SAW and
Rough-Undercut SMA Tee Weld-
ments

I = INITIAL CRACK LENGTH, in.
F = FINAL CRACK LENGTH, in.

9AS4 ±16 KSI

RUNOUT

2AS1 ±16 KSI

I = 1.469
F = TOTAL FAILURE

F

I

6AS3 ±14 KSI

TOTAL FAILURE

F

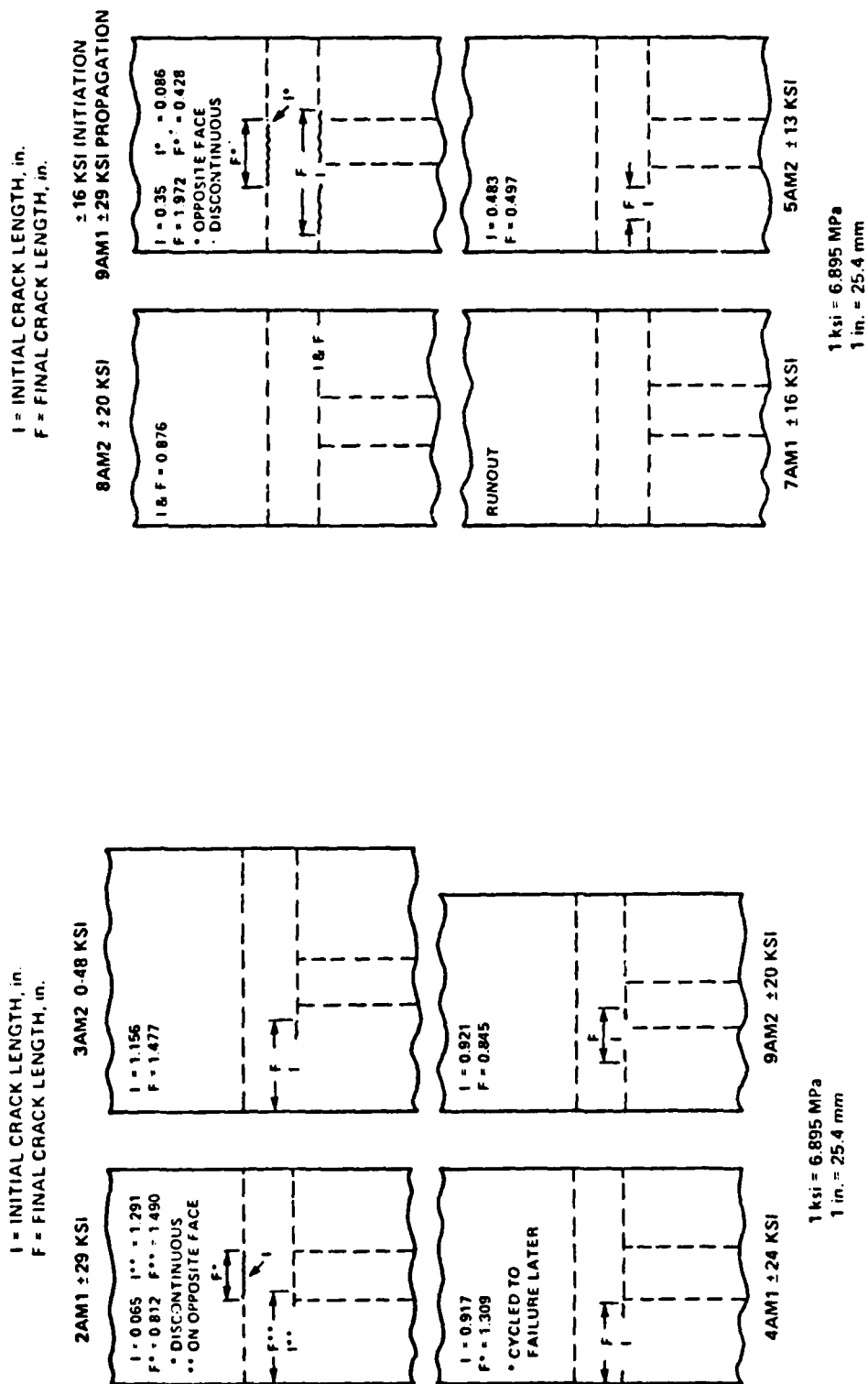6AS4 ±14.8 KSI

I & F = 0.900

I & F

1 in. = 25.4 mm
1 ksi = 6.895 MPa

Figure 5-5   Location and Surface
Length of Fatigue Cracks
in 1-Inch-Thick A537
Class 1 As-Welded SAW
Tee Weldments

25

I = INITIAL CRACK LENGTH, in.
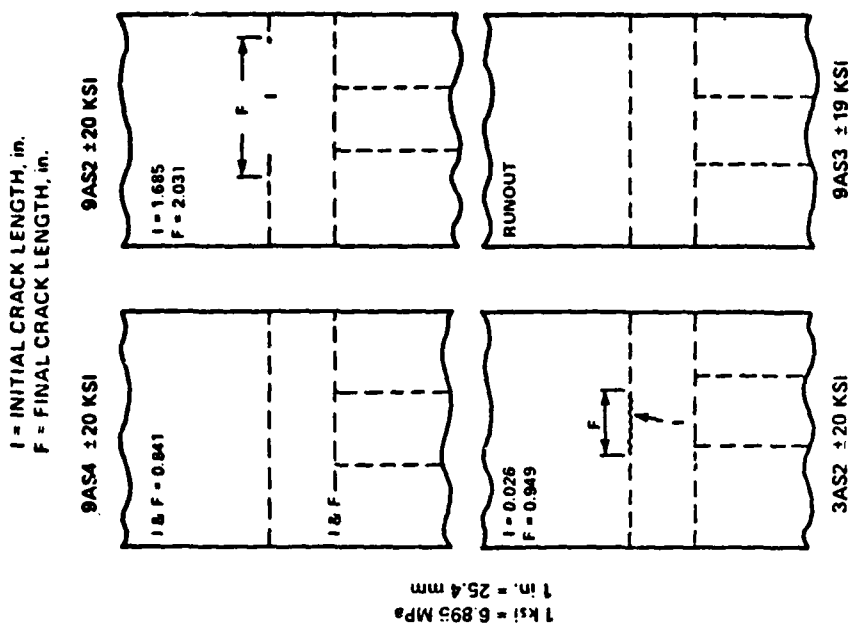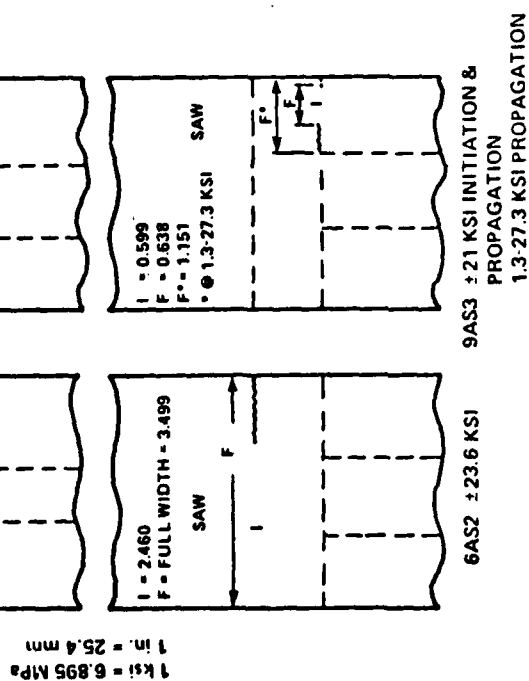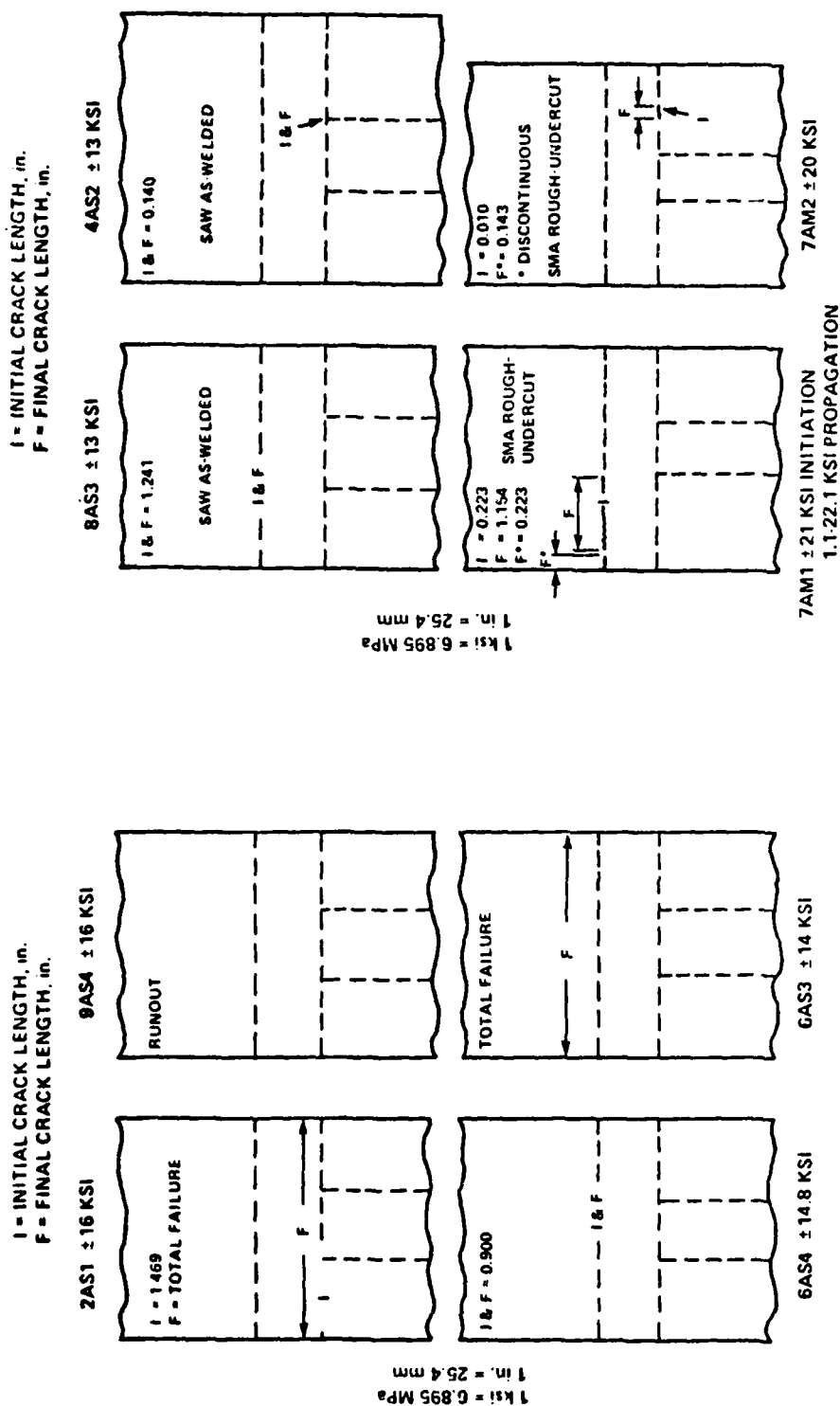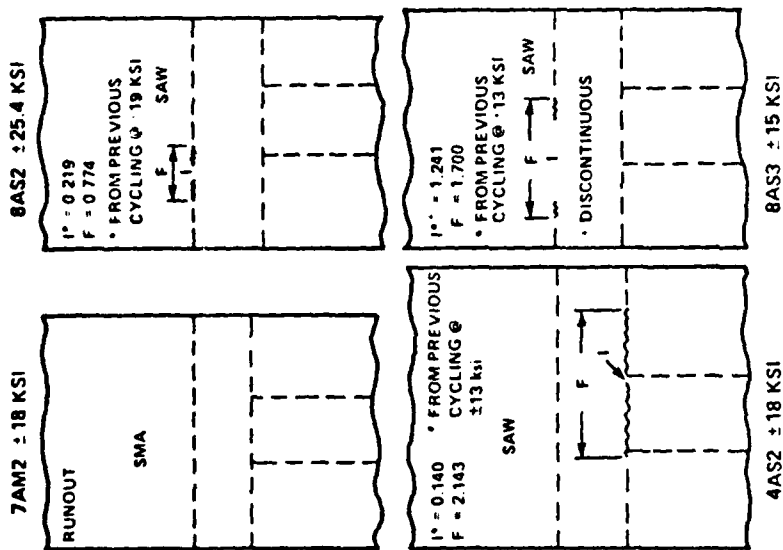F = FINAL CRACK LENGTH, in.

**2AM2 ±29 KSI**
TOTAL FAILURE
SMA

**4AM2 ±27 KSI**
I & F = 0.559
I° & F° = 0.809
* MAXIMUM INTERNAL LENGTH (INTERNAL INITIATION)
SMA
I & F
I° & F°

**8AM1 ±23 KSI**
I & F = 1.011
I° & F° = 1.172
* MAXIMUM INTERNAL LENGTH (INTERNAL INITIATION)
SMA
I & F
I° & F°

**4AS1 ±27 KSI**
TOTAL FAILURE°
° FROM INTERNAL INITIATION
SAW

1 ksi = 6.895 MPa
1 in. = 25.4 mm

Figure 5-8 Location and Surface Length of Fatigue Cracks in 1-Inch-Thick A537 Class 1 Smooth-Undercut SMA and SAW Tee Weldments

---

I = INITIAL CRACK LENGTH, in.
F = FINAL CRACK LENGTH, in.

**7AM2 ±18 KSI**
RUNOUT
SMA

**8AS2 ±25.4 KSI**
I° = 0.219
F = 0.774
* FROM PREVIOUS CYCLING @ -19 KSI
SAW
F

**4AS2 ±18 KSI**
I° = 0.140
F = 2.143
* FROM PREVIOUS CYCLING @ ±13 ksi
SAW
F

**8AS3 ±15 KSI**
I° = 1.241
F = 1.700
* FROM PREVIOUS CYCLING @ -13 KSI
* DISCONTINUOUS
SAW
F

1 ksi = 6.895 MPa
1 in. = 25.4 mm

Figure 5-7 Location and Surface Length of Fatigue Cracks in 1-Inch-Thick A537 Class 1 Rough-Undercut SMA and SAW Tee Weldments

26

I = INITIAL CRACK LENGTH, in.
F = FINAL CRACK LENGTH, in.

7AS3 ±25 KSI



RUNOUT

SAW SMOOTH UNDERCUT

I & F = 0.866
I* & F* = 0.900

* MAXIMUM INTERNAL
LENGTH INTERNAL
INITIATION

SAW SMOOTH

7AS2 ±33 KSI

| SAW SMOOTH | | |
|---|---|---|
| SPECIMEN NO. | $\sigma$, ksi | RESULT* |
| 1AS2 | ±40 | B |
| 1AS1 | ±40 | I |
| 5AS2 | ±38 | I |
| 7AS4 | ±36 | G |
| 1AS4 | ±36.1 | G |
| 4AS3 | ±29 | I |
| 7AS1 | ±29 | G |
| 6AS1 | ±25 | R |
| 4AS4 | ±23 | R |

* B, I, G: TOTAL FAILURE FROM
BASE PLATE, FROM INTERNAL
IMPERFECTION AT BOND LINE,
OR FROM GRIPPED REGION.

R: RUNOUT

1 ksi = 6.895 MPa
1 in. = 25.4 mm

Figure 5-9    Location and Surface Length of Fatigue Cracks in 1-Inch-
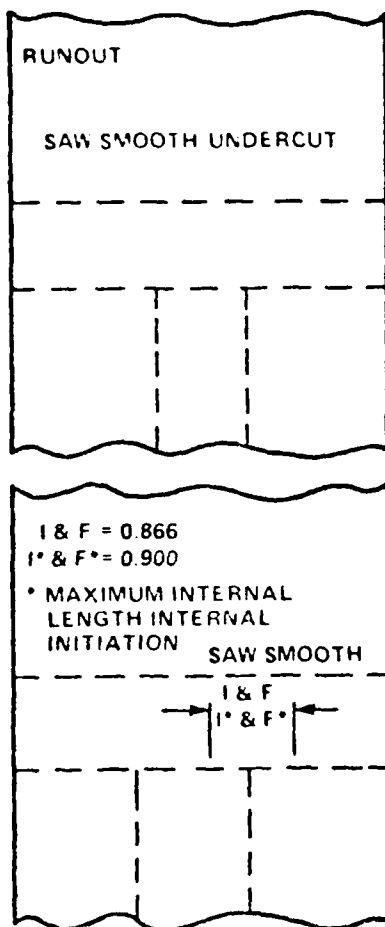Thick A537 Class 1 Smooth-Undercut and Smooth SAW Tee
Weldments (Total Failures and Runouts Also Indicated)

27

shown in Figure 6-1 for all the SMA weldments and in
Figure 6-2 for all the SAW weldments. The crack length at the
time the crack was first observed is indicated next to each data
point.

For the smooth specimens, the cracks started in the
base metal or from internal initiation sites located below the
specimen surface in the weld. These internal sites were near
the bond line of the transverse weld or within the longitudinal
weld. For the smooth-undercut specimens, internal cracks
initiated near the bond line of the transverse weld, whereas for
the as-welded and rough-undercut specimens the crack always
initiated on the surface of the specimen at the toe of the
transverse weld. In some specimens the crack initiated at a
sharp corner or in the gripped portion of the specimen, as noted
in Figure 6-2.

6.22  Fatigue-Crack-Initiation Tests at -60°F

To determine the fatigue-crack-initiation behavior of
weldments at low temperatures, four as-welded SAW Tee weldments
were cycled at a test temperature of -60°F at several stress
levels. The stress levels were selected on the basis of the
fatigue-crack-initiation behavior obtained at room temperature.
The primary purpose of these tests was to determine the fatigue
strength for one million cycles at a test temperature of -60°F.

The fatigue-crack-initiation tests at -60°F were
conducted at 124 cps on the same 150-kip resonant fatigue
machine as were some of the room-temperature tests. To maintain
the test temperature, a tank was mounted on the specimen,
filled with a coolant, and externally cooled fluid was circulat-
ed through the tank as required. The temperature was monitored
by a thermocouple attached to the specimen. The actual tempera-
ture during the tests ranged from -48 to -72°F (-44 to -58°C),
and for most of the duration of the tests the temperature was
between -52 and -68°F (-47 to -56°C). The total test time for
$10^6$ cycles was about two and one-quarter hours. Terminal
strips were bonded to the specimen surfaces to identify crack
initiation.

The results are compared with the room-temperature
S-N curves in Figures 7 and 8. Figure 7 indicates that at one
million cycles and a stress ratio of -1, the fatigue strength
at -60°F of the SAW as-welded specimens was about ±19 ksi
(131 MPa) versus less than ±13 ksi (90 MPa) at room temperature.

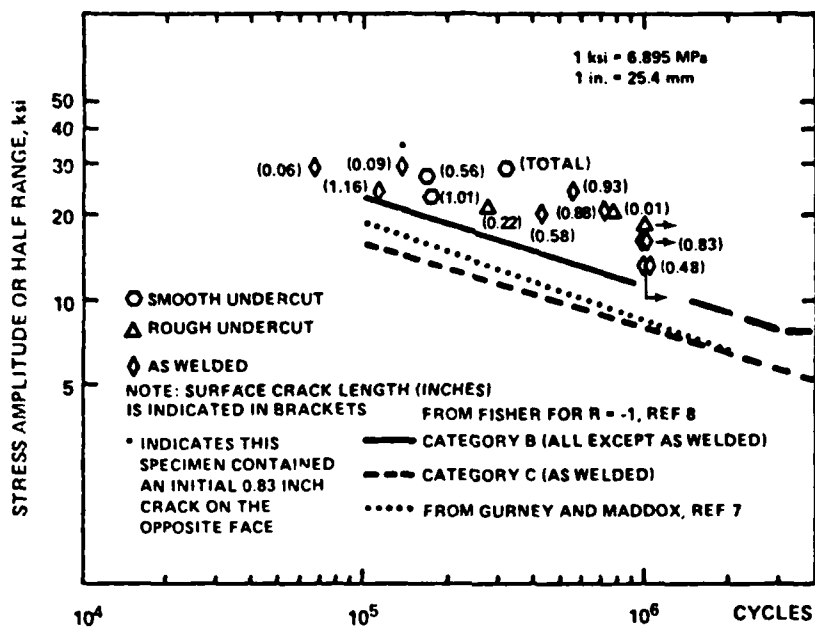Figure 6-1    Stress Amplitude and Cycles to Initiate
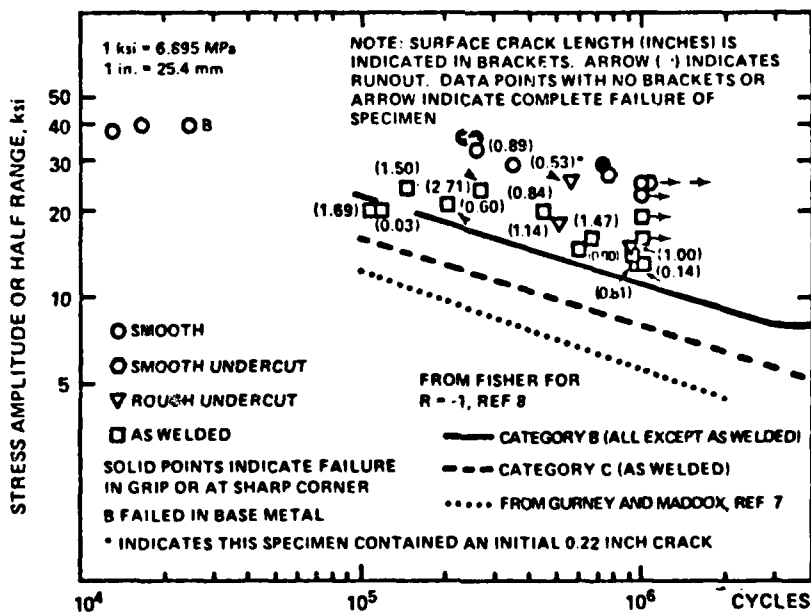Crack for SMA Tee Weldments



Figure 6-2    Stress Amplitude and Cycles to Initiate
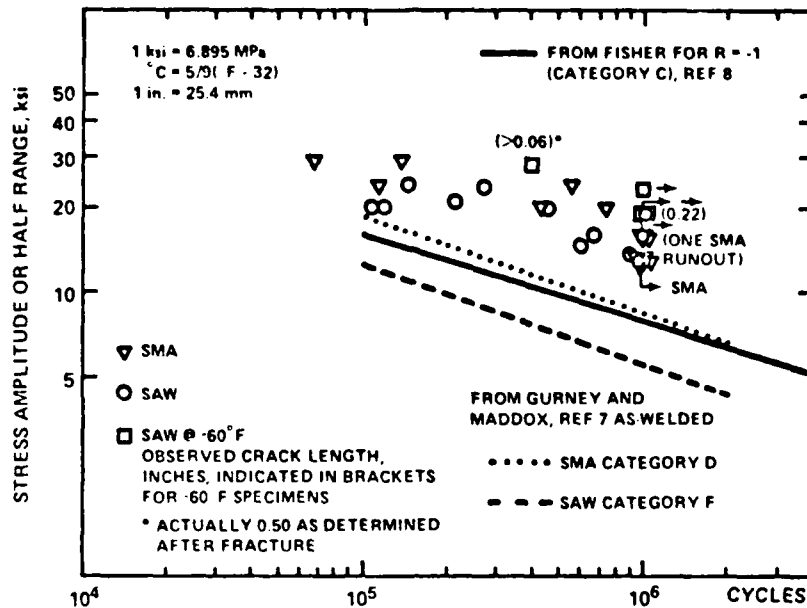Crack for SAW Tee Weldments

Figure 7    Stress Amplitude and Cycles to Initiate
Crack for SMA and SAW Tee Weldments in the
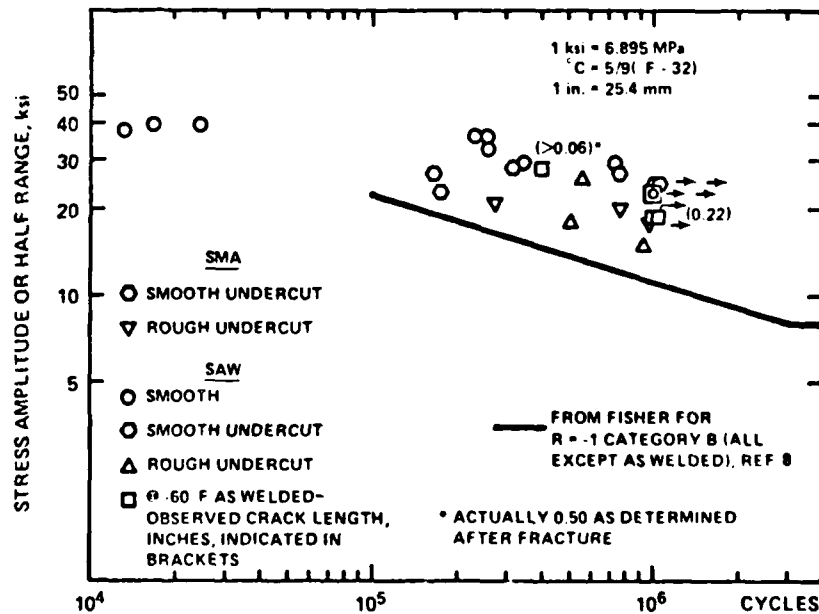As-Welded Condition



Figure 8    Stress Amplitude and Cycles to Initiate
Crack for SMA and SAW Tee Weldments with
Various Surface Conditions

30

## 6.3  Discussion of Results

### 6.31  As-Welded Specimens

The fatigue data for the as-welded 1-inch-thick SMA and SAW Tee-weld specimens showed no significant difference in behavior due to the difference in welding procedure, and the fatigue strength was about 12 ksi (83 MPa) (corresponding to a stress range of 24 ksi) at a life of $10^6$ cycles, Figure 7 and Appendix A.  All the fatigue cracks in the as-welded specimens initiated randomly at the toe regions of the transverse weld. In some cases multiple cracks were observed.  Because the stress concentration is greatest in this toe region, none of the as-welded specimens developed visible cracks from internal imperfections.

Although previous studies have determined the fatigue strength at different lives for butt-welded plates, the present data are perhaps best compared with compilations of data that were accumulated during extensive studies undertaken to develop fatigue design specifications.  Two such programs were 1) that of Fisher et al.[6] in preparing fatigue design curves for welded structural details for the American Association of State Highway and Transportation Officials (AASHTO) and 2) that of Gurney and Maddox[7] for design of British steel girder bridges.  Both the SMA and SAW as-welded specimens tested in the present study correspond to the Category C designation of the AASHTO specifications,[8] whereas the as-welded SMA specimens correspond to Class D and the as-welded SAW specimens correspond to Class F, respectively, of the British standards.[9]  Thus, unlike the

---

[6]  J. W. Fisher, K. H. Frank, M. A. Hirt, and B. M. McNamee, "NCHRP Report 102, Effect of Weldments on the Fatigue Strength of Steel Beams," Lehigh University, Bethlehem, Pennsylvania.

[7]  T. R. Gurney and S. J. Maddox, "Determination of Fatigue Design Stresses for Welded Structures From an Analysis of Data," Metal Construction and British Welding Journal, November 1972, Vol. 4, No. 11, pp. 11-15.

[8]  J. W. Fisher, "Guide to 1974 AASHTO Fatigue Specifications," American Institute of Steel Construction, New York, New York.

[9]  B. S. 153 "Steel Girder Bridges," British Standard Institution, London.

31

British standards, the AASHTO design procedures do not recognize differences between SMA and SAW weldments. The present results are consistent with the AASHTO design procedures in that no difference in results was observed for the two methods of welding. Although, after $10^6$ cycles, two SMA weldments did not show a visible crack (one at a stress amplitude of 16 ksi or 110 MPa and one at 13 ksi or 90 MPa, one SMA weldment showed a 0.48-inch-long (12.2 mm) crack after $10^6$ cycles at a stress amplitude of 13 ksi (89.6 MPa), Figure 6-1. Thus SMA weldments may statistically have fewer surface imperfections than SAW weldments, but the present data support the more conservative AASHTO philosphy of not allowing higher fatigue design strength for SMA weldments than for SAW weldments. The curves forming the basis for the AASHTO fatigue specifications correspond to the 95 percent confidence limits for 95 percent survival determined from experimental data[6] for a given category or severity of welded detail. Hence, the design curves are thought to represent very conservative estimates of fatigue performance.

The curve forming the basis for the AASHTO Category C specification is plotted in Figures 6-1, 6-2, and 7 as a comparison with the results from the present study. Similarly, the results of Gurney and Maddox[7] for the adjusted mean fatigue strength minus two standard deviations of the data examined are shown in the same figures for Class D (SMA butt welds) and Class F (SAW butt welds). Both design procedures recognize that the total stress range must be used for determining the fatigue performance of as-welded structural details because the tensile residual stresses after welding can be of yield-strength magnitude.

All the data from the present study lie above the AASHTO and British specification curves, Figures 6-1, 6-2, and 7. This is to be expected because 1) with one exception, the tests were conducted at an R ratio of -1 and thus, if the applied compressive stress exceeded the tensile residual stress, the actual tensile-stress range at the crack tip would be less than the total applied-stress range; 2) the present weldments were fabricated under ideal laboratory conditions; 3) the design curves are all based upon a conservative analysis of numerous sets of weldment results; and 4) the present fatigue results correspond to the number of cycles necessary to form a visible crack, whereas some of the British and all the AASHTO results are for the number of cycles necessary to fail large beams.

Fisher[6] observed that, generally, at least 75 percent of the life of large beams was required to form a detectable surface crack 1/2 to 1 inch long. In the present study, after

32

560,000 cycles at a stress amplitude of 24 ksi (165.5 MPa), a crack 0.917 inch (23.5 mm) in length was observed in the SMA Tee weld specimen 4AM1 (Appendix A). This specimen failed after 84,000 additional cycles, an increase of 15 percent. Similarly, after 663,000 cycles at a stress amplitude of 16 ksi (110.3 MPa), a crack 1.46 inches (37.1 mm) in length was observed in the SAW Tee weld specimen 2AS1. This specimen failed after 169,000 more cycles, an additional 25 percent. Thus, defining failure as a 1- to 1-1/2-inch-long (25.4 to 38.1 mm) surface crack versus total separation of the specimen may result in only a 1-3 ksi (7-21 MPa) difference in the fatigue-strength stress amplitude for lives of $5 \times 10^5$ to $10^6$ cycles.

One of the objects of the present study was to determine the number of cycles necessary to intitiate the first observable fatigue crack. The shortest surface crack observed was about 0.03 inch (0.75 mm) long, whereas the longest was about 2.7 inches (69 mm), Figures 6-1 and 6-2. In several instances, many short shallow cracks may have formed at about the same time and might not have been detected. However, with additional cycling, these short cracks would link up to form a few "long" surface cracks. This behavior, along with other factors, could produce a large variation in the length of surface cracks observed at about the same cyclic life. As noted above, sometimes only minor differences in fatigue strength, 1-3 ksi (7-21 MPa), were observed at the number of cycles necessary to develop 1-to 1-1/2-inch-long surface cracks versus the number of cycles for complete failure of a specimen.

### 6.32 Smooth SAW Specimens

In contrast, visible cracks initiated on the surface of the as-welded specimens at the toe of the weld reinforcement, weld-toe surface cracks did not initiate in the smooth SAW weldments. In fact, at the higher stress levels several of the specimens failed in the base metal or in the portion of the specimen gripped in the testing machine. Furthermore, because cracks grew from internal imperfections in the transverse and the longitudinal welds, the cyclic loading of only one SAW specimen (and two SMA specimens) could be stopped before complete fracture had occurred, Figure 6-2.

The primary reason is that during fatigue-crack growth, when a crack growing from an internal imperfection breaks through the specimen surface, the growth rate accelerates because the maximum stress intensity for the surface crack is greater than that of the corresponding internal crack; see Appendix B. For example, if a circular internal crack (perpendicular to the

direction of applied stress) becomes a surface crack, having the same depth as surface length, the stress-intensity factor increases 45 percent. Similarly, a 20 percent increase in the stress-intensity factor occurs when an internal crack having a major- to minor-axis ratio of two to one (with the major axis parallel to the surface) breaks through the surface and becomes a surface crack.

Because the internal fatigue cracks usually initiated well below the surface of the specimen, they were generally large when they became surface cracks. Thus, only three specimens that had internally initiated cracks (specimens No. 8AM1, 4AM2, and 7AS2) were obtained for the $K_c$ tests of surface-cracked specimens. The additional increase in the stress-intensity factor that occurred for the large internal cracks when they became surface cracks resulted in a very rapid fatigue-crack-growth rate and an attending low number of cycles to final fracture of the specimen.

Comparing the data for the as-welded and smooth SAW specimens, Figure 6-2, indicates a two-fold improvement in fatigue strength at $10^6$ cycles, from about 12 ksi (83 MPa) for the as-welded to about 24 ksi (165 MPa) for the smooth specimens. The AASHTO fatigue specifications[8] allow an increase of up to 60 percent in design stress (Category B versus Category C) if the weld reinforcement is removed. Hence, the present data are in reasonable agreement with the AASHTO results regarding the effect of the weld reinforcement on fatigue strength. The work of Gurney and Maddox[7] does not include results for weldments without the reinforcement.

## 6.33 Smooth- and Rough-Undercut Specimens

Although Gurney[10] has suggested that, typically, defects 0.006 to 0.016 inch (0.15 to 0.41 mm) in depth occur at the toe of the weld reinforcement and that the cyclic life of a weldment is spent only in extending these crack-like imperfections to fail the specimen, Maddox[11] has shown that an

[10] T. R. Gurney, "Some Recent Work Relating to the Influence of Residual Stresses on Fatigue Strength," Residual Stresses in Welded Construction and Their Effects, and international conference, London, Nov. 15-17, 1977, the Welding Institute, Abington Hall, Abington Cambridge.

[11] S. J. Maddox, "Fracture Mechanics Applied to Fatigue in Welded Structures," Proceedings of the Conference on Fatigue of Welded Structures, the Welding Institute, Abington, Cambridge, July 1970.

34

initiation life may also exist. To resolve these conflicting viewpoints, specimens were prepared with the weld reinforcement removed to eliminate the stress concentration due to the height of the weld reinforcement. Two sets of "undercut" specimens were machined and evaluated. The first set, designated smooth-undercut, had the weld reinforcement and the mill surface of the plate removed, whereas a second set of specimens, designated rough-undercut, had just the weld reinforcement removed without machining away any of the plate mill surface. For most of these latter specimens, the reinforcement height was reduced from an initial as-welded height of about 1/64 to 1/8-inch (0.5 to 3.0 mm) to less than 1/32-inch (0.8 mm) after machining.

Results from the SAW undercut specimens are discussed first because results were obtained for both as-welded and smooth SAW specimens (no smooth SMA specimens were tested). For the rough-undercut specimens, cracks always initiated in the "undercut" region and the results were coincident with the as-welded specimen data, whereas for the smooth-undercut specimens, the results were consistant with the smooth-specimen data (Figures 6-2 and 8). The one SAW smooth-undercut specimen that fractured did so as a result of an internal weld imperfection and not a surface-generated crack.

Thus, these data indicate that the removal of the weld reinforcement alone did not significantly affect the fatigue strength, whereas the removal of the reinforcement plus part of the "undercut" region resulted in a definite improvement in fatigue life. These data also support those investigators who believe that the difference between the fatigue strength of as-welded versus smooth specimens is primarily due to the dele-terious effect of "crack-like" imperfections existing at the toe of the weld. Because after the smooth-undercut specimens were machined, the length of the undercut region was no more than one-eighth the width of the specimen. It may be fortuitous that all SMA and SAW smooth-undercut specimens failed from internal imper-fections. It is not clear from the limited data whether the contour of the undercut region also acts as a significant stress concentration factor. However, for the SAW weldments examined, the weld reinforcement itself did not appear to add significantly to the stress concentration at the weld toe.

The data for the rough-undercut SMA Tee-weld specimens are not significantly different from those for the smooth-undercut or the as-welded specimens, and at about $10^5$ cycles, the data for the smooth-undercut specimens appear very similar to those for the as-welded specimens, Figures 6-1 and 8. Thus, unlike the SAW weldments, the SMA weldments show little differ-ence in the fatigue data regardless of the degree to which the

35

weld joint is ground. However, all the cracks in the smooth-undercut SMA specimens initiated internally near the bond line, whereas fatigue cracks in the rough-undercut specimens initiated at the toe of the weld as observed in the as-welded specimens.

Thus, all the results from the present investigation for both SMA and SAW Tee-weld specimens indicate that imperfections at the toe of the weld are the source of fatigue cracks leading to the failure of as-welded or rough-undercut specimens. The fatigue strength of the SAW weldments can apparently be improved significantly only by removing the weld reinforcement and the undercut region. Although the data for the smooth-undercut SAW specimens of the present investigation suggest that they had a high-fatigue strength at $10^6$ cycles, these results may only reflect the statistically small probability of a significant imperfection being present in the short undercut regions that remained on the specimen surface. In addition, an as-welded reinforcement height higher than that obtained in the present study may lead to a more severe stress concentration and attendant lower fatigue strengths.

## 6.34 Fatigue Threshold for Smooth-Undercut and Smooth Specimens

For both the smooth-undercut and smooth specimens all the fatigue cracks initiated internally from imperfections near the bond line of the weld, Figure 9. The dimensions and locations of these imperfections are given in Table 5. These dimensions were used to predict the threshold stress amplitude by treating the internal imperfections as sharp elliptical cracks or, alternatively, as rounded internal notches having a radius equal to half their narrowest dimension.

As described in Appendix C, assuming that the imperfections behave as sharp cracks and that a crack-propagation threshold exists at a $\Delta K$ (total range) of about 5.5 ksi$\sqrt{inch}$ (6.1 MPa $\sqrt{m}$) (as for base metal, that is, assuming no residual stresses are present),[12] the corresponding predicted threshold stress amplitude (half the stress range) varied from 11.5 to 21.3 ksi (79.3 to 146.9 MPa). Alternatively, assuming that the

---

[12] S. T. Rolfe and J. M. Barsom, Fracture and Fatigue Control in Structures, Prentice-Hall, Inc., Englewood Cliffs, New Jersey, 1977.

IMPERFECTION

FATIGUE
SURFACE

CROSS SECTION
THROUGH
IMPERFECTION

IMPERFECTION

FATIGUE
SURFACE

CROSS SECTION
THROUGH
IMPERFECTION

Figure 9    Internal Initiation Sites at Imperfections Near the Bond
Line Typical of Those Found in the Smooth-Undercut and
Smooth SMA and SAW Weldments-2X

Table 5

Prediction of Threshold Stress Amplitude, $\sigma_{th}$, and Cycles for Crack to Reach Surface From Dimensions and Locations of Internal Imperfections in SMA and SAW Weldments

| Specimen No. | Imperfection Dimensions Length, in. | Width, in. | Distance Below Surface, in. | Stress Amplitude, ksi | Predicted $\sigma_{th}$, ksi Sharp Cracks | Rounded Notches | Predicted Cycles to Reach Surface after Initiation | Actual Cycles to Failure or to Initiate and Reach Surface |
|---|---|---|---|---|---|---|---|---|
| | | | | SMA Smooth-Undercut | | | | |
| 2AM2 | 0.029 | 0.017 | 0.101 | 29.0 | 21.3 | 32.0 | 79,076 | 319,100* |
| 4AM2 | 0.098 | 0.042 | 0.282 | 27.0 | 12.5 | 29.2 | 49,693 | 165,980 |
| 6AM1 | 0.229 | 0.018 | 0.237 | 23.0 | 16.5 | 25.8 | 88,406 | 174,790 |
| | | | | SAW Smooth-Undercut | | | | |
| 4AS1 | 0.069 | 0.037 | 0.417 | 27.0 | 14.1 | 29.6 | 69,127 | 761,520* |
| | | | | SAW Smooth | | | | |
| 1AS1 | 0.158 | 0.011 | 0.230 | 40.0** | 21.0 | 24.8 | 21,629** | 16,790* |
| 5AS2 | 0.089 | 0.089 | 0.373 | 38.0** | 11.5 | 38.0 | 26,717** | 13,260* |
| 7AS2 | 0.045 | 0.045 | 0.331 | 33.0 | 16.2 | 38.0 | 65,110 | 261,080 |
| 4AS3 | 0.092 | 0.035 | 0.479 | 29.0 | 13.4 | 27.8 | 164,772 | 347,570* |

* Indicates cycles are to failure.

** Total stress range exceeded net section yield.

38

imperfections are rounded notches, the predicted threshold stress amplitude varied from 24.8 to 38.0 ksi (171 to 262 MPa). Because the actual threshold is greater than 11.5 ksi (79.3 MPa) but less than 24.8 ksi (171.0 MPa) and, in fact, residual stresses are present which if taken into account would lead to an even more conservative prediction of the threshold, the present investigation shows that the actual imperfections must be less severe than a crack but more severe than a notch.

## 6.35  Fatigue-Crack Initiation at -60°F

Because the fatigue-crack-initiation life for steels increases with increasing tensile or yield strength[12] and because the tensile and yield strengths of steels increase with decreased temperature, the fatigue-crack-initiation life of a steel tested at low temperature should be greater than at room temperature.[12]  Moreover, the fatigue-crack-propagation rate at low temperatures can be slower than at room temperature.[12] Consequently, the total fatigue life of a component tested at low temperature should be higher than at room temperature.

The results from the present investigation showed an improvement in fatigue performance at the reduced temperature and increased cyclic frequency.  As-welded SAW specimens cyclically loaded at -60°F had a fatigue strength of about 19 ksi (131 MPa) for $10^6$ cycles at a frequency of 124 cpm, compared with a fatigue strength of less than 13 ksi (90 MPa) when tested at room temperature and a frequency of 3.5 cpm.  Thus, the fatigue strength increased almost twofold at the lower test temperature and higher cyclic frequency.  The difference in fatigue strength is thought to be primarily related to the effect of temperature and not to cyclic test frequency.[12]

The observed increase in fatigue strength at -60°F is greater than would be expected as a consequence of increased yield strength.  On the basis of the hardness measurements, Figure 2-2, the tensile and yield strengths of the base plate are lower than those of the weld metal and, presumably, lower than those of the HAZ.  Thus, the effect of temperature and loading rate will produce the maximum estimated[12] _percentage_ change in fatigue strength for the base plate (lowest strength region of the weldment).  From a procedure suggested by Irwin,[13] the yield strength of the base metal during the cyclic loading at -60°F is estimated to be 86.9 ksi (599 MPa), in comparison with the

---

[13] R. Roberts, G. Irwin, G. Krishna, and B. Yen, "Fracture Toughness of Bridge Steels-Phase II Report," Report No. FHWA-RD-74-59, September 1974.

static room-temperature value of 57 ksi (393 MPa). From the work of Barsom,[12] this change in yield strength should correspond to an increase of only 33 percent in the fatigue-crack-initiation threshold of notched specimens. This suggests that, at most, only two thirds of the observed improvement in fatigue performance at -60°F were that at room temperature can be attributed to an increase in yield strength.

Additional studies would be necessary to determine whether the improvement was also a consequence of other factors such as improvement in crack-propagation behavior. What is most significant, however, is that the reduced temperature did not impair the fatigue performance. Because of fluctuations in the temperature of ship structures during service, it is questionable that designers could utilize improvements in fatigue performance that occur as a result of low temperatures.

## 7.0 FATIGUE-CRACK-PROPAGATION BEHAVIOR

### 7.1 Background

Current fracture-mechanics techniques allow the quantitative evaluation of fatigue-crack-growth rates in steels.[3,14] Evaluation of the cyclic stress-intensity factor, $\Delta K_I$, and the concomitant fatigue-crack-growth rate, da/dn, has shown that the crack-growth rate for ferrite-pearlite steels is described according to the equation[15]

$$da/dN = 3.6 \times 10^{-10} \, (\Delta K_I)^{3.0} \tag{1}$$

where da/dN is given in inches per cycle and $\Delta K$ is expressed in $ksi\sqrt{inch}$.

In the absence of residual tensile stresses, only the tensile or crack-opening portion of the applied $\Delta K_I$ is effective in crack growth. Variations in hardness or microstructure in the HAZ of a weldment are expected to have negligible influence on the fatigue-crack-growth rate and the crack path. A research project conducted by U. S. Steel Research Laboratory for the National Cooperative Highway Research Program included the examination of the fatigue-crack-growth behavior in electroslag weldments of A36 and A588 steels. The results from this work showed that different microstructures had no effect on fatigue-crack-growth rate.[16] Under zero-to-tension loading, residual tensile stresses have no effect on growth rate below the fatigue-rate transition (a transition from growth predictable from Equation 1 to rapidly accelerating growth), whereas residual compressive

---

[14] J. M. Barsom, E. J. Imhof, and S. T. Rolfe, "Fatigue Crack Propagation in High Yield-Strength Steels," Engineering Fracture Mechanics, Vol. 2, 1971.

[15] J. M. Barsom, "Fatigue-Crack Propagation in Steels of Various Yield Strengths," Transactions of the ASME, Journal of Engineering for Industry, Series B, Vol. 96, No. 4, November 1971.

[16] B. M. Kapadia and E. J. Imhof, Jr., "Fatigue-Crack Propagation in Electroslag Weldments," Flaw Growth and Fracture, ASTM STP 631, American Society for Testing and Materials, 1977, pp. 159-173.

stresses, causing crack closure, may cause a retardation in growth rate.[17] These data also showed a retardation of fatigue-crack propagation attributed to residual compressive stresses.

## 7.2   Test Procedures and Results

After cracks were detected in the Tee-weld specimens, cycling was continued to determine the fatigue-crack-propagation behavior for several SAW specimens both in the as-welded condition and with the weld reinforcement removed (undercut). Data were also obtained from several as-welded SMA specimens.

For the first few specimens tested, the base-plate region parallel to the path of the weld toe crack was polished and, with a hardness tester, marked with a series of diamond impressions 0.010 inch (0.254 mm) apart. The crack propagation could then be precisely monitored by using this scale on the specimen along with a 20X microscope. This method has been used by Barsom[18] to monitor crack growth in WOL specimens. However, after several tests it became apparent that, because the crack was propagating along a rough surface and because the active crack often branched, was discontinuous, or changed plane or location, the precision obtained with the aforementioned system was not warranted. Therefore, for the remaining crack-propagation tests, crack growth was monitored by using the scale on the micrometer slide of the 20X microscope used to observe the crack.

Figures 5-1 to 5-9 show both the location and initial and final surface length of the cracks in the specimens used to obtain the propagation data. Sample plots of surface-crack length versus cycles during propagation are presented in Figures 10-1 and 10-2.

---

[17] B. M. Kapadia, "Influence of Residual Stresses on Fatigue-Crack Propagation in Electroslag Welds," Fatigue Testing of Weldments, ASTM STP 648, D. W. Hoeppner, Ed., American Society for Testing and Materials, 1978, pp. 244-260.

[18] J. M. Barsom and S. R. Novak, "Subcritical Crack Growth in Steel Bridge Members," prepared for the Highway Research Board, National Cooperative Highway Research Program, National Academy of Sciences, U. S. Steel Research, Monroeville, PA, September, 1974.
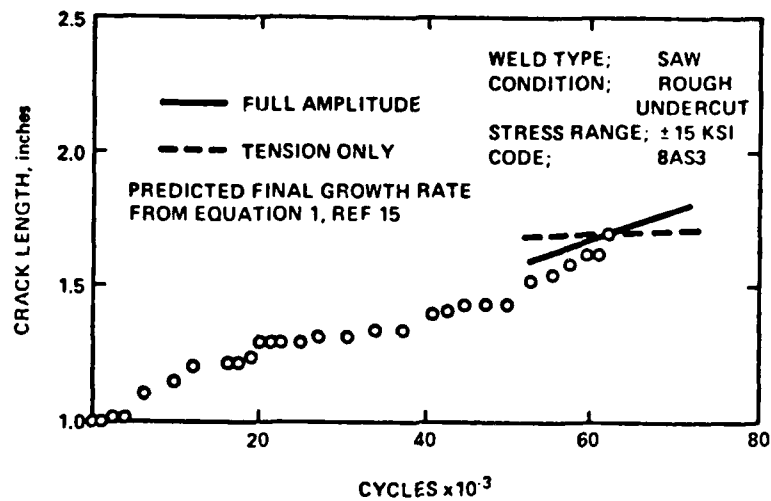
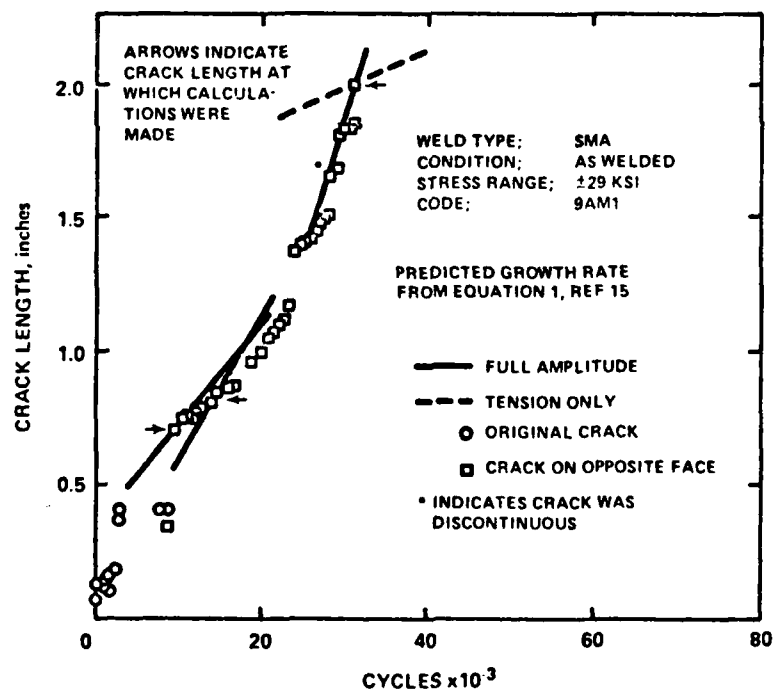Figure 10-1    Fatigue Crack Growth for SMA Tee-Weld Specimen



Figure 10-2    Fatigue Crack Growth for SAW Tee-Weld Specimen

43

## 7.3 Discussion of Results

With few exceptions, the fatigue cracks for both the SMA and SAW Tee welds propagated perpendicular to the direction of applied stress, Figure 11. This was true regardless of the location of the initiation site (surface or subsurface) or weldment contour. Thus, the propagating fatigue cracks showed no tendency to remain in a particular region of the HAZ during crack growth.

In some specimens, the cracks grew from multiple initiation locations and subsequently joined together to form a single crack with a lower aspect ratio (a/c value) than any of the separate cracks. In addition, even when only a single crack was observed, the aspect ratio often changed greatly during propagation.

## 7.31 As-Welded and Rough-Undercut Specimens

All the fatigue cracks for the as-welded and rough-undercut specimens initiated on the surface of the specimen at the toe of the transverse weld. Except for two cracks of shallow depths, the crack-growth rates measured on the surface of the specimens were consistent with the estimates made with Equation 1. This equation was developed to describe Region II (linear growth rate on a log-log plot) fatigue-crack growth in ferrite-pearlite steels. It should be noted that, because a surface crack has two crack tips on the surface of the specimen, the total surface-crack-growth rate is twice the value obtained from Equation 1. For corner cracks Equation 1 could be used to estimate the growth rate both on the surface and in the thickness direction. Also, even though all but one of the specimens was tested under fully reversed loading (R = -1), because of the presence of residual tensile stresses in the weldments, the compressive as well as the tensile portion of the cyclic stress must be included when calculating the value of $\Delta K$ to be used in Equation 1 above.

For two typical specimens, the final slope of crack length vs. fatigue cycles (da/dN) predicted by Equation 1 (doubled for other than corner cracks to account for growth from both crack tips) is shown in Figures 10-1 and 10-2 superimposed on plots of the actual surface-crack length and corresponding cycles during crack propagation. In addition, the final predicted and actual da/dN values, including data for the remainder of the specimens, are shown in Table 6. The K values for the surface-cracked specimens were calculated from an equation

44

FATIGUE
CRACK
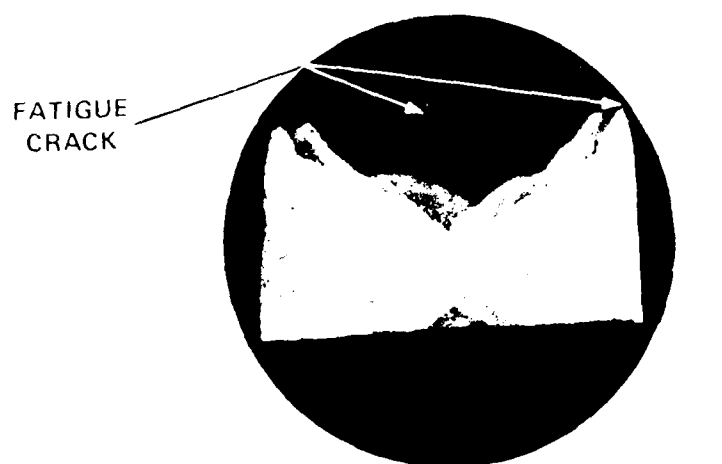
SMA                              9AM1
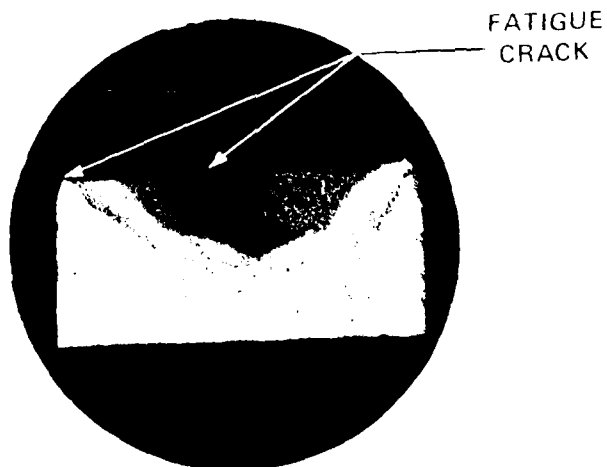
FATIGUE
CRACK

SAW                              8AS2

Figure 11    Fatigue-Crack Propagation Path in SMA and SAW T
Weldments-Section at Deepest Point on Crack Front - 2X

## Table 6

### Predicted and Actual Crack-Growth Rates
### for SMA and SAW Tee Weldments

| Specimen No. | Stress Amplitude, ksi* | Surface Crack Length, in. | a/2c Ratio | Growth Rate,** in/cycle x $10^{-5}$ Predicted | Actual |
|---|---|---|---|---|---|
| | | SMA As-Welded | | | |
| 2AM1[†] | 29 | 1.464 | 0.209 | 6.73 | 5.56 |
| 2AM1 | 29 | 1.464 | 0.209 | 24.87[†] | 6.67[†] |
| 9AM1[††] | 29 | 1.979 | 0.285 | 10.62 | 22.73 |
| 9AM1 | 29 | 0.827 | 0.405 | 5.52 | 3.31 |
| 9AM1 | 29 | 0.711 | 0.370 | 3.80 | 2.72 |
| 3AM2[†] | 24 (R=0) | 1.482 | 0.166 | 2.41 | 3.27 |
| 3AM2 | 24 (R=0) | 1.482 | 0.166 | 12.94[†] | 12.20[†] |
| 4AM1[†] | 24 | 1.312 | 0.170 | 1.94 | 0.24 |
| 4AM1 | 24 | 1.312 | 0.170 | 1.22[†] | 0.45[†] |
| 9AM2[††] | 20 | 0.768 | 0.495 | 2.20 | 1.80 |
| 9AM2 | | 0.612 | 0.415 | 1.19 | 1.21 |
| | | SAW As-Welded | | | |
| 9AS1 | 24 | 2.805 | 0.236 | 6.65 | 6.85 |
| 3AS2 | 20 | 1.333 | 0.048 | 0.02 | 10.64 |
| | | SAW Rough Undercut | | | |
| 4AS2 | 18 | 1.818 | 0.329 | 2.93 | 1.94 |
| 8AS3 | 15 | 1.651 | 0.341 | 1.01 | 1.89 |

\* R=-1 except as noted.
\** Surface crack growth rate except as noted.
[†] Corner crack. Second line gives growth rate in thickness direction.
[††] Values for intermediate crack length also given.

46

developed by Irwin.[19] For the deepest point on the crack front, this equation may be expressed in the form

$$K = \sigma \left[ \frac{1.2 \pi a}{\phi^2 - 0.212(\sigma/\sigma y)^2} \right]^{1/2} \qquad (2)$$

where

$\sigma$ = the applied gross stress,
$a$ = the crack depth,
$\sigma y$ = the material yield strength,

and $\phi$ = a function of the aspect ratio of the crack given by Equation C-2 in Appendix C.

(A simplified equation for calculating $\phi$ is discussed in Reference 20.)  The free-surface correction factor, 1.2, in Equation 2 was squared for the case of corner cracks.  Also, to obtain the K value at the two crack tips at the surface of the specimen, the right side of Equation 2 must be multiplied by $(a/c)^{1/2}$ to account for the variation in K along the crack front[12] (values for the yield strength used in Equation 2 were estimated[21] from the hardness at the 3-mm HAZ and the yield-to-tensile ratio of the base plate).

A second set of calculations was made by assuming that residual stresses were not present (that is, only the tensile component of the cyclic stress was considered) to verify that, for fully reversed loading, the full stress range must be used to calculate the crack-growth rate when significant residual tensile stresses are present and that the use of the full-stress-range results in conservative estimates of the fatigue life.  With few exceptions, these calculations resulted in nonconservative estimates of the crack-growth rate, as shown by the examples in Figures 10-1

---

[19] G. R. Irwin, "Crack Extension Force for a Part Through Crack in a Plate," Journal of Applied Mechanics, Vol. 29, No. 4, 1962, pp. 651-654.

[20] J. C. Newman, Jr., "A Review and Assessment of the Stress-Intensity Factors for Surface Cracks," presented at the ASTM Symposium on Part-Through Crack Life Prediction, San Diego, California, October 13-14, 1977.

[21] Metals Handbook, 8th Edition, Vol. 1, Properties and Selection of Metals, edited by T. Lyman, American Society for Metals, Novelty, Ohio.

and 10-2. However, when tensile residual stresses were con-
sidered, Figures 10-1 and 10-2 and Table 6 show that, for all but
a few specimens, the growth rates predicted from Equation 1 were
conservative.

One exception was specimen 3AS2, which contained a very
long, shallow crack no deeper than 0.064 inch (1.6 mm). The
extension of this very shallow crack may have occurred, in part,
by the linking up of multiple cracks which initiated at various
locations ahead of the primary crack on the surface of the speci-
men as was observed for specimen 9AS1. The changing aspect ratio
(a/c) of a semi-elliptical crack extending in this manner also
results in an increasingly severe crack shape and an accompanying
increase in the K value at the deepest point on the crack front.
Other factors that may have contributed to greater than predicted
growth rates for this specimen include the possible nonconser-
vatism of Equation 1 for very shallow cracks, the possible addi-
tive effect of the geometrical stress concentration existing at
the weld toe, and the possible contribution of residual tensile
stresses to increased crack-growth rates.

An attempt was also made to mark the instantaneous
crack shape during propagation by decreasing the stress range
intermittently. The actual crack shape could then be determined
and used to calculate $\Delta K$ values corresponding to several surface-
crack lengths. In a few instances, it was possible to correlate
these intermediate crack shapes with observations of the actual
surface-crack length. As shown in Figure 10-1 and Table 6, when
these intermediate crack shapes were known, the crack-growth rate
predicted using Equation 1 was in good agreement with the actual
data.

The number of cycles accumulated between the first
observation of the crack and either final fracture or the com-
pletion of precracking is presented in Appendix A and Figure 12.
Additional fatigue life, significant in some cases, was observed
after the initial observation of the surface crack. The longer
lives were probably related to the very shallow depth of some of
these cracks. Appendix A also lists the predicted minimum number
of cycles necessary to obtain the observed crack extension as
calculated from integration of Equation 1. From Appendix A and
Figure 13, the ratio of the actual number of cycles necessary for
a given amount of crack extension to the number of cycles esti-
mated by using Equation 1 ranged from 0.05 to 36.02.
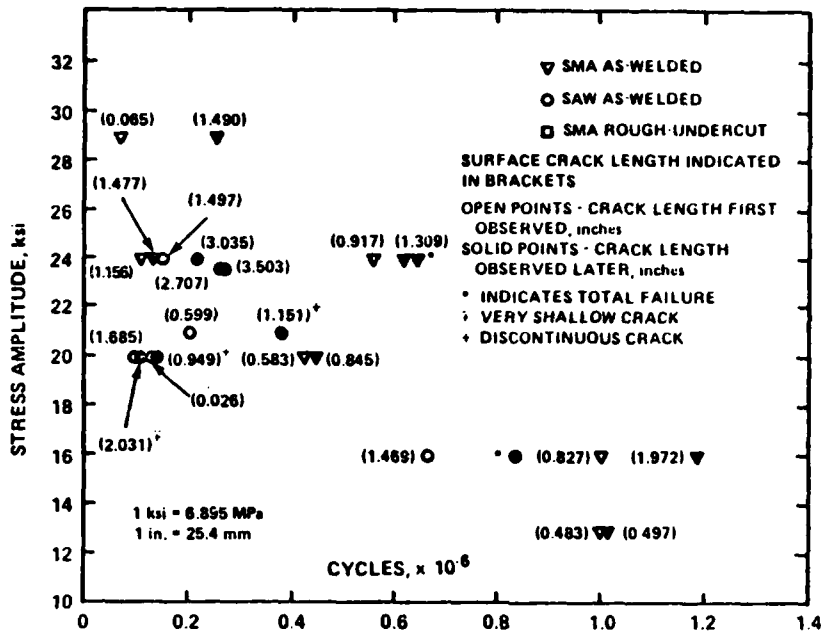
48

Figure 12    Comparison of Cycles Required for
            Crack Initiation Only with Cycles Re-
            quired for Crack Initiation and Pro-
            pagation for SMA and SAW Tee Weldments
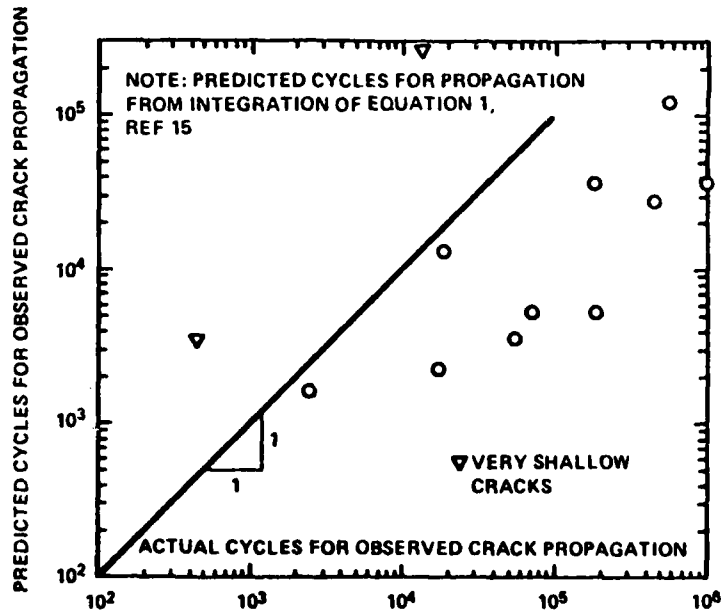


Figure 13    Actual VS Predicted Minimum Number
            of Cycles Required for Surface Crack
            Propagation for As-Welded and Rough-
            Undercut SMA and SAW Tee Weldments

## 7.32  Smooth-Undercut and Smooth Specimens

For all the smooth and smooth-undercut specimens the fatigue cracks initiated internally from imperfections located near the bond line of the weld, Figure 9, and thus the crack-growth rate could not be determined directly during propagation. The dimensions and locations of the internal imperfections are presented in Table 5.

Crack propagation in these specimens was characterized by comparing the actual number of cycles necessary for either final fracture of the specimen or for a crack to initiate and reach the surface, with the predicted minimum number of cycles (from Equation 1) required for a crack that has already initiated to extend from the internal imperfections to the surface of the specimen, Table 5. The ratio of the actual to predicted cycles for crack extension ranged from 0.50 to 11.02. However, the two specimens for which nonconservative estimates were obtained had been cycled at a total net-section stress range exceeding the estimated monotonic yield strength of the weldments. Therefore, as the crack grew, the K levels for these specimens increased to values much greater than for the others, and much of the crack propagation was probably representative of Region III (rapidly accelerating crack growth) rather than Region II (crack growth according to Equation 1) of a log-log plot of crack growth rate and $\Delta K$. The growth rate would, therefore, be expected to be much greater than predicted from Equation 1.

## 8.0 FRACTURE-TOUGHNESS (UNSTABLE CRACK EXTENSION) BEHAVIOR

### 8.1 Background

In 1953, Williams and Ellinger[22] reported the results of an extensive investigation of structural failures in welded ships. They noted that an arc strike or a small weld can cause rapid cooling, creating a hard and brittle zone (the heat-affected zone or HAZ). This brittle zone may be accompanied by residual stresses due to restrained thermal contraction and volume changes associated with the metallurgical transformations.

In their study, Williams and Ellinger[22] concluded that over half the failures in 100 ships, including cargo ships, tankers, and others, could be attributed to a stress concentration resulting from some type of mechanical notch almost always in combination with an embrittled zone resulting from welding, flame cutting, or mechanical working. One third of these fractures were in defective welds. In addition, several initiated at the junction of welds where the HAZ's overlapped. To demonstrate that the HAZ displayed lowered fracture toughness, a test similar to the present NDT test[23] was conducted[22] by making an arc strike on a small piece of ship plate, cooling it, and fracturing it with a hammer. The fracture energy absorbed by a sample taken close to this region was found to be only 60 percent of that in the base plate. However, arc strikes and welds may produce different HAZ microstructures and toughnesses in steel plates.

The present standard CVN[1] test was used in the 1940's to examine the fracture toughness of base plate involved in many catastrophic failures of ships. By the late 1940's, a technique had been developed by Nippes and Savage[24] for heat treating

---

22) M. L. Williams and G. A. Ellinger, "Investigation of Structural Failures of Welded Ships," The Welding Journal, Vol. 32, No. 10, 1953 Research Supplement 498s-527s.

23) "Conducting Drop-Weight Test to Determine Nil-Ductility Transition Temperature of Ferritic Steels," ASTM Standards Part 10, 1978, pp. 364-383.

24) E. F. Nippes and W. F. Savage, "Tests of Specimens Simulating Weld Heat-Affected Zones," The Welding Journal, Vol. 28, No. 12, 1956, Research Supplement 599s-616s.

specimens to simulate the material in a weld HAZ. However, in 1956 Hatch and Hartbower[25] noted that this procedure might be an oversimplification of the actual situation because the structure in the vicinity of the HAZ is actually not as uniform as that of the simulation specimen. Therefore, Hatch and Hartbower[25] tested edge-notched CVN specimens taken from a bead-on-plate weld and oriented such that a crack would initiate and run parallel to the weld, sampling half weld metal and half HAZ. This test was also an oversimplification of the fracture event because of the lack of a complete weld and the fact that normally actual cracks were not found to exist half in the weld metal and half in the HAZ.

Pellini,[26] in 1956, cautioned that for transverse loading of weldments in the plastic range, the relative flow strength of the weld compared with that of the base plate will determine where the strain will be concentrated. He concluded from the results of Kinzel tests conducted by Murphy and Stout[27] that a specimen with a notch simultaneously situated in the weld, HAZ, and base plate could be used to evaluate the fracture toughness of the HAZ. However, Murphy, McMullen and Stout[28] noted that sometimes the HAZ in the NDT specimen can be tougher than the base plate.

25) W. P. Hatch, Jr., and C. E. Hartbower, "V-Notch Charpy Impact Testing of Weld Metal and Heat-Affected Zone Simultaneously," The Welding Journal, Vol. 35, No. 3, 1956, Research Supplement 120s-126s.

26) W. S. Pellini, "Notch Ductility of Weld Metal," The Welding Journal, Vol. 35, No. 5, 1956, Research Supplement 217s-233s.

27) W. J. Murphy and R. D. Stout, "Effect of Electrode Type in the Notch Slow Bend Test," The Welding Journal, Vol. 33, No. 7, 1954.

28) W. J. Murphy, W. D. McMullen, and R. D. Stout, "Relative Behavior of Notch Toughness Tests for Welded Steel," The Welding Journal, Vol. 36, No. 6, 1957, Research Supplement 307s-311s.

In 1965, Masubuchi, Monroe, and Martin,[29] summarizing the results of an extensive literature survey, reported that SMA and SAW were the two major weld processes used in ship-hull construction. About three fourths of the total length of welds were fillet joints, primarily made with the SMA process, and about one fourth were butt welds, two thirds made with the SMA and one third made with the SAW process. This same literature survey contained extensive references to the fracture toughness of weldments and reviewed numerous studies that evaluated the CVN toughness at various locations of the weld and HAZ.

Although numerous research programs had studied cracking in the HAZ and hardenability of the HAZ, only limited information had been obtained on the toughness of the HAZ.[29] (In those instances where HAZ CVN specimens were tested, the notch tip was usually situated in a particular microstructure.) For .SMA welds, the transition temperature of the HAZ sometimes was a maximum at a particular location and improved both closer to and further away from the bond line. In addition, in synthetic HAZ specimens, the lowest CVN values were sometimes obtained in a region far outside the zone normally considered as the HAZ, although actual fractures were not found to initiate in or propagate through this region. For 1/2-inch SMA and SAW weldments the lowest toughness region was found somewhat outside the HAZ.

In 1974, Rolfe, Rhea, and Kuzmanovic[30] proposed specific fracture-control guidelines for welded steel ship hulls. They stated that these moderate levels of fracture toughness in the hull plate should be accompanied by a design philosophy incorporating the use of crack arrestors.

Citing a lack of information on specific loading rates in ship structures, Rolfe, et al.[30] assumed dynamic loading rates and suggested that there is a high probability of critical regions in welded ship hulls being subjected to dynamic yield-strength loading (particularly in regions of stress concentration where residual stresses from welding may be present). On the other hand, research conducted by the Ship Structure Committee on

---

[29] K. Masubuchi, R. E. Monroe, and D. C. Martin, "SSC-169, Interpretative Report on Weld Metal Toughness," National Academy of Sciences—National Research Council, July, 1965.

[30] S. T. Rolfe, D. M. Rhea, and B. O. Kuzmanovic, "SSC-224 Fracture-Control Guidelines for Welded Steel Ship Hulls," U. S. Coast Guard Headquarters, Washington, D.C., 1974.

actual ships[31] showed that the measured maximum nominal-strain rate in ships during "slamming" conditions was of the order of intermediate loading rates ($10^{-3}$ in./in./sec or loading times of about 1 sec) rather than dynamic loading rates (10 in./in./sec). This is consistent with the fact that only very small structural members have a high enough frequency response to be excited to such high straining rates. In addition, the massive ribbing construction of a ship hull should be a very effective damping mechanism for high-frequency (high strain rate) excitation waves. Programs to determine actual loading rates in ship structures are in progress.[32]

On the basis of the assumption of dynamic loading, Rolfe, et al.[30] recommended that at the minimum service temperature the ratio of the dynamic fracture toughness to the dynamic yield strength, $K_{ID}/\sigma_{yD}$, should be equal to 0.9. Because this level of ductility cannot be measured directly, they recommended that the plate NDT should be 32°F (18°C) below the minimum service temperature. This requirement was proposed to ensure that for dynamic loading conditions the brittle-to-ductile transition begins below the minimum service temperature.

A second requirement by Rolfe et al.[30] was recommended to ensure that the fracture-transition behavior of the plate occurs within a small temperature range above the NDT temperature and that the plate does not exhibit a "low-energy" ductile tearing behavior. This requirement states that 5/8-inch dynamic-tear-test[33] (5/8 DT) energy-absorption values should be obtained 43°F (24°C) above the minimum service temperature. The required energy value increases in proportion to the yield strength of the material; for example, 290 ft-lb (394 J) is required for a yield strength of 50 ksi (345 MPa), whereas 500 ft-lb (678 J) is required for a yield strength of 100 ksi (690 MPa). The particular energy requirements were derived from extrapolation of empirical correlations of the 5/8 DT energy absorption and the corresponding NDT temperatures for various steel plates and were adjusted for differences in yield strength.

---

[31] J. W. Wheaton, C. H. Kano, P. T. Diamant, and F. C. Bailey, "Analysis of Slamming Data from the S. S. Wolverine State," Ship Structure Committee Report SSC-210, 1970.

[32] "Review and Recommendations for the Interagency Ship Structure Committee's Fiscal 1980 Research Program," Ship Research Committee, National Academy of Sciences, Washington, D.C., March 1979.

[33] Dynamic Tear Energy of Metallic Materials, ASTM Standards, Part 10, 1978, pp. 617-625.

Commenting on the work of Rolfe, et al.[30], Hawthorne and Loss[34] cautioned that, on the basis of their own study, a given ratio of fracture toughness to yield strength may not always be associated with a fixed temperature above NDT. In their study of numerous ship steels, Hawthorne and Loss[34] found that CVN results did not correlate with either P3 NDT specimen results or results obtained from slightly modified 1-inch DT specimens. However, unpublished[35] independent results for 5/8-inch-thick specimens from some of the identical plates tested by Hawthorne and Loss[34] showed that the 5/8-inch DT energy estimates obtained from 1-inch DT specimens were significantly in error.

As evidenced by the background information presented above, development of proper toughness criteria to prevent unstable crack extension in steel weldments is a complex problem. Variations in yield strength, fracture toughness, and residual stress, coupled with the stress concentration caused by a weld reinforcement and possible welding defects, have resulted in a multiplicity of interpretations and toughness criteria for different service applications. The problem is further complicated by the need to use small-scale specification test specimens to predict full-thickness-weldment fracture behavior.

Today, the most commonly used test for evaluating toughness is the CVN test. Current Coast Guard specifications require that for ship-hull weldments, the CVN toughness must be evaluated in the weld metal, at the fusion line, and at 1 mm, 3 mm, and 5 mm from the fusion line—until the base-metal toughness is reached. These specifications generally require that the average toughness of each area of the weldment be no lower than some minimum specified toughness value, independent of the hardness or the volume of the part of the weldment being tested or its location relative to the weld reinforcement.

Another commonly used fracture-toughness test is the NDT test.[23] This test method is used primarily for evaluating base-metal and weld-metal behavior. The NDT of a steel plate has

---

[34] J. R. Hawthorne and F. J. Loss, "SSC-248, Fracture Toughness Characterization of Shipbuilding Steels," U. S. Coast Guard Headquarters, Washington, D.C., 1974.

[35] Private communication, T. B. Heberling, Armco Steel Co., Middletown, Ohio.

been shown by Shoemaker and Rolfe[36,37] to correspond to the upper bound of valid <u>dynamic</u> plane-strain fracture toughness, $K_{Id}$, for a 1-inch-thick plate. Thus, the NDT is both a qualitative ranking test of steels and a quantitative assessment of the maximum temperature at which dynamic plane-strain fracture behavior (brittle behavior) will occur in a 1-inch-thick specimen.

More recently, the 5/8-DT test specimen has been used to assess fracture-toughness behavior.[38] This test specimen has a greater thickness and, therefore, more through-thickness constraint than the CVN specimen and has a pressed notch rather than the V-notch employed in the CVN specimen.

Qualitative correlations between DT data and $K_{IC}$ behavior have also been shown.[39] However, for low-strength steels, insufficient data have been developed to properly separate and assess the influence of specimen loading rate (static versus dynamic behavior) for the static and dynamic $K_{IC}$ values and for the corresponding static and dynamic DT data.

In 1977, Willens[2] reported test results for HAZ toughness of an A537 Class 1 (formerly Grade A) sulfide-shape-controlled (SSC) material joined by SMA and SAW welding processes. This work showed that, although sulfur and sulfide-shape control have a beneficial effect on base-metal CVN values, the HAZ toughness degradation for this material was between 50 and 100 ft-lb (70 to 136 J) energy absorption, whereas the HAZ

---

36) A. K. Shoemaker and S. T. Rolfe, "Static and Dynamic Low-Temperature $K_{IC}$ Behavior of Steels," <u>Journal of Basic Engineering</u>, <u>Trans. ASME</u>, September 1969.

37) A. K. Shoemaker and S. T. Rolfe, "The Static and Dynamic Low-Temperature Crack-Toughness Performance of Seven Structural Steels," <u>Engineering Fracture Mechanics</u>, Vol. 2, 1971.

38) W. S. Pellini, "Design Options for Selection of Fracture Control Procedures in the Modernization of Codes, Rules and Standard," Welding Research Council Bulletin, No. 186, August 1973.

39) F. J. Loss and W. S. Pellini, "Coupling of Fracture Mechanics and Transition Temperature Approaches to Fracture-Safe Design," <u>Practical Fracture Mechanics for Structural Steels</u>, Chapman and Hall, London, 1969.

toughness degradation for the standard A537A material was only about 6 to 10 ft-lb (8 to 14 J) energy absorption. Willens[2] noted that the lowest HAZ toughness shifted from 3 mm in the standard plate to the fusion line in the SSC plate and attributed this shift to the large difference in the weld metal versus the base metal CVN values. Thus, the toughness level of the base metal (or the weld metal) can bias the "apparent" location of the lowest region in the HAZ.

Willens[2] also concluded that the large amount of scatter in the CVN results was a result of localized variations within the material, accentuated by variations in the positioning of specimens and the amount of weld metal included in the HAZ specimens. Because these variations might not affect the ultimate performance, Willens[2] recommended that the CVN test should be replaced by a new test more representative of the fracture toughness of the material.

The primary purpose of the present study was to assess the use of various toughness tests and criteria to predict the fracture behavior of weldments containing a low-toughness HAZ. Natural fatigue cracks were initiated (Section 6.0) and propagated (Section 7.0) to various sizes in SAW and SMA butt-welded Tee joints including those machined to various weld-reinforcement heights. Thus, the crack fronts resided in the various regions of the weldments. The most severe service conditions of the secondary containment shell of an LNG ship were used by loading these fatigue-cracked (surface cracked) specimens to failure at an intermediate loading rate at a temperature of -60°F.

## 8.2   Test Procedures and Results

The fracture toughness of various regions of the SMA and SAW weldments was first assessed by using standard[1] Charpy V-notch (CVN) specimens. Emphasis was given to determining the lowest toughness region in the HAZ at the specification temperature of -60°F. After the lowest toughness region of the weldment was determined from the CVN tests, the toughness behavior of the weld metal, lowest toughness HAZ, and transverse base-plate material were assessed by using standard P-3 nil-ductility-transition (NDT)[23] and standard 5/8-inch dynamic-tear (DT)[33] specimens.

As a quantitative comparison with the fracture-toughness behavior predicted from the above tests, standard three-point-bend fracture-mechanics-type specimens[40] were

[40]   "Plane-Strain Fracture Toughness of Metallic Materials," ASTM Standards, Part 10, 1978, pp. 512-533.

57

tested. The fatigue-crack tip was situated in the lowest tough-
ness region of the HAZ, and the specimens were tested at -60°F
at an intermediate loading rate (corresponding to a strain rate
of about $10^{-3}$ $sec^{-1}$) that was near the maximum measured during a
study of slamming conditions in the structure of an actual
ship.[31] Finally, to more closely simulate conditions that might
occur in a ship structure, several of the fatigue-cracked Tee-
weld specimens were tested to failure at -60°F under an inter-
mediate loading rate.

## 8.21  CVN Tests

Standard[1] CVN specimens were oriented according to the
rules of the American Bureau of Shipping (ABS)[41] and the
U. S. Coast Guard,[42] so that the notch was perpendicular to the
plate surface and parallel to the weld, and the region being
evaluated was located at the center of the notch. The one varia-
tion from the specified specimen location was for 1-inch plate in
which specimens were taken from the quarter-thickness position
closer to the first welded side as well as that closer to the
second welded side. For testing purposes, the base plate was
treated according to Sections 24.11 and 24.59 of the afore-
mentioned ABS rules[41] as Grade V-051, a material for hull
members which may be subjected to temperatures as low as
-50°F or -46°C.

8.211  <u>CVN Test Procedure</u>. For the 1-inch plate, CVN blanks were
machined from the weld metal and HAZ of SMA and SAW weldments
made by joining two 32- by 9-inch (813 by 229 mm) plates oriented
with the rolling direction (32-inch dimension) parallel to the
weld. In a similar manner, CVN blanks were taken from weldments
of the 1/2-inch plate.

Charpy blanks were etched to reveal the weld and HAZ,
then marked for final machining. Specimens were machined with
the center of the notch located at the centerline of the weld, at
the bond line, and in the HAZ at positions 1, 3, and 5 mm from
the bond line, Figure 14. Base-metal longidutinal and transverse

---

[41] "Rules for Building and Classing Steel Vessels," Section
24.65 "Welding Procedure Qualification Tests," American
Bureau of Shipping, 1975.

[42] Code of Federal Regulation, Title 46, Section 54.05-15,
Office of the Federal Register, National Archives and
Records Service, General Services Administration, U. S.
Government Printing Office, Washington, 1976.

SINGLE-VEE BUTT WELD
FOR 1/2-INCH-THICK PLATE
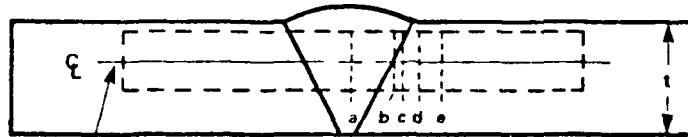
SPECIMEN POSITIONED AS CLOSE TO SURFACE AS POSSIBLE

DOUBLE-VEE BUTT WELD
FOR 1-INCH-THICK PLATE
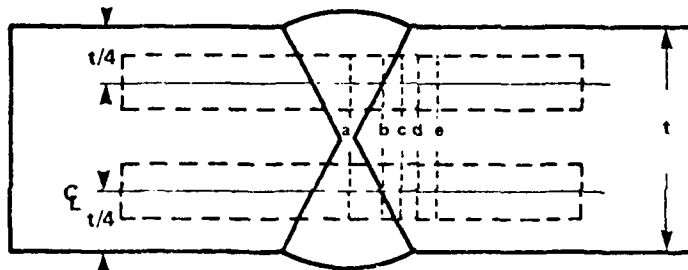
NOTCH LOCATION
  a  CENTER OF WELD
  b  ON FUSION LINE
  c  IN HAZ, 1 mm (0.039 in.) FROM FUSION LINE
  d  "    "    3 mm (0.118 in.)    "         "        "
  e  "    "    5 mm (0.197 in.)    "         "        "

Figure 14    Orientation and Location of CVN Specimens Taken from
             1- and 1/2-Inch-Thick SMA and SAW Weldments

59

specimens were also obtained.  The CVN specimens were then tested
to determine the lowest toughness (lowest energy absorption)
region of the HAZ at a temperature of -60°F.  The transition
behavior, including the fracture energy absorbed and percent
fibrous fracture, was determined for each location.

8.212  CVN Test Results.  All the CVN results are presented in
Appendix D, Tables D-1 to D-5, and the results for the weld
metal, the HAZ region exhibiting the lowest toughness at -60°F,
and the transverse base plate are compared in Figures 15-1 to
15-4.  These data show that, at -60°F, for the 1-inch SMA and SAW
weldments, the location in the HAZ having the lowest toughness
occurred from 3 to 5 mm from the bond line.  However, the 3-mm
position consistently appeared to have the lowest toughness
values.  For the 1/2-inch SMA weldments the lowest toughness
region in the HAZ was found 3 mm from the bond line, and for the
1/2-inch SAW weldments the lowest toughness region in the HAZ was
found 1 mm from the bond line.

For the 1-inch plate, the energy absorption at -60°F
for the lowest toughness HAZ region was 13 ft-lb (18 J) for the
SMA weldments and 14 ft-lb (19 J) for the SAW weldments, Fig-
ures 15-1 and 15-2.  The corresponding energy absorption for the
SMA and SAW weld metal was 62 ft-lb (84 J) and 46 ft-lb (62 J),
whereas the energy absorption for the longitudinal and transverse
base plate was 93 and 63 ft-lb (127 and 86 J) respectively.

For the 1/2-inch plate at -60°F, the energy absorption
for the lowest toughness region was 7 ft-lb (9 J) for the SMA
weldments and 11 ft-lb (15 J) for the SAW weldments, Fig-
ures 15-3 and 15-4.  The corresponding energy absorption for the
SMA and SAW weld metal was 82 ft-lb (111 J) and 20 ft-lb (27 J),
whereas the energy absorption for the longitudinal and transverse
base plate was 108 and 92 ft-lb (147 and 125 J) respectively.

The CVN values for both the base plate and weld metal
for both the 1-inch and 1/2-inch SMA and SAW weldments, Fig-
ures 15-1 to 15-4, exceed the minimum requirement of 20 ft-lb
(2.8 kg·m or 27 J) for the average energy values for three
specimens (ABS rules[41]) with the exception of the 1/2-inch SAW
weld metal for which the results would only be marginal.  Fig-
ures 15-1 and 15-3 show that the CVN values for the lowest
toughness regions of the 1- and the 1/2-inch SMA weldments would
marginally not meet and would not meet the toughness requirement,
respectively.  However Figures 15-2 and 15-4 suggest that for the
1- and the 1/2-inch SAW weldments the CVN values of the lowest
toughness regions would marginally not meet and would meet the
20 ft-lb requirement, respectively.  It is important to note that

Figure 15-1    Absorbed Energy of Charpy V-Notch
Specimens from 1-Inch-Thick A537
Class 1 SMA Weldments


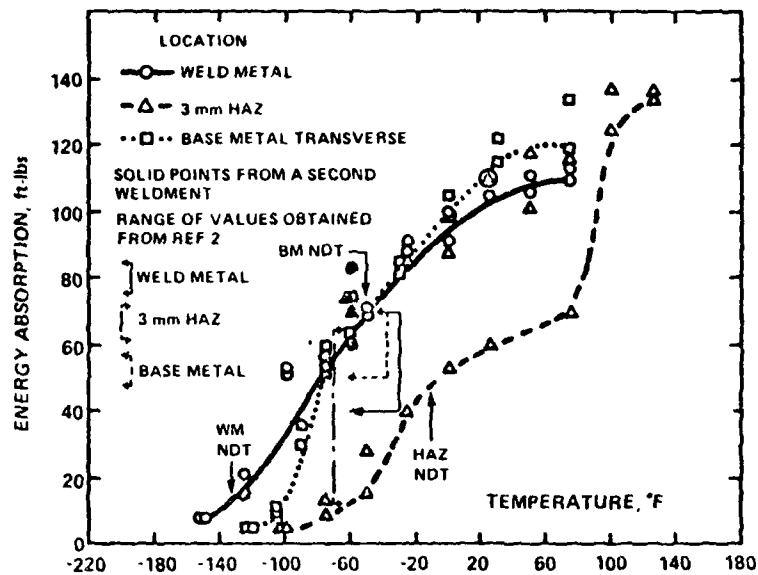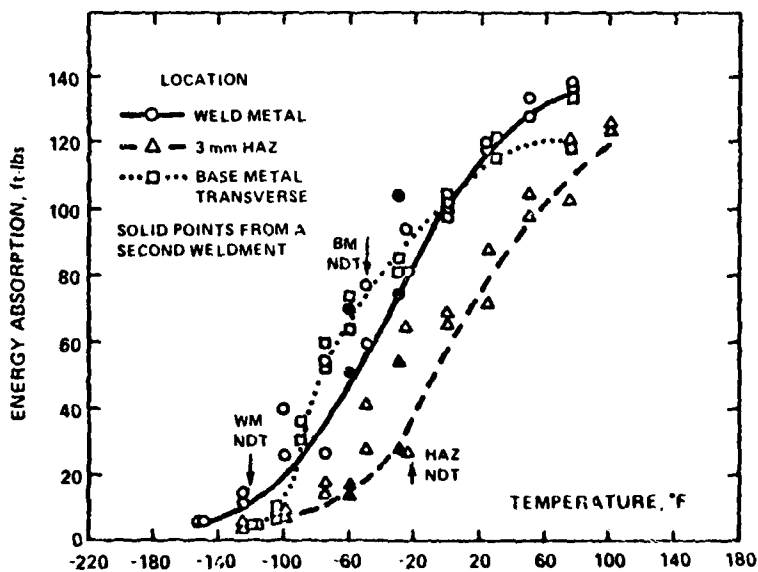
Figure 15-2    Absorbed Energy of Charpy V-Notch
Specimens from 1-Inch-Thick A537
SAW Weldments

61
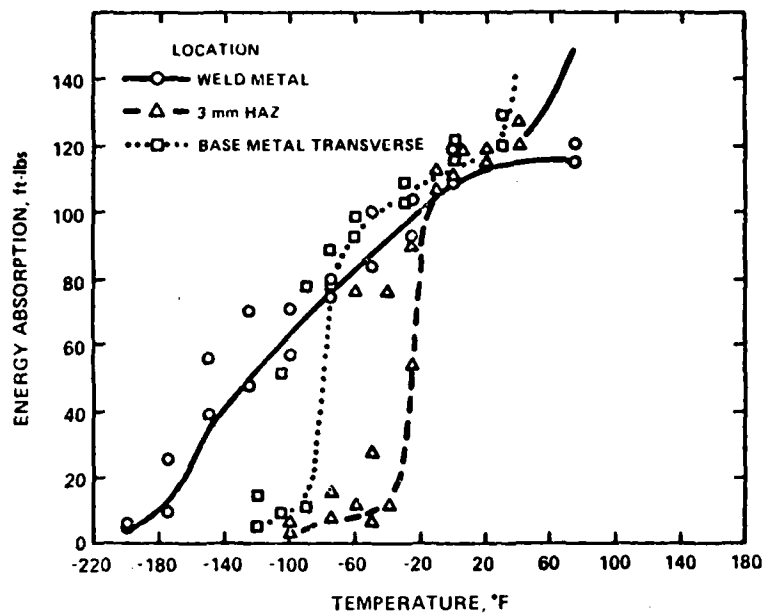
Figure 15-3    Absorbed Energy of Charpy V-Notch
                Specimens from 1/2-Inch-Thick A537
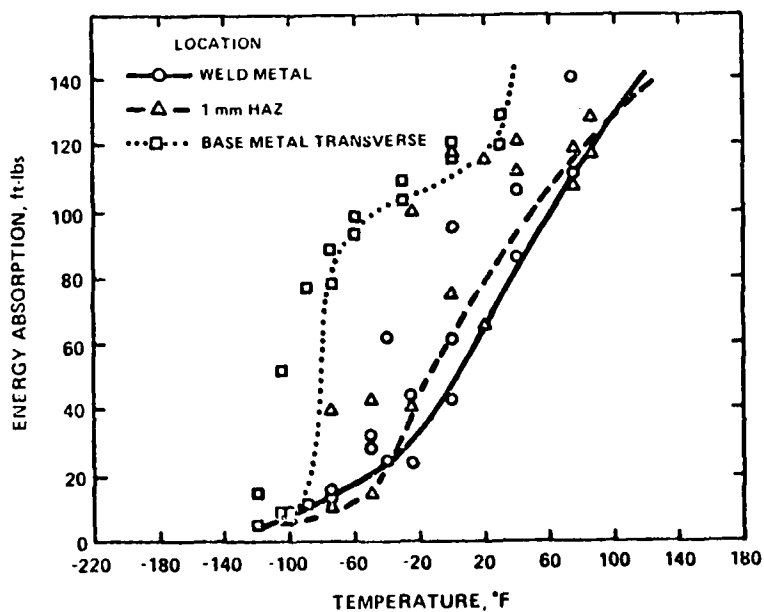                SMA Weldments



Figure 15-4    Absorbed Energy of Charpy V-Notch
                Specimens from 1/2-Inch-Thick A537
                SAW Weldment

62

the ABS specification requires a 20 ft-lb minimum average for three specimens as well as a minimum of 13.5 ft-lb (1.9 kg·m or 18 J) for any one specimen tested.

## 8.22   5/8-Inch DT Tests

Standard[33] 5/8-inch DT specimens were tested for the 1-inch-thick plate only.  The specimens were obtained from the transverse orientation for the base plate, the centerline of the weld metal, and in the HAZ 3 mm from the bond line, which corresponded to the lowest toughness HAZ found in the earlier CVN tests.

8.221   5/8-Inch DT Test Procedures.  Extra-long DT blanks were first machined from the mid-thickness location of the SMA and SAW weldments, then etched to reveal the weld and HAZ as was done with the CVN specimens.  The blanks were than marked for final machining with the same notch orientation as the CVN specimen, but with the 3-mm HAZ located at the two 1/3-thickness points of the specimen.  This location was chosen so that the low-toughness HAZ would be located in the highly constrained center portion of the specimen, while at the same time a minimum amount of the higher toughness weld and base metal would be sampled.  From a subsequent examination of several specimens, the actual location of the notch tip at the 1/3-thickness points of the specimen varied from 2 mm to 3 mm from the bond line for the SMA specimens and from 6 mm up to the bond line for the SAW specimens.

8.222   5/8-Inch DT Test Results.  At -60°F the average energy absorption for the 3-mm HAZ was 82 ft-lb (111 J) for the SMA welds and 130 ft-lb (176 J) for the SAW welds compared with 82 ft-lb (111 J) for the base plate in the transverse direction, 254 ft-lb (344 J) for the SMA weld metal and 155 ft-lb (210 J) for the SAW weld metal, Figure 16.  Thus, at -60°F the toughness of the region 3 mm from the bond line ranked lower than that of the base plate with the CVN test but greater than or equal to that of the base plate with the 5/8-inch DT test.

## 8.23   NDT Tests

Standard[23] NDT specimens were prepared and tested for the 1-inch-thick plate to evaluate the centerline weld metal, the 3-mm HAZ position, and the transverse base plate.

8.231   NDT Test Procedures.  As for the CVN and the 5/8-inch DT specimens, extra-long NDT blanks were first machined from the SMA and SAW weldments, then the edges of the blanks were etched to reveal the weld and HAZ.  For the specimens used to evaluate the
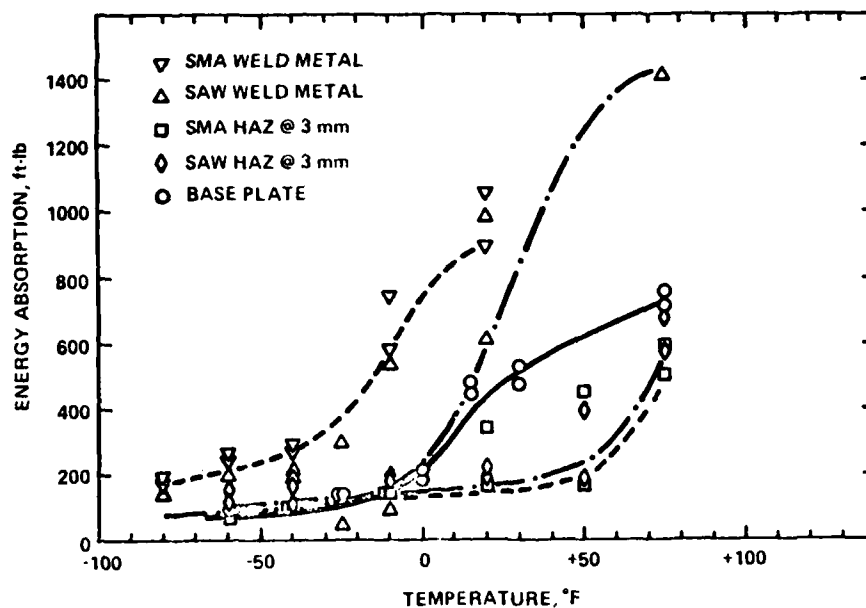
Figure 16    Energy Absorbed in 5/8-Inch-Dynamic-Tear-Test
             Specimens of SMA and SAW Weldments and Trans-
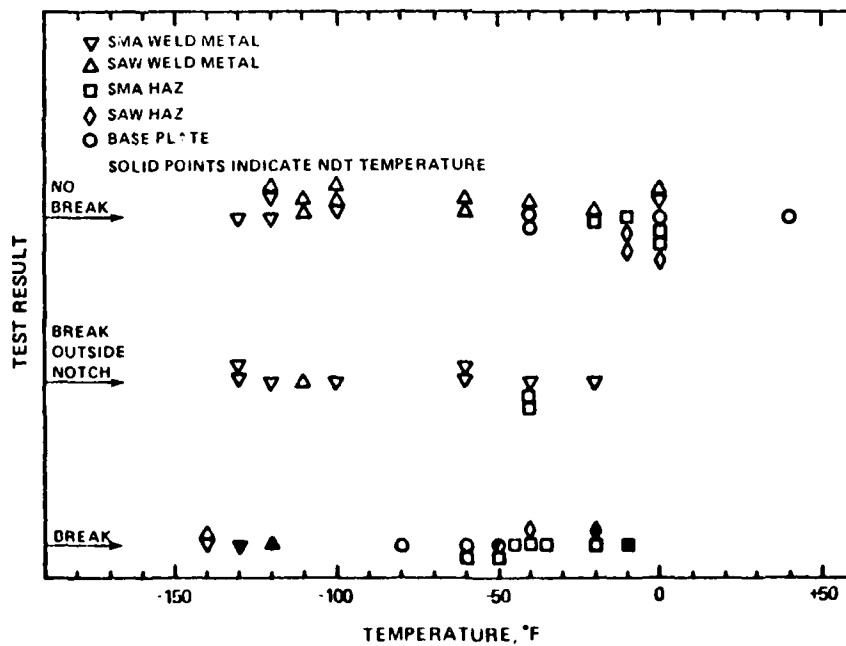             verse Base Plate



Figure 17    Type P3 NDT Test Results for 1-Inch-Thick SMA
             and SAW Weldments and Transverse Base Plate

3-mm position, the blanks were marked for the location of the brittle weld bead and the crack-starter notch such that a crack generated from the brittle-weld starter notch would intersect the 3-mm position at the quarter-thickness location in the NDT specimens. For the crack shape determined from preliminary tests, this kept the 3-mm position close to the surface, and at the same time, close to the tip of the crack produced when the brittle weld bead breaks and a crack "pops" into the base plate. A few of the SMA and SAW HAZ specimens that did not fracture completely were heat-tinted to mark the crack and then fractured at liquid-nitrogen temperature to reveal the extent of the crack "pop-in." The cross sections revealed that the running crack would sometimes intercept the 3-mm HAZ at a location closer to or farther from the surface than the quarter-thickness location. In addition, the actual crack tip after pop-in was located at various positions ranging from 1.5 to 4 mm from the bond line.

8.232 NDT Test Results. The NDT temperature was -130°F (-90°C) for the SMA weld metal and -10°F (-23°C) for the 3-mm HAZ, whereas the NDT temperature was -120°F (-84°C) for the SAW weld metal and -20°F (-29°C) for the 3-mm HAZ, Figure 17. Thus, the measured NDT for both weld metals was similar, and the measured NDT for the 3-mm location in both weldments was similar. The NDT for the weld metals occurred 75°F (42°C) below that for the base plate, whereas the NDT at the 3-mm location occurred about 35°F (19°C) above the base-plate value of -50°F (-46°C). Therefore, the NDT test ranked the toughness of the 3-mm position, compared with that of the base plate, in the same order as the CVN test but in the opposite order from the DT test.

8.24 Three-Point-Bend $K_c$ Tests

As a means of quantitatively assessing the fracture toughness of the lowest toughness position in the HAZ, as determined from the results of the CVN, DT, and NDT tests, three standard[40] full-thickness fracture-toughness specimens were prepared from the low-toughness location. The specimens were tested at -60°F at a loading rate that produced maximum load in 1.2 to 3.4 seconds if linear elastic fracture behavior occurred.

8.241 Three-Point-Bend $K_c$ Test Procedures. Extra-long blanks were machined, etched to reveal the weld and HAZ, then marked for final machining. The specimens were then edge-notched with the notch parallel to the weld such that the lowest toughness region was located at the two 1/3-thickness points of the specimen as for the 5/8-inch DT specimens. As for the DT specimens, this procedure located the 3-mm HAZ in the highly constrained portion of the specimen and, at the same time, minimized the amount of

65

the higher toughness weld and base metal sampled. However, because of the uneven nature of both the bond line and the fatigue-crack tip, in some cases the fatigue crack at the 1/3-thickness positions actually intercepted the 3- to 7-mm HAZ of the SMA specimens and the 7- to 9-mm HAZ of the SAW specimens.

Earlier[43] studies had been conducted to obtain fatigue cracks that sample parts of the weld metal, bond line, and HAZ of weldments. Because these studies indicated that it is difficult to obtain an even fatigue crack front, the normal fatigue-cracking procedure[40] was modified. The specimens were first precracked in three-point-bending compression-compression loading at an R ratio of 0.1, with the same loads that would have been used in tension-tension loading. After a crack initiated and had grown an average of at least 0.050 inch (1.27 mm), the specimens were reversed and the precracking was completed in the usual manner. During this final precracking stage, the maximum K-level was less than about 27 ksi$\sqrt{inch}$ (29.6 MPa$\sqrt{m}$) for all except specimen 11AM1 for which the maximum K-level was 35.5 ksi$\sqrt{inch}$ (39 MPa$\sqrt{m}$). The total surface-crack extension was 0.249 to 0.882 inch (6.3 to 22.4 mm).

Even with this modified precracking procedure, it was found, after testing, that the fatigue cracks were much shorter in the HAZ or base metal located in the mid-thickness portion of the specimen than in the weld metal or HAZ located near the surfaces of the specimen. The difference in crack length at these two locations varied from 0.063 to 0.307 inch (1.60 to 7.80 mm). The fatigue-cracked specimens were tested at -60°F at the intermediate loading rate described above. Load versus clip-gage displacement and load versus time records were obtained.

8.242  Three-Point-Bend $K_c$ Test Results. Sample load versus clip-gage displacement (P vs. Vg) and load versus time records are shown in Figure 18, and the test results are presented in Table 7. No valid[40] $K_{IC}$ values were obtained because (1) the measurement capacity was limited by the one-inch-thick specimen, (2) the fatigue-crack front for most specimens was uneven, and (3) except for one SAW specimen, the ratio of the fracture load to the five percent secant load exceeded 1.1. $K_Q$ values ranged from 65.1 to 69.7 ksi$\sqrt{inch}$ (71.5 to 76.5 MPa$\sqrt{m}$) for the SMA specimens and from 71.6 to 78.2 ksi$\sqrt{inch}$ (78.6 to 85.9 MPa$\sqrt{m}$) for the SAW specimens, whereas $K_{max}$ values ranged from 78.7 to

[43] A. K. Shoemaker and J. F. Sovak, unpublished research, U. S. Steel Research, Monroeville, PA, July 1978.
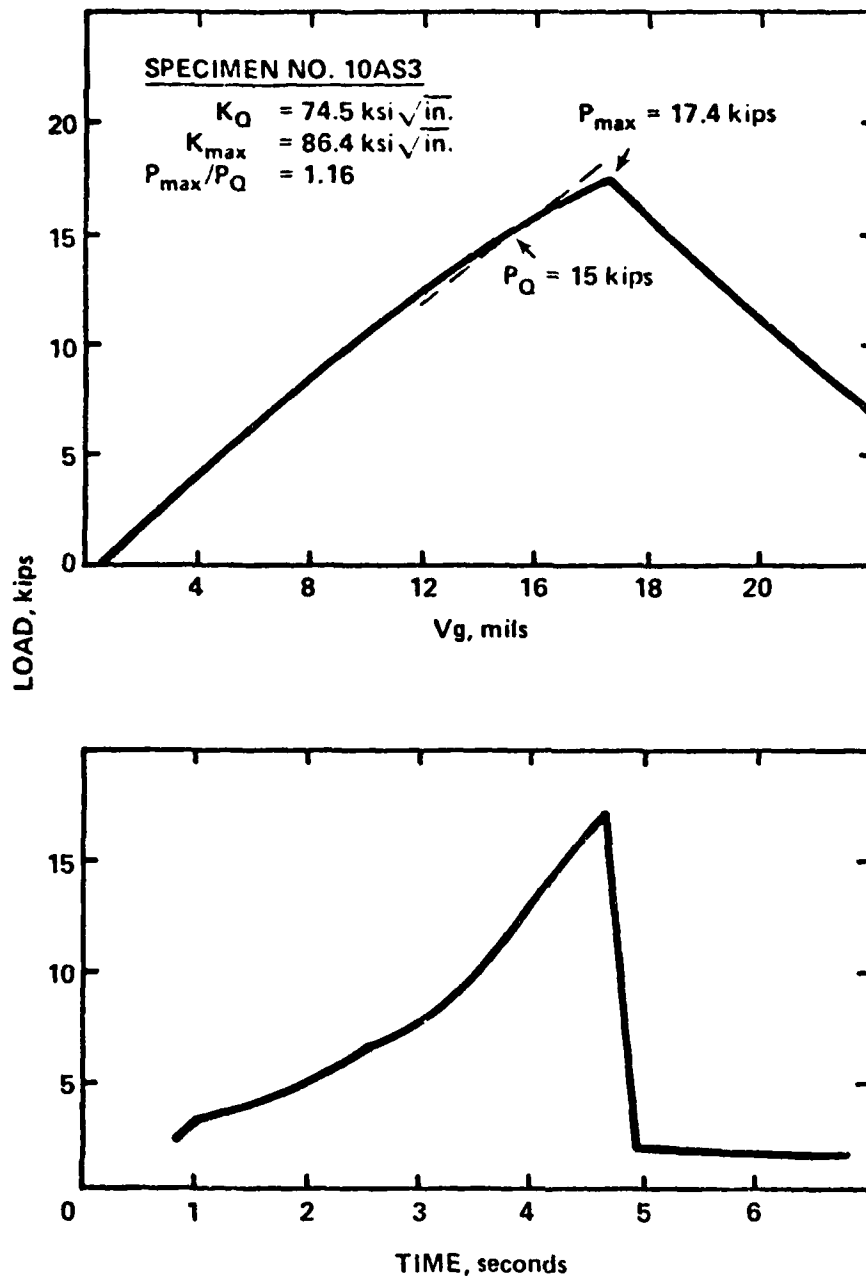
Figure 18    Sample Test Records of Intermediate-Strain-
Rate Three-Point-Bend Fracture-Mechanics
Specimen at -60°F (-51°C) SAW Weldment with
Crack in 3mm Zone of HAZ

67

Table 7

Intermediate-Strain-Rate Three-Point-Bend $K_{Ic}$ Specimen Results

at -60°F for 1-Inch SMA and SAW Weldments (Crack in 3-mm Region of HAZ)

| Specimen No. | Precrack Cycles x 10³ Compression | Tension | $K_f$(max), ksi√inch | $K_Q$, ksi√inch | $K_{max}$, ksi√inch | $\frac{P_{max}}{P_Q}$ | Maximum Valid $K_{Ic}$ for Specimen Dimensions, ksi√inch Based on Thickness | Based on Crack Length | Reasons* for Invalid Test Result | COS, mils, @ "Pop-In" |
|---|---|---|---|---|---|---|---|---|---|---|
| | | | | SMA Weldment | | | | | | |
| 11AM-1 | 25,402 | 1316 | 35.5 | 69.7 | 91.4 | 1.31 | 43.0 | 64.3 | 1, 2, 3, 4 | 4.54 |
| 11AM-2 | 6903 | 868 | 18.8 | ND | 78.7 | ND | 43.0 | 56.9 | 2, 3, 5 | ND** |
| 11AM-3 | 6699 | 444 | 23.6 | 65.1 | 86.7 | 1.33 | 43.0 | 56.9 | 1, 2, 3, 5 | 0.59 |
| | | | | SAW Weldment | | | | | | |
| 10AS-1 | 7920 | 2428 | 21.4 | 78.2 | 81.7 | 1.04 | 42.1 | 58.9 | 2, 3 | 1.28 |
| 10AS-2 | 26,683 | 1245 | 25.7 | 71.6 | 88.7 | 1.24 | 42.1 | 58.2 | 1, 2 | 3.26 |
| 10AS-3 | 14,602 | 527 | 26.5 | 74.5 | 86.4 | 1.16 | 42.1 | 58.8 | 1, 2 | 2.29 |

*The numbers 1 through 5 indicate that the $K_{Ic}$ test results were invalid by ASTM E399, Reference 40, for one or more of the following reasons:

1. $P_{max}/P_Q > 1.10$.
2. B or a < 2.5 $(K_Q/\sigma_y)^2$.
3. a varies more than 0.05 $a_{AV}$.
4. The crack plane angle is >10 degrees to the width direction.
5. a/w < 0.45.

**ND Not determined

91.4 ksi√inch (86.4 to 100.4 MPa√m) for the SMA specimens and from 81.7 to 88.7 ksi√inch (89.7 to 97.4 MPa√m) for the SAW specimens. The K values were calculated by using the following equation[40]

$$K = \frac{PS}{BW^{3/2}} \cdot f\left(\frac{a}{W}\right) \qquad (3)$$

where

P = the applied load,
S = the 3-point bend span,
a = the crack length,
W = the specimen depth,
B = the specimen thickness, and

$f\left(\frac{a}{W}\right)$ = a function of the relative crack length given in Reference 40.

## 8.25 Fracture-Toughness Tests for Surface-Cracked Specimens

The most meaningful assessment of the significance of a low-toughness HAZ in a weldment is that determined from tests in which the weldment is cylically loaded to develop a fatigue crack in a natural and not an artificial or predetermined manner. A series of fatigue-cracked specimens were obtained and tested to serve as the "base-line" data to which all of the other toughness-test results were compared. These surface-cracked specimens were cyclically loaded to extend the fatigue cracks generated during the fatigue tests of the various types of 1-inch-thick Tee weldments. A variety of crack sizes was deliberately obtained to assess any differences that might occur in the fracture behavior of the weldments when the fatigue-crack front was located in various regions of the HAZ. The specimens were loaded to fracture at -60°F at intermediate loading rates.

8.251 **Fracture-Toughness Test Procedures for Surface-Cracked Specimens**. Because there is no standard test method for this type of specimen, specimens selected for the fracture tests were representative of those containing both small and large cracks. The cracks were usually thumbnail shaped. The surface fatigue-crack length ranged from 0.792 to 3.499 inches (20.1 to 88.9 mm) and the crack-depth to surface-crack-length (a/2c) ratio ranged from 0.048 to 0.556, Table 8. The ratio of the net to gross section area varied from 0.486 to 0.978. On each specimen, a clip gage was mounted on two blocks bonded to the surface of the specimen across the crack mouth at the location estimated to have the maximum crack depth. Thus, the clip gage recorded the surface

69

crack-opening displacement. A strain gage was bonded to the opposite surface of the specimen at the location opposite that of the clip gage. In addition, on several specimens strain gages were mounted at other locations. For example, strain gages were mounted on opposite faces of the specimen to determine whether bending stresses occurred as a consequence of the unsymmetrical nature of the fatigue-cracked cross section.

8.252  Fracture-Toughness Test Results for Surface-Cracked Specimens. The results from the surface-cracked specimens are presented in Table 8, and the fracture surfaces are shown in Figures 19-1 to 19-4. The maximum nominal gross stress ranged from 19.6 to 82.5 ksi (135 to 569 MPa) and the maximum nominal net stress ranged from 40.3 to 85.1 ksi (278 to 587 MPa). However, because the surface cracks extended primarily from one face of the specimens, creating an eccentric geometry, the actual net section stress at the cracked surface of the specimen was increased because of bending, with the amount of bending stress dependent on the size and shape of the crack.

The difference in stress between the front and back surfaces of the specimen was estimated (by a method similar to that of Bryan, et al.[44]) by assuming that the resultant of the nominal stress that would have been supported by the cracked area acts at the centroid of the crack area. This force creates a bending moment in the plane of the crack, which is then resisted by a stress differential between the front and back faces of the specimen. The value of this differential stress is shown in Table 8 and was used in calculating the stress-intensity factor ($K_c$).

The clip-gage displacement across the mouth of the crack at instability or maximum load ranged from 1.2 to more than 74.7 mils* (0.030 to 1.897 mm), and the strain opposite the crack ranged from -50 to 16,880 microinches/inch, Table 8.

## 8.3  Discussion of Results

### 8.31  Charpy V-Notch Toughness Results

The sulfide-shaped-controlled A537 Class I plate and welding conditions chosen for the present investigation were

---

[44] R. H. Bryan, et al., "Tests of 6-Inch Thick Pressure Vessels. Series 2: Intermediate Test Vessels V-3, V-4, and V-6," ORNL-59-59, Oak Ridge National Laboratory, Oak Ridge, Tennessee, November 1975.

* 1 mil = 0.001 in. = 0.0254 mm

## Table 8

### Intermediate-Strain-Rate Surface-Cracked (PTC) Specimen Results at -60°F for SMA and SAW Tee Weldments

| Specimen No. | Surface Crack Length, $a_s$, in. | Crack Depth, $a_t$, in. | a/2c Ratio* | $\sigma_G$, ksi | $\sigma_N$, ksi | $\Delta\sigma$, ksi, Between Faces | Displacement Across Crack Vg, mils | Microstrain Opposite Crack | Time, sec |
|---|---|---|---|---|---|---|---|---|---|
| | | | | | | | | | |
| | | | | | SMA As-Welded | | | | |
| 9AM2 | 0.808 | 0.380 | 0.470 | 74.6 | 79.6 | 12.5 | >>37.9 | +16,880 | 34.0 |
| 9AM2** | | | | 62.8 | 67.0 | 10.5 | 10.0 | +6900 | 16.0 |
| 9AM1 | 1.978 | 0.564 | 0.285 | 54.4 | 72.3 | 30.9 | 8.8 | -50 | 0.55 |
| 2AM1 | 1.467 | 0.612 | 0.209*** | 56.5 | 71.7 | 25.1 | 44.0 | +10,860 | 26.5 |
| 8AM2 | 0.792 | 0.377 | 0.476 | 63.4 | 69.6 | 10.7 | 14.1 | +4080 | ~17.5 |
| 8AM2** | | | | 63.0 | 69.1 | 10.6 | 12.0 | +2940 | ~13.5 |
| | | | | | SAW As-Welded | | | | |
| 9AS2 | 2.137 | 0.082 | 0.048 | 82.5 | 85.1 | 7.6 | >>37.5 | >>+14,300 | <74.0 |
| 9AS2** | | | | 60.5 | 62.4 | 5.6 | 4.4 | 4520 | <74.0 |
| 3AS2 | 1.850 | 0.064 | 0.048 | 79.8 | 81.6 | 4.5 | >>37.8 | +6300 | 35.0 |
| 3AS2** | | | | 67.1 | 68.6 | 3.8 | 6.6 | +5000 | <35.0 |
| 9AS1 | 2.808 | 0.662 | 0.236 | 42.0 | 71.4 | 37.5 | 8.6 | +200 | 0.5 |
| 6AS4 | 0.911 | 0.247 | 0.271 | 66.0 | 69.5 | 9.1 | <19.8+ | >+6600+ | >51.0 |
| 6AS4** | | | | 62.6 | 65.9 | 8.6 | 13.6 | >+6600 | ND++ |
| 6AS2 | 3.499 | 0.795 | 0.124*** | +++ | +++ | 43.2 | 21.0 | +930 | 13.5 |

(Continued)

71

Table 8 (Continued)

| | | | | | | | Values at Maximum Load | | |
| | | | | | | | Displacement | | |
| Specimen No. | Surface Crack Length, $a_s$, in. | Crack Depth, $a_t$, in. | a/2c Ratio* | $\sigma_G$, ksi | $\sigma_N$, ksi | $\Delta\sigma$, ksi Between Faces | Across Crack $V_g$, mils | Microstrain Opposite Crack | Time, sec |
|---|---|---|---|---|---|---|---|---|---|
| | | | | *SAW Rough-Undercut* | | | | | |
| 4AS2 | 1.815 | 0.598 | 0.329 | 56.3 | 70.4 | 25.2 | 12.4 | +1330 | 0.9 |
| 8AS3 | 1.733 | 0.563 | 0.325 | 53.7 | 68.5 | 26.6 | 8.7 | +1040 | 1.0 |
| 8AS2 | 0.828 | 0.394 | 0.476 | 56.7 | 60.0 | 10.4 | 10.8 | >4050 | 0.85 |
| 8AS2** | | | | 53.4 | 57.5 | 9.8 | 1.15 | +1550 | 0.7 |
| | | | | *SMA Smooth-Undercut* | | | | | |
| 8AM1 | 1.078 | 0.513 | 0.476 | 74.6 | 84.7 | 19.5 | >>74.7 | >>+13,130 | 1.5 |
| 8AM1** | | | | 66.0 | 74.9 | 17.3 | 11.8 | +2440 | 0.5 |
| 4AM2 | 0.829 | 0.493 | 0.297*** | 73.5 | 80.5 | 14.7 | >>37.5 | +7515 | 1.24 |
| 4AM2** | | | | 67.4 | 73.8 | 13.5 | 12.5 | +2850 | 0.6 |
| | | | | *SAW Smooth* | | | | | |
| 7AS2± | ~0.866 | ~0.580 | 0.556 | 71.7 | 79.7 | 17.5 | >70.8 | >+13,130 | ± |
| 7AS2** | | | | 66.2 | 73.6 | 16.2 | 20.3 | +6800 | 0.6 |

* a/2c = $a_t/a_s$. For a corner crack a/2c = $a_t/2a_s$.
** Values at first maximum in load record.
*** Corner crack.
+ "Pop-in" occurred before maximum load. Also specimen pulled out of grips.
++ Not determined.
+++ Very large fatigue crack resulted in large bending stress, $\sigma_G$ = 19.6 ksi, $\sigma_N$ = 40.3 ksi.
± Specimen did not fracture—held at maximum of load range.

72

9AM1



9AM2





8AM2



Figure 19-1    Fracture Surfaces of As-Welded SMA Tee Weldments
               Tested at Intermediate Strain Rate at -60 F
               (-51°C) - 1XMagnification

6AS2

6AS4

3AS2

9AS1

Figure 19-2    Fracture Surfaces of As-Welded SAW Tee Weldments
             Tested at Intermediate Strain Rate at -60°F
             (-51°C) - 1XMagnification

**4AS2**
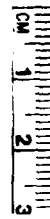


**8AS3**
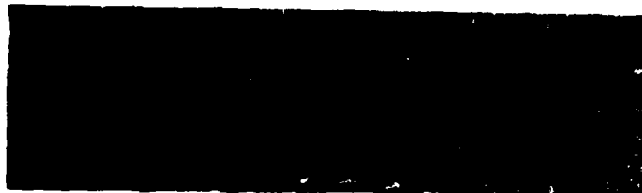


**8AS2**



Figure 19-3    Fracture Surfaces of Rough-Undercut SAW Tee
Weldments Tested at Intermediate Strain Rate
at -60°F (-51°C) - 1XMagnification

75

**4AM2**



**SMA SMOOTH-UNDERCUT**

**8AM1**



**SMA SMOOTH-UNDERCUT**

**7AS2**



**SAW SMOOTH**

Figure 19-4    Fracture Surfaces of Smooth-Undercut SMA and Smooth
SAW Tee Weldments Tested at Intermediate Strain Rate
at -60°F (-51°C) - 1XMagnification

selected to deliberately obtain a weldment exhibiting a low-toughness HAZ. Earlier investigations[2] of this plate and SMA welding found a toughness range of 12 to 65 ft-lb (16 to 88 J) in the 3-mm region of the HAZ at -60°F, Figure 15-1.

The weldment is atypical because the marginal-toughness region in the HAZ occurred even though the base-plate toughness was 50 to 70 ft-lb (68 to 95 J) in the transverse direction of the 1-inch-thick plate, Figure 15-1. The corresponding weld metal toughness, also shown in Figure 15-1, was 40 to 70 ft-lb (54 to 95 J). Hence, the lowest toughness region in the HAZ had only 25 to 30 percent of the energy absorption of the base metal and weld metal. Conversely, the steel initially chosen for the present investigation was ABS-CS plate. Even utilizing a wide range of welding consumables and heat inputs, the lowest tough-ness region in the HAZ at -60°F always had a toughness at least as great as that of the base metal or weld metal, Appendix Supplement.

Because of the wide variation between the minimum-toughness region of the HAZ and the adjacent base metal and weld metal, attention was focused on the minimum rather than the average toughness. The Charpy specimen orientation required by the specification,[41] Figure 14, will always locate a significant portion of the notch in the base metal and/or weld metal even though the notch is centered on the specific location in the HAZ that is to be tested. Hence, the higher toughness of the base metal or weld metal will "mask" the actual toughness of small regions in the HAZ. For example, for the 1-inch plate two differ-ent SMA and two different SAW weldments were used to determine the CVN results. For each welding procedure, a preliminary weldment, A, was used to evaluate the Charpy values at -60°F whereas a second weldment, B, was used to obtain data at other temperatures (full Charpy transition curves), Appendix Table D-1 and D-2.

Table 9 summarizes the lowest toughness values at -60°F obtained from each set of weldments. For weldment B, the average and minimum values were evaluated at -60°F by calculating the values in proportion to the corresponding results obtained at -50° and -75°F, Appendix Tables D-1 to D-4. The data scatter within a weldment and between weldments that may be partially attributed to the aforementioned "masking" is exemplified by the results obtained for the 1-inch-thick SAW weldment. At the 3-mm position of SAW weldment B, the calculated minimum and average values were 23 and 27 ft-lb respectively, whereas the values measured at -60°F for weldment A were 14 and 16 ft-lb, respectively. Thus, in the present study, attention was focused on the minimum or lower bound values for each set of weldments, which represents a conservative viewpoint.

The salient feature of the Charpy results for all four weldments is that some region in the HAZ always exhibited toughness values less than 20 ft-lb, Table 9. Because the weld-metal and base-plate toughness values were at least twice as high as these minimums, the adjacent high-toughness regions tended to mask the measurement of the minimum-toughness regions. To further document this "masking" effect, surface-notched Charpy specimens were obtained from the 1-inch-thick SMA weldments, Table 9. The notch was oriented parallel to the plate surface so that the entire tip of the notch was located in the region of the HAZ to be evaluated. Whereas the conventional Charpy specimen orientation resulted in a minimum toughness value of 12 ft-lb at the 3-mm location, the surface-notch-orientation result was a minimum of 8 ft-lb (11 J). Thus, it must be assumed that very small regions in the HAZ have toughness values lower than those indicated by the results in Table 9.

A prediction of the flaw tolerance at -60°F can now be made from the weldment Charpy data. Barsom[45] has shown that at a specified strain rate the brittle-to-ductile fracture-initiation transition occurs at the same temperature in the Charpy test as in the fracture-mechanics $K_{IC}$ test. This transition occurred at the temperature corresponding to about 15 to 25 ft-lb (20 to 34 J) energy absorption in the Charpy specimen for the 3-mm HAZ of the present weldments, Figures 15-1 and 15-2. If a value of 20 ft-lb is used, the brittle-to-ductile fracture-initiation transition for impact loading occurs at -45°F (-43°C) for the 3-mm position in the 1-inch SMA and SAW weldments, Figures 15-1 and 15-2, respectively.

In assessing flaw tolerance for an intermediate rather than impact strain rate (a rise time of about one second rather than one millisecond), Barsom[46] has shown that the fracture-initiation transition temperature is shifted downward from that obtained with impact loading according to the equation

$$\Delta T = 2/3 \ (215 - 1.5\sigma_{ys}) \tag{4}$$

[45] J. M. Barsom, "Relationship Between Plane-Strain Ductility and $K_{IC}$ for Various Steels," Journal of Engineering for Industry, November 1971, pp. 1209-1215.

[46] J. M. Barsom, "Development of the AASHTO Fracture-Toughness Requirements for Bridge Steels," Engineering Fracture Mechanics, Vol. 7, No. 3, September 1975.

## Table 9

### Charpy V-Notch Energy Absorption (ft-lb) at -60°F for 1- and 1/2-Inch A537 SMA and SAW Weldments

| | Weld Metal | Bond Line | 1 mm | 3 mm | 5 mm | Base Plate Longitudinal | Transverse |
|---|---|---|---|---|---|---|---|
| **1-Inch SMA*** | | | | | | | |
| Average | 64 | 35 | 42 | 17 | 14 | 169 | 69 |
| Minimum | 63 | 32 | 21 | 12 | 13 | 109 | 64 |
| **1-Inch SAW*** | | | | | | | |
| Average | 57 | 34 | 19 | 16 | 20 | | |
| Minimum | 46 | 30 | 17 | 14 | 15 | | |
| **1/2-Inch SMA** | | | | | | | |
| Average | 86 | 75 | 34 | 15 | 46 | 114 | 96 |
| Minimum | 80 | 43 | 21 | 7 | 16 | 109 | 93 |
| **1/2-Inch SAW*** | | | | | | | |
| Average | 25 | 26 | 28 | 66 | 61 | | |
| Minimum | 23 | 25 | 13 | 56 | 55 | | |
| **1-Inch SMA (Surface Notched)** | | | | | | | |
| Average | | | 56 | 14 | 50 | | |
| Minimum | | | 46 | 8 | 36 | | |

* Average and minimum values are the smaller of the values determined from two different weldments, Weldment A tested at -60°F and Weldment B tested at -50 and -75F (value at -60F determined in proportion to values measured at -50 and -75F).

where

$\Delta T$ = the temperature shift, °F

and $\sigma_{ys}$ = the room temperature static yield strength, ksi.

Hardness surveys of the weldments showed that the 3-mm location in both the SMA and SAW weldments was a maximum of about 193 DPH, corresponding[21] to a tensile strength of 89.2 ksi (615 MPa), Table 10. If it is assumed that the yield to tensile ratio for the HAZ is the same as that for the base plate (57.0/76.2 = 0.75), then the 3-mm positions in both the SMA and SAW weldments would have a maximum yield strength of about 67 ksi (462 MPa). Use of 67 ksi in Equation 4 predicts a shift in the fracture-initiation transition temperature from a dynamic to an intermediate loading rate of -76°F (-42°C).

Hence, if an energy absorption of 20 ft-lb (27 J) corresponds to the brittle-to-ductile transition temperature in the impact test of the Charpy specimen, for an intermediate loading rate in the structure, the 3-mm positions in the SMA and SAW weldments should exhibit transition-temperature behavior at about -121°F (-85°C). For several structural steels of up to 50 ksi (345 MPa) yield strength, the temperature at which non-plane-strain (ductile) behavior occurs is about 50°F (28°C) above this transition temperature. Thus, applving a 50°F shift predicts elastic-plastic fracture-initiation behavior at inter-mediate loading rates down to -71°F (-57°C) in the 3-mm location of the 1-inch SMA and SAW weldments. If the actual yield to tensile ratio is 0.85 rather than 0.75, the predicted minimum temperature for elastic-plastic behavior increases 10°F (6°C).

Thus, the predicted fracture behavior of specimens containing real cracks tested at -60°F and an intermediate loading rate is predicted to be elastic-plastic (non plane strain). If the yield strength of a region in the HAZ is significantly higher than estimated or if the actual Charpy toughness at -60°F is less than the required 20 ft-lb, as was actually measured, then fracture under plane-strain conditions might be expected.

## 8.32 Nil-Ductility Transition-Temperature Results

Because of the variation in strength and toughness in the various regions of the weldments, many of the NDT specimens exhibited cracking away from the crack-starter notch in the brittle weld bead, Figure 17. This was particularly evident in specimens used to establish the SMA weld-metal NDT temperature. Because the weld metal had higher strength and toughness than the

80

## Table 10

### Room-Temperature Static Tensile and Yield Strengths in Various Regions of the HAZ of 1-Inch SMA and SAW Weldments (Estimated from Hardness (DPH) Measurements)

| Location | Maximum Hardness, DPH | $\sigma_{ts}$,* ksi | $\sigma_y$,** ksi |
|----------|-----------------------|---------------------|-------------------|
| SMA Weldment | | | |
| Bond Line | 245 | 114.0 | 85.5 |
| 1 mm | 247 | 114.8 | 86.1 |
| 3 mm | 193 | 89.2 | 66.9 |
| 5 mm | 185 | 86.0 | 64.5 |
| SAW Weldment | | | |
| Bond Line | 216 | 99.4 | 74.6 |
| 1 mm | 213 | 98.2 | 73.7 |
| 3 mm | 193 | 89.2 | 66.9 |
| 5 mm | 187 | 86.8 | 65.1 |

\* Estimated using Reference 21.
\** Assuming $\sigma_y/\sigma_{ts}$ = 0.75.

adjacent regions of the HAZ, cracks would initiate and propagate
in the HAZ rather than from the root of the notch cut in the
brittle crack-starter bead located above the weld metal. The
measured NDT for the SMA and SAW weld metals were -130 and
-120°F (-90 and -84°C), respectively. The measured NDT for the
corresponding 3-mm HAZ in these weldments were -10°F and -20°F
(-23 and -29°C), respectively, whereas the NDT for the base plate
was -50°F (-46°C).

As indicated in the previous section, the high-tough-
ness regions of the weld and base plate may have "masked" the
actual Charpy toughness values in the lowest toughness region of
the HAZ. The NDT values for the HAZ of both the SMA and SAW
weldments add further credence to this concern. In many hot-
rolled structural steels and weld metals of about 50 ksi
(345 MPa) yield strength, a 10 to 30 ft-lb (14 to 41 J) Charpy
V-Notch energy absorption is obtained at the NDT tempera-
ture.[47,48] Although minimums near these energy levels were
observed at -40 to -60°F (-40 to -51°C) in the HAZ of the 1-inch-
thick SMA and SAW weldments, the respective NDT temperatures
were -10 and -20°F (-23 and -29°C) or about 40 to 50°F (22 to
28°C) higher than expected on the basis of the CVN results.
Although the CVN energy absorption can increase rapidly over a
small temperature range for some steels, these higher than expec-
ted NDT temperatures suggest that 15 ft-lb (20 J) values in the
3-mm position could be obtained at much higher temperatures.

The reduction in toughness of the HAZ of the base plate
is further exemplified by the difference between the base plate
NDT temperature of -50°F (-46°C) and the base plate 15 ft-lb
Charpy energy temperature of -100°F (-73°C). An embrittled
region can also occur in the HAZ as a result of the deposition of
the hard-X crack-starter weld bead on the base- plate samples.
If this embrittled region has very low toughness, a larger crack
is produced at "pop-in" from the brittle weld bead, and a corres-
pondingly higher NDT temperature is obtained than for a steel
that does not exhibit a low-toughness HAZ. Thus, the NDT values
obtained can be representative of the HAZ created by the brittle
crack-starter weld rather than the base plate.[47] In comparison,
the 1-inch SMA and SAW weld metals each exhibited 15 ft-lb Charpy

---

47) J. H. Gross, "Comparison of Charpy V-Notch and Drop-Weight
    Tests for Structural Steels," The Welding Journal, Vol. 39,
    No. 2, February 1960, Research Supplement 59s-69s.

48) W. S. Pellini, "Notch Ductility of Weld Metal," The Welding
    Journal, Vol. 35, No. 5, May 1956, Research Supplement
    217s-233s.

energy-absorption values at their respective NDT temperature, namely -130 and -120°F (-90 and -85°C), Figures 15-1 and 15-2.

The limit of plane strain or brittle, unstable crack extension for testing at an intermediate loading rate at -60°F can now be estimated from the NDT results. Shoemaker and Rolfe[36,37] have shown that the NDT temperature represents the limit of dynamic plane-strain behavior in 1-inch-thick plate. On the basis of the same arguments discussed in the previous section for the Charpy results, the predicted brittle to ductile transition temperature for intermediate loading rates (assuming a yield to tensile ratio of 0.75) should occur 76°F (42°C) below the NDT temperature obtained under impact loading. Hence, for the 3-mm positions in the SMA and SAW weldments, completely brittle fracture would be expected only at temperatures below -86°F and -96°F (-66 and -71°C), respectively, at an intermediate loading rate. Thus, elastic-plastic behavior at -60°F is predicted from the NDT data and an intermediate rate of loading.

## 8.33  5/8-Inch Dynamic-Tear-Test Specimen Results

Like the CVN results, the 5/8-inch DT test results also indicated that an increase in energy absorption (fracture transition from brittle to ductile behavior) occurred for specimens from the 3-mm positions of the SMA and SAW weldments at a temperature about 40 to 50°F (22 to 28°C) above the transition temperature of the base plate, Figure 16. Because the thickness of the DT specimen, namely 5/8-inch (15.9 mm), is greater than that of the CVN specimen (0.394-inch or 10 mm), the actual low-toughness region and corresponding energy value may be "masked" by the adjacent higher toughness weld metal or base metal to a greater extent in the dynamic tear than in the CVN test.

Rolfe et al.[30] have suggested criteria, alleged to ensure a reasonable level of fracture toughness, that incorporate tests of 5/8-DT and NDT specimens and the assumption that a ship hull is subjected to impact loading. With the assumption of impact loading, an NDT temperature at least 32°F (18°C) below the minimum service temperature is required. Because the minimum service temperature for the material of the present investigation is -50°F (-46°C), an NDT lower than -82°F (-63°C) is required. In addition, a minimum 5/8-DT energy 75°F (42°C) above the maximum permissible NDT temperature, or -7°F (-22°C) for the present material, is also required. The required minimum 5/8-DT energy absorption is a function of the yield strength according to the equation[30]

$$DT = \left(\frac{\sigma_y + 20}{60}\right) 250 \qquad (5)$$

where

     DT = the 5/8-DT energy absorption, ft-lb.
and   $\sigma_y$ = the static yield strength at the test temperature, ksi.

Thus, for the different yield strengths of the various regions of the weldments, the minimum required energy varies from 340 ft-lb (461 J) for the base plate to 449 ft-lb (609 J) for the SMA weld metal, Table 11.

     Examination of the 5/8-DT energy curves shows that the only region of the weldments that would meet these criteria is the SMA weld metal, Figure 16. The base metal and 3-mm positions in both weldments would fail to meet both the maximum-NDT-tempera-ture criterion of -82°F and the 5/8-DT energy-absorption criterion at -7°F.

     If, however, the Rolfe et al.[30] criteria are examined with the assumption of an intermediate rather than impact loading rate for the structure, both the maximum allowable NDT tempera-ture and the specified temperature for the 5/8-DT requirement will be shifted (assuming a yield strength of 67 ksi or 462 MPa) +76°F according to Equation 4. Thus, the maximum allowable NDT temperature will be -6°F (-82°F + 76°F) or -21°C and the tempera-ture at which the required 5/8-DT energy absorption is to be obtained will be +69°F (NDT + 75°F) or +21°C, respectively, for a structure subjected to an intermediate loading rate. The NDT temperatures for the 3-mm locations in the SMA and SAW weldments were 5 to 15°F lower than that required for the intermediate loading rate, whereas the required 363 ft-lb was measured about 5°F below the 69°F DT test temperature, Figure 16. Thus the Rolfe criteria for NDT and 5/8 DT, when adjusted for intermediate loading rate, indicate that the present results would be marginally acceptable.

     Rolfe[30] has also presented a CVN requirement equiva-lent to the 5/8-DT criteria for dynamic loading. The CVN require-ment is 32 ft-lb (44J) at 43°F (24°C) above the service tempera-ture. The 3-mm locations for both weldments meet this require-ment, Figures 15-1 and 15-2. If the requirement is adjusted for intermediate loading rates (temperature shifted upward 76°F), then 32 ft-lb would be required at about +69°F for -50°F service. The CVN values at the 3-mm positions for both 1-inch-thick weld-ments exceed this requirement by a factor of two to three, Fig-ures 15-1 and 15-2.

     Thus, it is concluded that both weldments would exceed the equivalent CVN criterion but would not meet the NDT or

## Table 11

### Required* 5/8-Inch-DT Energy Absorption For Various Regions of the 1-Inch Weldments Using the Criterion of Reference 30

| Location in Weldment | Estimated** Static Yield Strength, ksi, at -7°F | Energy Absorption, ft-lb, at -7°F | |
|---|---|---|---|
| | | Required | Actual Minimum (from Curves) |
| **SMA Weldment** | | | |
| Weld Metal | 87.7 | 449 | 615 |
| 3 mm HAZ | 71.3 | 380 | 120 |
| **SAW Weldment** | | | |
| Weld Metal | 80.3 | 418 | 170 |
| 3 mm HAZ | 71.3 | 380 | 185 |
| Transverse Base Plate | 61.7 | 340 | 155 |

* Required at 75°F above the required NDT temperature which is 32°F below the service temperature (-50 -32 +75 = -7). The requirement varies with the static yield strength at the test temperature.

** From Reference 13 and for the HAZ also from the maximum hardness using Reference 21 and assuming $\sigma_y / \sigma_{ts} = 0.75$.

5/8-DT criteria proposed by Rolfe[30] for dynamic loading. However, for intermediate loading rates, the data from the 3-mm position marginally meet the NDT and DT Rolfe criteria, whereas the CVN values far exceed those required.

## 8.34   Three-Point-Bend Fracture-Mechanics Specimen Results

As discussed earlier, all the three-point-bend specimens exhibited invalid $K_{IC}$ behavior consistent with the Charpy V-Notch, NDT, and 5/8-DT data which predicted marginal elastic-plastic fracture behavior in the HAZ for an intermediate loading rate at -60°F.  The proximity of the low-toughness 3-mm position to the center of the crack front did not lead to valid low-toughness behavior in the fracture-mechanics type of specimen.

Critical crack-opening-displacement (COD) or crack-opening-stretch (COS) values were calculated from the clip-gage displacement for each fracture-mechanics test according to British Standard BS5762:79.  Although the Standard is for three-point-bend cross-sectional geometries of TxT and Tx2T (where the first dimension, T, is the thickness and the second dimension is the depth), the Tx4T geometry used in the present investigation should give similar results.  The COS values of 0.59 mil (0.015 mm) for the SMA weldment and 1.28 mils (0.033 mm) for the SAW weldment, Table 7, are generally considered inadequate for acceptable performance.  Values of about 3 mils (0.08 mm) or more, however, are considered as representing acceptable ductility.  Hence, unlike the other fracture-toughness tests, which indicate marginal fracture behavior, <u>the COD test results indicate unacceptable fracture behavior of the 3-mm location</u>. Because a significant amount of data scatter occurred, when average values of the COS are used the toughness would appear acceptable, whereas lower-bound values suggest marginal or unacceptable fracture performance.

The three-point-bend results can also be compared with the behavior predicted from the CVN results as shown by Barsom.[46]  At the same temperature and loading rate, the dynamic critical stress-intensity factor at fracture, $K_{Id}$, can be estimated from the CVN energy absorption in the transition region by using the equation[46]

$$K_{Id} = \sqrt{5E(CVN)} \qquad (6)$$

where $K_{Id}$ is given in psi$\sqrt{inch}$, E is the modulus of elasticity of the material in psi, and the CVN energy absorption is in ft-lb. When an estimate of $K_{IC}$ is desired at a loading rate other than that of the impact CVN test, the CVN curve must be shifted toward a lower temperature to account for the difference in loading rate.  The amount of the shift depends on the yield strength.

86

For an intermediate loading rate, the shift is given by Equation 4. Thus, for the present SAW 3-mm HAZ, with an estimated maximum yield strength (Table 10) of 66.9 ksi, the minimum CVN of 27 ft-lb (37 J) at -25°F (-32°C), Figure 15-2, predicts an intermediate loading rate $K_{IC}$ of 63.6 ksi$\sqrt{inch}$ (70.0 MPa$\sqrt{m}$) at -101°F (-74°C).

Similarly, the COD results obtained in the three-point-bend test can be used to estimate the minimum actual $K_{IC}$ values by using the equation[49]

$$K_{Ic} = \sqrt{E\sigma_{ys}(COS)} \tag{7}$$

where $K_{Ic}$ is given in psi$\sqrt{inch}$; E is modulus of elasticity of the material in psi, $\sigma_{ys}$ is the yield strength under the test conditions in psi, and the COS is in inches. Estimating the yield strength from Table 10 and Reference 21, the estimated $K_{IC}$ at -60°F at an intermediate loading rate is 38.1 to 105.6 ksi$\sqrt{inch}$ (41.9 to 116 MPa$\sqrt{m}$).

## 8.35 Surface-Cracked Specimen Results

The average values of the results from the quality-control tests suggest that the toughness in the 3-mm location of both types of weldments is marginal, but acceptable, that is, elastic-plastic fracture behavior should occur at -60°F at the intermediate strain rate. However, the fracture behavior predicted from the lower-bound values of the CVN test data indicates unacceptable fracture performance, that is, a brittle fracture can occur. Because a brittle fracture occurred in one surface-cracked specimen tested at -60°F and an intermediate strain rate, the minimum values for the CVN results and the fracture-toughness results from the surface-notched CVN specimens were considered to be the best quality-control-test assessment of the fracture performance of the weldments used in this study.

Thus, to a great extent, the extreme values of the sets of data are consistent. That is, the lowest values or worst-case results from tests of the CVN and surface-cracked specimens both indicate brittle fracture. Alternatively, the average or mean values for these two sets of data both predict consistent elastic-plastic performance. Use of extreme values for all variables of interest is a very conservative approach to the problem, and the

---

[49] J. G. Merkle, "Analytical Relations Between Elastic-Plastic Fracture Criteria," International Journal of Pressure Vessels and Piping, Volume 4, 1976, pp. 197-206.

low probability that all these extremes will occur simul-
taneously, in a sense, has lead to the recent development of
probabilistic fracture mechanics.

The fatigue cracks were grown to various sizes,
Table 8, to locate the crack front in various regions of the HAZ
of the weldments. For a crack-shape ratio, a/2c, of 0.24,
assuming an ideal weld bond-line included angle of 60°, the crack
tip would be located at the 3-mm position when the crack depth is
0.2 inch (5 mm). Thus, all but two of the 15 surface-cracked
specimens would theoretically have some part of the crack front
residing in the 3-mm or lowest toughness portion of the weld-
ments. However, because of the nonuniformity of the actual HAZ
zones and bond lines, some of the 12 specimens theoretically
having cracks in the 3-mm position, in fact, did not.

As previously discussed, the shortest loading times
observed during slamming conditions of ships would correspond to
a rise time of about one second. This loading time, and there-
fore the corresponding strain rate (referred to as an inter-
mediate strain rate in comparison to impact loading in a Charpy
V-notch specimen), was attained in only about half the surface-
cracked specimens tested, Table 8, even when calculated on the
basis of the initial linear portion of the load-time curve. For
the remaining specimens the rise time was longer. The nominal
K-rate of loading at the crack tip ranged from about 1 to 16 ksi
√inch/sec.

8.351 Gross- and Net-Section Stress Behavior. Table 8 lists
both the gross-($\sigma_G$) and net-($\sigma_N$) section stresses for each
specimen. The gross-section stress at fracture is not signifi-
cant because the value will vary with the crack size as well as
the fracture ductility of the weldment. However, when the net-
section stress is below the yield strength, linear-elastic-
fracture-mechanics calculations can be made and brittle-fracture
behavior is possible. The net-section stress, $\sigma_N$, was calculated
(assuming pure tension loading) by using the fracture load
divided by the net section (excluding the cracked area). At the
test temperature and loading rate, the base-plate yield strength
is about 67 ksi. In some tests, a maximum load was followed by a
decreasing load (not an abrupt "pop-in"), in turn followed by a
further increase in load. Although it is not possible to deter-
mine whether brittle crack extension or general yielding of the
net section occurred, in most of these cases it is probable that
general yielding was the cause of the load drop because of the
proximity of the net section stress to the yield stress. Table 8
presents data corresponding to the first maximum as well as the
final maximum in the load record.

88

Because of the inherent eccentricity of loading on the net section of a surface-cracked specimen, a bending component should be added to $\sigma_N$ to determine the maximum value of the net-section stress. As described in Section 8.252, the bending stress is given in Table 8 as $\Delta\sigma$—the total stress differential between the two faces of the specimen. The bending stress, $\Delta\sigma$, was determined by first calculating the location of the centroid of the surface crack (cracked area) and assuming that a resultant force, equal to the nominal stress times the cracked area, acts at this centroid. The differential stress between the two faces of the specimen was then calculated by solving for the linearly varying stress across the thickness of the specimen, which would produce a moment about the back face equal to that produced by the resultant force acting at the centroid of the cracked area. Then, by assuming the specimen to be a simple beam, the additional stress at the front face due to bending was taken as half the value shown in Table 8.

For example, for specimen 9AM2 the maximum net-section tensile stress for the first maximum in the load record would be 67.0 + 5.8 or 72.8 ksi (502 MPa). Thus, the cracked face of the specimen was significantly above the estimated base-plate yield stress of 67 ksi (462 MPa). Similarly, the bending-plus-tension net-section stress for specimen 6AS4 was greater than the yield strength. On the other hand, for specimen 8AS2 the maximum net-section stress was below the base-plate yield strength, and, even when bending is taken into account, large plastic straining did not occur prior to crack extension. These observations do not consider the effects of residual stresses or their redistribution during the development of the crack under cyclic loading.

## 8.352 Crack-Opening-Displacement Behavior

### 8.3521 Crack-Opening-Displacement Values for Surface-Cracked Specimens.
In addition to net-section stress, another indicator of ductility was the clip-gage displacement, $V_q$, across the crack mouth. Unacceptable fracture behavior would be consistent with clip-gage displacements of only a few thousandths of an inch (mils) or about 0.1 mm. Thus, the values listed in Table 8 again indicate brittle fracture behavior for specimen 8AS2.

Another method of characterizing elastic-plastic fracture behavior is the crack-opening-displacement (COD) value for each test. The critical COD or crack opening stretch (COS) for fracture is the calculated value of the deformation or blunting at the crack tip that occurs just prior to crack extension. For the surface-cracked specimens, the critical COS values were estimated from the clip-gage displacement measured across the

center of the surface crack and the strain-gage readings obtained directly opposite this location on the opposite face. For corner cracks both the clip gage and the strain gage were mounted near the edge of the specimen. The strain-gage readings were first converted to displacement by assuming that the strain was uniform over the active gage length (generally 0.060 in. or 1.52 mm). From this calculated displacement and that obtained from the clip-gage on the opposite face, the COS was estimated by linear interpolation.

The COS values ranged from 0.7 to 15.6 mils, (0.18 to 0.40 mm) or more, Table 12. A "rule-of-thumb" value to assure elastic-plastic rather than brittle fracture is a minimum COS of 3 to 5 mils (0.08 to 0.13 mm). Two SAW weldments, 9AS1 and 8AS2, had calculated COS values of less than 3 mils (0.08 mm) at instability. However, as discussed above, specimen 9AS1 had a very long surface crack (2.8 inches or 71 mm) and a net-section stress well in excess of the yield strength. Because the surface crack was also deep (0.662 in. or 16.8 mm), the bending stress imposed on the specimen was large and lead to a calculated differential stress between the front and back faces of 37.5 ksi (259 MPa), Table 8. In addition, the fracture-initiation site (identified after the test) was only 0.203 in. (5.2 mm) from the surface rather than at the deepest point on the crack front. Thus, because of the significant bending stress, it is probable that the COS at the fracture-initiation site was greater than the value of 2.5 mils (0.064 mm) calculated at the deepest point on the crack front. In contrast, virtually a linear-elastic fracture was observed in specimen 8AS2.

8.3522 Comparison of Actual Critical Crack Size With Estimates Obtained From Three-Point-Bend Test Results. The results from the three-point-bend tests can be used with the British COD design curve[50] to estimate conservative tolerable crack sizes for the surface-cracked-specimen tests. Because a factor of safety of at least two in flaw tolerance is included in the design curve, use of this procedure does not establish critical crack sizes for design but only estimates noncritical or safe sizes. The procedure requires establishing the critical COD value, $\delta$, (referred to as the COS in previous sections) and yield

---

[50] F. M. Burdekin and M. G. Dawes, "Practical Use of Linear Elastic and Yielding Fracture Mechanics with Particular Reference to Pressure Vessels," Practical Application of Fracture Mechanics to Pressure Vessel Technology, Institute of Mechanical Engineering, London, May 1971.

strength, $\sigma_y$, for the material at the design temperature and maximum expected loading rate. From the design curve, Figure 20, for gross stresses near or below yield, the ratio of the equivalent elastic stress of the uncracked member to the yield strength can be used to establish the value of the nondimensional parameter $\Psi$. Knowing the value of $\Psi$, a conservative tolerable half-crack-length value, $a_{cct}$, for an infinite center-cracked (through-cracked) plate specimen under tension loading is established for the particular material properties, $\sigma_y$, $\delta$, and the modulus of elasticity, E.

The results from the surface-cracked specimens were compared with corresponding estimates of conservative flaw tolerance based upon the results from the three-point-bend tests of the same weldments. The comparison, however, was made for equivalent crack lengths in a center-cracked specimen. From the three-point-bend tests of the SMA weldments, $\delta$, or COS, varied from 0.59 to 4.54 mils (0.015 to 0.115 mm), whereas the SAW weldment values varied from 1.28 to 3.26 mils (0.033 to 0.083 mm), Table 7.

As shown in Table 12, for each surface-cracked specimen test these $\delta$ values were used along with the gross-section stress to estimate a range of conservative tolerable crack lengths for infinite center-cracked specimens using the COD design curve. Because the values of half-crack length, $a_{cct}$, from the design curve are for an infinite center-cracked-tension (CCT) specimen, the critical flaw sizes from the surface-cracked-specimen tests were converted to equivalent CCT half-crack lengths by solving for the CCT half-crack length, $a_{cct}$, which, under the same gross stress, produces the same crack-tip K level at the deepest point of the surface crack.

For an infinite CCT specimen the K level is given by the equation[51]

$$K = \sigma_G \, (\pi a_{CCT})^{1/2} \qquad (8)$$

where

$\sigma_G$ = the applied gross stress,
and $a_{CCT}$ = the half-crack length.

---

[51] P. C. Paris and G. C. Sih, "Stress Analysis of Cracks," Fracture Toughness Testing and its Applications, ASTM STP 381, American Society for Testing and Materials, Philadelphia, PA, April 1965, pp. 30-81.
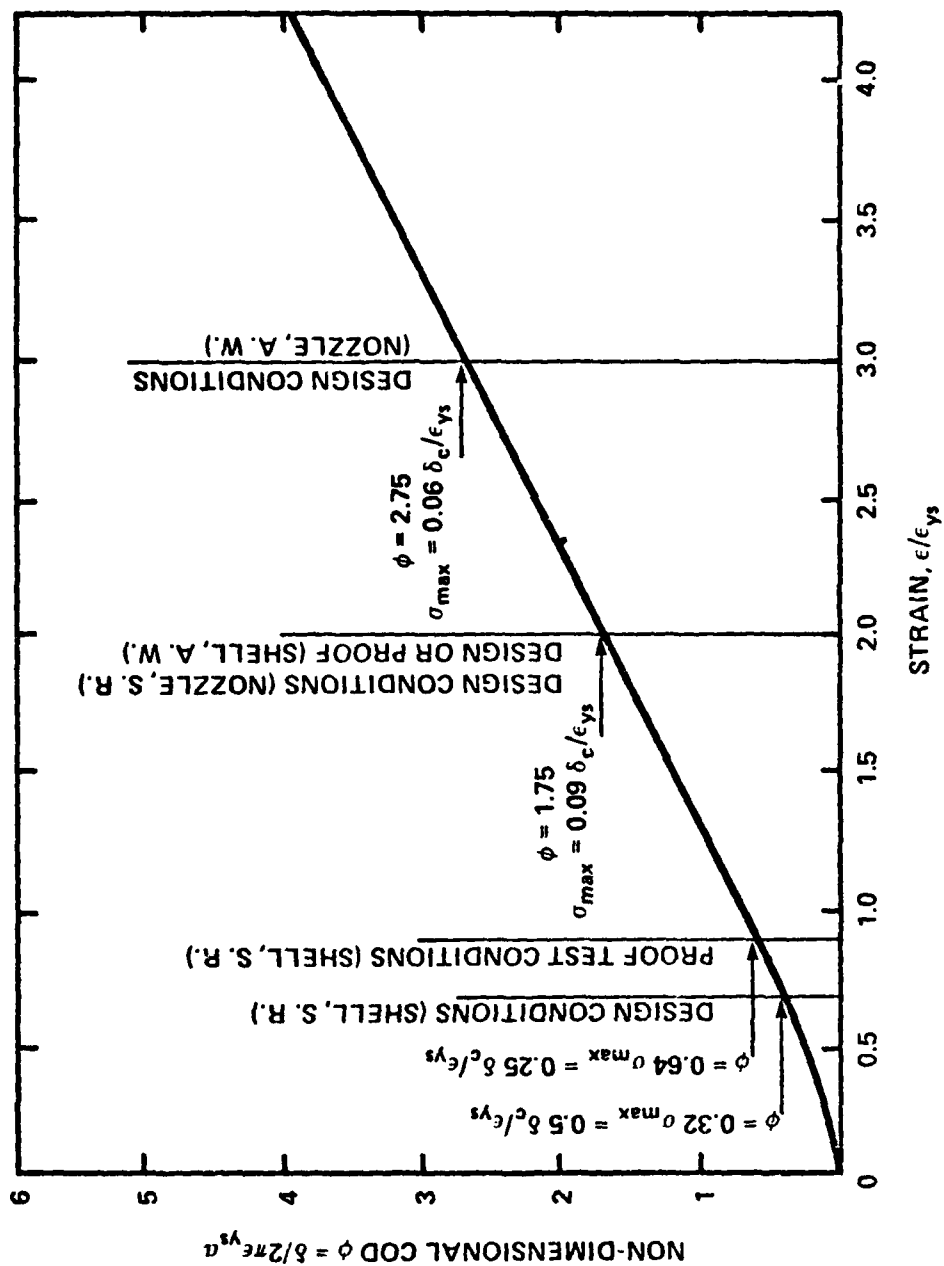
Figure 20    Design Curve for COD, Strain, and Crack Size Relationship
as Proposed by Burdekin and Dawes, Reference 50

92

Table 12

Intermediate-Strain-Rate Surface-Cracked-Specimen Results at -60°F and -100°F for Tee Welds Analyzed by the COD Method

| Specimen No. | $\sigma_G$,* ksi | Conservative Tolerable CCT Crack Length,** in. Predicted from COD Design Curve, Ref. 50, and 3-Point-Bend Results of Table 7 | Actual Surface Crack Depth from Test, $a_{act}$, in. | CCT Crack Length Corresponding*** to $a_{act}$, in. | Estimated COS, mils, at $\sigma_G$ | K, ksi√inch, from COD+ |
|---|---|---|---|---|---|---|
| SMA As-Welded (-60°F) | | | | | | |
| 9AM2[++] | 62.8[++] | 0.047-0.361 | 0.380 | 0.178 | 5.4 | 105.6 |
| 9AM1 | 54.4 | 0.080-0.617 | 0.564 | 0.549 | 3.1 | 80.0 |
| 2AM1[+++] | 56.5 | 0.074-0.572 | 0.612 | 0.840 | 15.6 | 179.4 |
| 8AM2[++++] | 63.0[++] | 0.047-0.357 | 0.377 | 0.184 | 6.4 | 114.9 |
| SAW As-Welded (-60°F) | | | | | | |
| 9AS2[+] | 82.5 | 0.077-0.195 | 0.082 | 0.103 | >>34.5 | >>261.8 |
| 3AS2 | 79.8 | 0.079-0.202 | 0.064 | 0.079 | >>30.0 | >>244.1 |
| 9AS1 | 42.0 | 0.253-0.618 | 0.662 | 0.847 | 2.5 | 70.5 |
| 6AS4[++] | 66.0[++] | 0.097-0.245 | 0.247 | 0.202 | ND | ND |
| 6AS2[+++] | [†††] | 2.154-5.465 | 0.795 | 2.197 | ND | ND |

93

Table 12 (Continued)

| Specimen No. | $\sigma_G$,* ksi | Conservative Tolerable CCT Crack Length,** in. Predicted from COD Design Curve, Ref. 50 and 3-Point Bend Results of Table 7 | Actual Surface Crack Depth from Test, $a_{act}$, in. | CCT Crack Length Corresponding*** to $a_{act}$, in. | Estimated COS, mils, at $\sigma_G$ | K, ksi√inch, from COD |
|---|---|---|---|---|---|---|
| | | SAW Rough-Undercut (-60°F) | | | | |
| 4AS2 | 56.3 | 0.160-0.405 | 0.598 | 0.505 | 4.5 | 94.5 |
| 8AS3 | 53.7 | 0.178-0.452 | 0.563 | 0.448 | 3.5 | 83.4 |
| 8AS2‡ | 53.4† | 0.160-0.405 | 0.394 | 0.196 | 0.7 | 37.3 |
| | | SMA Smooth-Undercut (-60°F) | | | | |
| 8AM1 | 74.6 | 0.039-0.301 | 0.513 | 0.269 | >>29.0 | >>244.7 |
| 4AM2‡‡ | 73.5 | 0.040-0.306 | 0.493 | 0.476 | >>14.7 | >>170.9 |
| | | SAW Smooth (-60°F) | | | | |
| 7AS2 | 71.7 | 0.089-0.225 | 0.580 | 0.322 | >33.7 | >258.7 |
| | | SMA Rough-Undercut (-100°F) | | | | |
| 7AM1‡‡‡ | 70.0 | ND | 0.292 | ND | 2.8⁋ | 60.0⁋⁋ |
| | | SAW As-Welded (-100°F) | | | | |
| 9AS3++ | 61.5 | ND | 0.450 | ND | 2.2 | 69.7⁋⁋⁋ |

* Gross stress at maximum load unless otherwise noted.
** Half crack length for an infinite plate with a through-thickness crack under tension loading. CCT denotes "center-cracked tension."

Table 12 (Continued)

*** Obtained by solving for the CCT crack length producing the same crack-tip K level as at the deepest point of the surface crack when both are under pure tension loading using Equation 51 and Equation 9 Reference 52.

+ Assumes $\sigma_y$ = 68.8 ksi for the SMA and 66.2 ksi for the SAW specimens unless otherwise noted.

++ At the first maximum in the load record.

+++ Corner crack.

++++ Contained two cracks.

† Failed in base plate.

†† Initial loading. Brittle crack extension occurred but specimen slipped through grips before total failure.

††† Large corner crack. $\sigma_G$ = 19.6 ksi

‡ At "pop-in."

‡‡ Incomplete corner crack.

‡‡‡ Multiple cracks.

∏ At fracture location rather than at deepest point.

∏∏ Assumes $\sigma_y$ = 76.2 ksi.

∏∏∏ Assumes $\sigma_y$ = 73.6 ksi.

95

Likewise, the K level at the deepest point of a surface-cracked specimen under pure tension loading can be calculated by using an equation developed by Newman[52]

$$K = \sigma_G \left(\frac{\pi a}{2}\right)^{1/2} F \qquad (9)$$

where

$\sigma_G$ = the gross applied stress,
$a$ = the crack depth,
$\phi$ = a function of the a/c ratio as shown in Equation C-2,
and $F$ = a function of the crack-depth to specimen-thickness ratio, a/t, given in Reference 52 ($f_w$ given in Reference 52 was not included in $F$).

Equating the K values

$$a_{CCT} = a \left(\frac{F}{\phi}\right)^2 \qquad (10)$$

The values for the equivalent through crack for a CCT specimen based upon the results from the surface-crack specimens (column 5 in Table 12) can now be compared with the predicted conservative flaw tolerance based upon the bend-specimen results (column 3 in Table 12). For the SMA weldments, four of the equivalent-crack-length values obtained from the surface-cracked-specimen test results were within the predicted range, whereas the values for two specimens (2AM1 and 4AM2) were greater than the predicted range. For the SAW weldments, however, one of the surface-cracked specimens, 3AS2, had an equivalent crack length equal to the minimum predicted from the bend tests, whereas the crack lengths for the others were within or greater than the predicted range.

It is obvious that the reason for the less conservative prediction for the SAW weldments was that the minimum δ value from the SAW bend tests was 1.28 mils (0.033 mm), whereas the minimum δ values from the SMA bend tests was 0.59 mil (0.015 mm). Because the lowest toughness region of the weldments was at the 3-mm location in the HAZ rather than in the weld metal, the lowest δ for both sets of weldments should have been used as the minimum of the predicted range for all tests. Use of 0.59 mil (0.015 mm) as the minimum for

---

[52] J. C. Newman, Jr. and I. S. Raju, "Analyses of Surface Cracks in Finite Plates Under Tension or Bending Loads," NASA TP (in preparation), 1979.

96

the SAW weldments would have reduced all the predicted minimum
lengths by half; thus, all equivalent crack lengths of the
surface-cracked specimens would have been greater than the
predicted minimum crack tolerance values by at least a factor of
two. Hence, the COD design curve and the minimum COS value from
the three-point-bend specimen results conservatively predicted
tolerable flaw sizes in the surface-cracked-specimen tests.

Only the most conservative results from the bend tests
would have conservatively predicted all the critical flaw sizes
of the surface-cracked-specimen tests. Again, it appears that
the high toughness of the 3-mm zones. The minimum $\delta$ value of
0.59 mil (0.015 mm) indicates a brittle fracture, that is, linear-
elastic fracture behavior.

8.353 Fracture Toughness From Critical-Stress-Intensity Factors
of Surface-Cracked Specimens. For the surface-cracked specimens,
the stress-intensity factor (K) at the crack tip, corresponding
to either the first or final maximum in the load record, was
first calculated by an elastic analysis, assuming that no bend-
ing stress was applied to the specimen because of the presence of
the surface crack. The equation[19] used was the same as Equa-
tion 2, described earlier in the discussion of fatigue-crack-
propagation behavior. The results are listed in Table 13. The
analysis was then modified to include the effects of bending due
to the surface crack as described in Appendix E.

The most meaningful critical-stress-intensity factor,
$K_c$, estimates for the surface-cracked specimens are those that
include bending and are obtained for the fracture-initiation
site, Table 13. The value of 32.9 ksi$\sqrt{\text{inch}}$ (36.2 MPa$\sqrt{\text{m}}$) for
specimen 3AS2 is not significant because the net-section stress
was significantly greater than the yield stress because of the
shallow depth of the crack. Likewise, the value of 42.5 ksi
$\sqrt{\text{inch}}$ (46.8 MPa$\sqrt{\text{m}}$) for specimen 6AS2 is in question because the
crack depth was 80 percent of the specimen depth, which may give
significant errors in the K analyses. Thus, the minimum $K_c$
value obtained from the surface-cracked-specimen tests is about
46 ksi$\sqrt{\text{inch}}$ (50.6 MPa$\sqrt{\text{m}}$) for specimen 8AS2, and is assumed to be
representative of the minimum-toughness 3-mm location in the
HAZ.

As indicated in Section 8.34, the maximum valid $K_{IC}$
value for a 1-inch-thick plate having a yield strength of
67.5 ksi (465 MPa) is 42.5 ksi$\sqrt{\text{inch}}$ (46.8 MPa$\sqrt{\text{m}}$). Thus, the
fracture-toughness value of 46 ksi$\sqrt{\text{inch}}$ (50.6 MPa$\sqrt{\text{m}}$), measured
at -60°F (-51°C) with an intermediate loading rate, is considered
a nearly valid $K_{IC}$ value. Therefore, the fracture behavior of

97

## Table 13

### $K_c$ Results for Surface-Cracked
### Specimens (at -60°F Except as Noted)

| Specimen No. | $\sigma_N$, ksi* | Crack Depth, in. At Deepest Point | At Initiation Site | $K_c$, ksi$\sqrt{inch}$ at Crack Tip From Simple Tension Analysis** | $K_c$, ksi$\sqrt{inch}$, Including Bending At Crack Tip*** | At Initiation Site[+] |
|---|---|---|---|---|---|---|
| | | | | SMA As-Welded | | |
| 9AM2 | 67.0[++] | 0.380 | 0.281 | 50.0 | 51.9 | 51.8 |
| 9AMl | 72.3 | 0.564 | 0.542 | 67.8 | 73.9 | 72.3 |
| 2AMl[+++] | 71.7 | 0.612 | 0.502 | 90.1 | 96.5 | 88.1 |
| 8AM2± | 69.1[++] | 0.377 | 0.053 | 51.0 | 53.0 | 52.9 |
| | | | | SAW As-Welded | | |
| 9AS2±± | 85.1± | 0.082 | ±± | >51.8 | >53.8 | ±± |
| 3AS2± | 81.6 | 0.064 | 0.034 | >44.1 | >45.1 | >32.9 |
| 9ASl | 71.4 | 0.662 | 0.203 | 58.6 | 65.0 | 46.9 |
| 6AS4±±± | 67.8 | 0.247 | 0.130 | <56.9 | <5ᵒ.4 | <50.1 |
| 6AS2[+++] | † | 0.795 | 0.263 | 30.7 | 4C.0 | 42.5 |
| | | | | SAW Rough-Undercut | | |
| 4AS2 | 70.4 | 0.598 | 0.544 | 68.5 | 72.3 | 70.4 |
| 8AS3 | 68.5 | 0.563 | 0.150 | 62.4 | 66.9 | 55.6 |
| 8AS2 | 57.5[††] | 0.394 | 0.235 | 44.6 | 46.4 | 45.8 |
| | | | | SMA Smooth-Undercut | | |
| 8AMl | 84.7 | 0.513 | 0.355 | 71.7 | 75.7 | 74.7 |
| 4AM2[++++] | 80.5 | 0.493 | 0.459 | 93.7 | 96.5 | 94.3 |
| | | | | SAW Smooth | | |
| 7AS2 | 79.7[†††] | 0.580 | ††† | >70.2 | >73.6 | ††† |
| | | | | SMA Rough-Undercut @ -100°F | | |
| 7AMl± | 75.9 | 0.292 | 0.200 | 63.6 | 66.8 | 59.4 |

Table 13 (Continued)

| Specimen No. | $\sigma_N$, ksi* | Crack Depth, in. | | $K_c$, ksi√inch at Crack Tip From Simple Tension Analysis** | $K_c$, ksi√inch, Including Bending | |
| | | At Deepest Point | At Initiation Site | | At Crack Tip*** | At Initiation Site+ |
|---|---|---|---|---|---|---|

__SAW As-Welded @ -100°F__

| 9AS3+++ | 69.2 | 0.450 | 0.278 | 85.9 | 91.5 | 74.7 |

\* At maximum load except as noted.

\*\* Using Equation 2, Reference 19.

\*\*\* Using Equation 2, Reference 19 and Equation E-1 Reference 52.

+ _Using Equation E-2, References 19 and Reference 1, Appendix E, and interpolation of solutions presented in Reference 52._

++ At first maximum in load record.

+++ Corner crack.

++++ Incomplete corner crack.

± Multiple cracks.

±± Failed in base plate.

±±± Initial loading. Brittle crack extension occurred but specimen slipped through grips before total failure.

† Very large fatigue crack resulted in large bending stress, $\sigma_N = 40.3$ ksi.

†† At pop-in. Load increased during fracture.

††† Did not fracture at maximum of load range.

the surface-cracked specimen 8AS2 is near plane strain and consistent with the conservative (low) estimates of the fracture toughness obtained from the minimum values measured in the CVN test.

8.354 Surface-Cracked Specimen Tests at -100°F. Because the brittle-fracture test result of specimen 8AS2 was unique, that is, not duplicated in any of the other test results, two additional tests were conducted at -100°F (-73°C) and at an intermediate loading rate. Specimen 7AM1 had a surface-crack length of 0.988 inch (25.1 mm) and a depth of 0.292 inch (7.4 mm), whereas specimen 9AS3 had a surface-crack length of 1.112 inches (28.2 mm) and a depth of 0.450 inch (11.4 mm). The purpose for conducting two tests at a temperature below -60°F was to verify that the result from specimen 8AS2 was an extreme in data scatter and that the overall toughness behavior of the weldment was not approaching brittle-fracture behavior. As shown in Table 13, the $K_c$ values for the tests at -100°F and an intermediate loading rate were similar to those at -60°F and an intermediate loading rate. However, the two estimated COS values at -100°F were less than 0.003 inch and, therefore, indicate unacceptable ductility at this temperature. Thus, although the $K_c$ values indicated acceptable elastic-plastic performance, the COS values from two tests of surface-cracked specimens at -100°F and an intermediate loading rate indicate that the fracture performance at -100°F is unacceptable and confirm the marginal fracture behavior at -60°F and an intermediate strain rate.

## 9.0 Recommendations and Future Research

1) The Charpy specimen is the best "quality control" type of specimen to use for assessing fracture toughness in ship-steel weldments. CVN tests at different locations in the weldment are necessary and should be continued as a requirement. The 5/8-inch-thick dynamic-tear specimen samples too many regions of the weldment and is, therefore, not recommended for use in qualifying the toughness behavior of the HAZ in weldments. Although the NDT specimen gave meaningful and correct toughness evaluations when care was taken in testing and interpreting the results, this specimen is not recommended for quality control because of these difficulties in testing and interpretation and because the additional HAZ of the hard-x bead may complicate the results.

2) Further research is needed to establish a basis for determining when weldments should be classified as having a "significantly" degraded region in the HAZ. Because the base metal selected for this work had a known excessive degradation of the HAZ toughness, it is not clear that the weldments examined in this work are "typical." Thus, it is not reasonable to recommend more stringent toughness requirements for all weldments on the basis of results from one weldment that is unique. On the other hand, the results from this work showed that, for the base metal examined, a small region of very-low toughness in the HAZ was masked by the higher toughness regions surrounding it. In such circumstances, the absorbed energy measured with the Charpy specimen may be fictitiously greater than that representative of this low-toughness zone, and only the lowest values measured may be true indications of the low-toughness region. Because the lowest values were necessary to predict the brittle fracture obtained from one of the surface-cracked specimens, consideration should be given to;

   a. requiring that five rather than three Charpy specimens from the low-toughness HAZ region be tested at the specification temperature.

   b. requiring that three additional specimens having a surface-notched rather than an edge-notched orientation be tested in the low-toughness region (at the specification temperature).

101

3) Additional measurements of actual strain <u>rates</u> in ship structures should be undertaken to further verify that it is proper to assume intermediate loading rates (of the order of 1 second loading times) when setting fracture-toughness requirements for ships.

# 10.0 References

1. "Mechanical Testing of Steel Products," ASTM Standards, Part 10, 1978, pp. 28-83.

2. K. Willens, "Final Report of Phase I, MARAD/NBS/General Dynamics Ship Steel Improvement Program," General Dynamics, Quincy Shipbuilding Division, May 17, 1977.

3. J. M. Barsom, "Fatigue Behavior of Pressure-Vessel Steels," Welding Research Council Bulletin, No. 194, May 1974.

4. R. Roberts, J. M. Barsom, S. T. Rolfe, and J. M. Fisher, "Fracture Mechanics for Bridge Design," Report No. FHWA-RD-78-68, Federal Highway Administration, Department of Transportation, Washington, D. C., July 1977.

5. B. A. Graville and F. Watkinson, "Research Programs to Investigate the Fatigue of High Strength Steels; Initiation in Fillet Welds," Fatigue Performance of Welded High Strength Steels, The Welding Institute, 1974.

6. J. W. Fisher, K. H. Frank, M. A. Hirt, and B. M. McNamee, "NCHRP Report 102, Effect of Weldments on the Fatigue Strength of Steel Beams," Lehigh University, Bethlehem, Pennsylvania, 1970.

7. T. R. Gurney and S. J. Maddox, "Determination of Fatigue Design Stresses for Welded Structures from an Analysis of Data," Metal Construction and British Welding Journal, November 1972, Vol. 4, No. 11, pp. 11-15.

8. J. W. Fisher, "Guide to 1974 AASHTO Fatigue Specifications," American Institute of Steel Construction, New York, New York.

9. BS. 153, "Steel Girder Bridge," British Standard Institution, London.

10. T. R. Gurney, "Some Recent Work Relating to the Influence of Residual Stresses on Fatigue Strength," Residual Stresses in Welded Construction and Their Effects, an international conference held in London, November 15-17, 1977, The Welding Institute, Abington Hall, Abington, Cambridge.

11. S. J. Maddox, "Fracture Mechanics Applied to Fatigue in Welded Structures," Proceedings of the Conference on Fatigue of Welded Structures, The Welding Institute, Abington, Cambridge, July 1970.

12. S. T. Rolfe and J. M. Barsom, Fracture and Fatigue Control in Structures, Prentice-Hall, Inc., Englewood Cliffs, New Jersey, 1977.

13. R. Roberts, G. Irwin, G. Krishna, and B. Yen, "Fracture Toughness of Bridge Steels—Phase II Report," Report No. FHWA-RD-74-59, September 1974.

14. J. M. Barsom, E. J. Imhof, and S. T. Rolfe, "Fatigue-Crack Propagation in High Yield-Strength Steels," Engineering Fracture Mechanics, Vol. 2, 1971.

15. J. M. Barsom, "Fatigue-Crack Propagation in Steels of Various Yield Strengths," Transactions of the ASME, Journal of Engineering for Industry, Series B, Vol. 93, No. 4, November 1971.

16. B. M. Kapadia and E. J. Imhof, Jr., "Fatigue-Crack Propagation in Electroslag Weldments," Flaw Growth and Fracture, ASTM STP 631, American Society for Testing and Materials, 1977, pp. 159-173.

17. B. M. Kapadia, "Influence of Residual Stresses on Fatigue-Crack Propagation in Electroslag Welds," Fatigue Testing of Weldments, ASTM STP 648, D. W. Hoeppner, Ed., American Society for Testing and Materials, 1978, pp. 244-260.

18. J. M. Barsom and S. R. Novak, "Subcritical Crack Growth in Steel Bridge Members," prepared for the Highway Research Board, National Cooperative Highway Research Program, National Academy of Sciences, U. S. Steel Research, Monroeville, Pa., September, 1974.

19. G. R. Irwin, "Crack Extension Force for a Part Through Crack in a Plate," Journal of Applied Mechanics, Vol. 29, No. 4, 1962, pp. 651-654.

20. J. C. Newman, Jr., "A Review and Assessment of the Stress-Intensity Factors for Surface Cracks," presented at the ASTM Symposium on Part-Through Crack Life Prediction, San Diego, California, October 13-14, 1977.

21. Metals Handbook, 8th Edition, Vol. 1, Properties and Selection of Metals, edited by T. Lyman, American Society for Metals, Novelty, Ohio.

22. M. L. Williams and G. A. Ellinger, "Investigation of Structural Failures of Welded Ships," The Welding Journal, Vol. 32, No. 10, Research Supplement 498s-527s.

23. "Conducting Drop-Weight Test to Determine Nil-Ductility Transition Temperature of Ferritic Steels," ASTM Standards, Part 10, 1978, pp. 364-383.

24. E. F. Nippes and W. F. Savage, "Tests of Specimens Simulating Weld Heat-Affected Zones," The Welding Journal, Vol. 28, No. 12, 1956, Research Supplement 599s-616s.

25. W. P. Hatch, Jr., and C. E. Hawthorne, "V Notch Charpy Impact Testing of Weld Metal and Heat-Affected Zone Simultaneously," The Welding Journal, Vol. 35, No. 3, 1956, Research Supplement 120s-126s.

26. W. S. Pellini, "Notch Ductility of Weld Metal," The Welding Journal, Vol. 35, No. 5, 1956, Research Supplement 217s-233s.

27. W. J. Murphy and R. D. Stout, "Effect of Electrode Type in the Notch Slow Bend Test," The Welding Journal, Vol. 33, No. 7, 1954 Research Supplement 305s.

28. W. J. Murphy, W. D. McMullen, and R. D. Stout, "Relative Behavior of Notch-Toughness Tests for Welded Steel," The Welding Journal, Vol. 36, No. 6, 1957, Research Supplement 307s-311s.

29. K. Masubuchi, R. E. Monroe, and D. C. Martin, "Interpretative Report on Weld Metal Toughness," National Academy of Sciences—National Research Council, SSC-169, July 1965.

30. S. T. Rolfe, D. M. Rhea, and B. O. Kuzmanovic, "Fracture-Control Guidelines for Welded Steel Ship Hulls," U. S. Coast Guard Headquarters, Washington, D.C., SSC-244, 1974.

31. J. W. Wheaton, C. H. Kano, P. T. Diamant, and F. C. Bailey, "Analysis of Slamming Data from the S. S. Wolverine State," U. S. Coast Guard Headquarters, Washington, D. C., SSC-210, 1970.

32. "Review and Recommendations for the Interagency Ship Structure Committee's Fiscal 1980 Research Program," Ship Research Committee, National Academy of Sciences, Washington, D. C., March, 1979.

33. "Dynamic Tear Energy of Metallic Materials," ASTM Standards, Part 10, 1978, pp. 617-625.

34. J. R. Hawthorne and F. J. Loss, "SSC-248, Fracture Toughness Characterization of Shipbuilding Steels," U. S. Coast Guard Headquarters, Washington, D.C., 1974.

35. Private communication, T. B. Heberling, Armco Steel Co., Middletown, Ohio.

36. A. K. Shoemaker and S. T. Rolfe, "Static and Dynamic Low-Temperature $K_{Ic}$ Behavior of Steels," Journal of Basic Engineering, Trans. ASME, September 1969.

37. A. K. Shoemaker and S. T. Rolfe, "The Static and Dynamic Low-Temperature Crack-Toughness Performance of Seven Structural Steels," Engineering Fracture Mechanics, Vol. 2, 1971.

38. W. S. Pellini, "Design Options for Selection of Fracture Control Procedures in the Modernization of Codes, Rules, and Standards," Welding Research Council Bulletin No. 186, August 1973.

39. F. J. Loss and W. S. Pellini, "Coupling of Fracture Mechanics and Transition Temperature Approaches to Fracture-Safe Design," Practical Fracture Mechanics for Structural Steels, Chapman and Hall, London, 1969.

40. "Plane-Strain Fracture Toughness of Metallic Materials," ASTM Standards, Part 10, 1978, pp. 512-533.

41. "Rules for Building and Classing Steel Vessels," Section 24.65 "Welding Procedure Qualification Tests," American Bureau of Shipping, 1975.

42. Code of Federal Regulations, Title 46, Section 54.05-15, Office of the Federal Register, National Archives and Records Service, General Services Administration, U. S. Government Printing Office, Washington, 1976.

43. A. K. Shoemaker and J. F. Sovak, unpublished research, U. S. Steel Research, Monroeville, Pa., July 1978.

44. R. H. Bryan, et al., "Tests of 6-Inch Thick Pressure Vessels, Series 2: Intermediate Test Vessels V-3, V-4, and V-6," ORNL-5059, Oak Ridge National Laboratory, Oak Ridge, Tennessee, November 1975.

45. J. M. Barsom, "Relationship Between Plane-Strain Ductility and $K_{IC}$ for Various Steels," Journal of Engineering for Industry, November 1971, pp 1209-1215.

46. J. M. Barsom, "Development of the AASHTO Fracture-Toughness Requirements For Bridge Steels," Engineering Fracture Mechanics, Vol. 7, No. 3, September 1975.

47. J. H. Gross, "Comparison of Charpy V-Notch and Drop-Weight Tests for Structural Steels," The Welding Journal, Vol. 39, No. 2, February 1960, Research Supplement 59s-69s.

48. W. S. Pellini, "Notch Ductility of Weld Metal," The Welding Journal, Vol. 35, No. 5, May 1956, Research Supplement 217s-233s.

49. J. G. Merkle, "Analytical Relations Between Elastic-Plastic Fracture Criteria," International Journal of Pressure Vessels and Piping, Vol. 4, 1976, pp 197-206.

50. F. M. Burdekin and M. G. Dawes, "Practical Use of Linear Elastic and Yielding Fracture Mechanics with Particular Reference to Pressure Vessels," Practical Application of Fracture Mechanics to Pressure Vessel Technology, Institute of Mechanical Engineering, London, May 1971.

51. P. C. Paris and G. C. Sih, "Stress Analysis of Cracks," Fracture Toughness Testing and It's Applications, ASTM STP 381, American Society for Testing and Materials, Philadelphia, Pa., April 1965, pp 30-81.

52. J. C. Newman, Jr. and I. S. Raju, "Analysis of Surface Cracks in Finite Plates Under Tension or Bending Loads," NASA TP (in preparation), 1979.

Initial and Final Surface-Crack Length and Prediction
of Cycles Required for Observed Crack Extension in 1-Inch
A537 Class 1 SMA and SAW Tee Weldments

| | Crack Initiation | | | Crack Propagation | | | |
|---|---|---|---|---|---|---|---|
| Specimen No. | Stress Amplitude, ksi | Initial Length, in. | Cycles | Stress Amplitude, ksi | Final Length, in. | Additional Cycles | Predicted* Additional Cycles |
| | | | | SMA As-Welded | | | |
| 2AM1 | 29.0 | 0.065 | 66,840 | 29.0 | 1.490** | 185,400 | 36,631 |
| 3AM2 | 24.0 | 1.156 | 110,140 | 24.0 | 1.477 | 17,170 | 2236 |
| 4AM1 | 24.0 | 0.917 | 559,691 | 24.0 | 1.309** | 56,300 | 3550 |
| | | | | 24.0 | T*** | 24,840 | - |
| 9AM2 | 20.0 | 0.583 | 425,540 | 20.0 | 0.845 | 18,730 | 13,145 |
| 8AM2 | 20.0 | 0.876 | 730,370 | - | - | - | - |
| 9AM1 | 16.0 | 0.827 | 1,000,000 | 29.0 | 1.972 | 186,810 | 5187 |
| 7AM1 | 16.0 | Runout | 1,000,000 | - | - | - | - |
| 5AM2 | 13.0 | 0.483 | 1,000,000 | 13.0 | 0.497 | 8180 | - |
| 7AM2 | 13.0 | Runout | 1,000,000 | - | - | - | - |
| | | | | SAW As-Welded | | | |
| 9AS1 | 24.0 | 1.497 | 145,850 | 24.0 | 3.035** | 70,790 | 5262 |
| 6AS2 | 23.6 | 2.707 | 270,200 | 23.6 | 3.503 | 2450 | 1654 |
| 9AS3 | 21.0 | 0.599 | 216,540 | 13.0 | 1.151+ | 165,410 | - |
| 9AS4 | 20.0 | 0.841 | 453,400 | - | - | - | - |
| 9AS2 | 20.0 | 1.685 | 109,670 | 20.0 | 2.031 | 450 | 3510++ |
| 3AS2 | 20.0 | 0.026 | 117,350 | 20.0 | 0.949** | 13,840 | 264,520++ |
| 9AS3 | 19.0 | Runout | 1,000,000 | - | - | - | - |
| 2AS1 | 16.0 | 1.469 | 663,680 | 16.0 | T*** | 168,940 | |
| 9AS4 | 16.0 | Runout | 1,000,000 | - | - | - | - |
| 6AS4 | 14.8 | 0.911 | 599,530 | - | - | - | - |
| 6AS3 | 14.0 | T*** | 929,900 | - | - | - | - |
| 8AS3 | 13.0 | 1.241+ | 1,000,000 | - | - | - | - |
| 4AS2 | 13.0 | 0.140 | 1,000,000 | - | - | - | - |

| | Crack Initiation | | | Crack Propagation | | | |
|---|---|---|---|---|---|---|---|
| Specimen No. | Stress Amplitude, ksi | Initial Length, in. | Cycles | Stress Amplitude, ksi | Final Length, in. | Additional Cycles | Predicted* Additional Cycles |
| **SMA Rough-Undercut** | | | | | | | |
| 7AM1 | 21.0 | 0.223 | 273,110 | 10.5 | 1.154 | 490,140 | - |
| 7AM2 | 20.0 | 0.010 | 770,060 | 20.0 | 0.143+ | 412,280 | - |
| 7AM2 | 18.0 | Runout | 1,000,000 | - | - | - | - |
| **SAW Rough-Undercut** | | | | | | | |
| 8AS2 | 25.4 | 0.219 | +++ | 25.4 | 0.774 | 448,360 | 27,585 |
| 4AS2 | 18.0 | 0.140 | +++ | 18.0 | 2.143 | 570,490 | 118,550 |
| 8AS3 | 15.0 | 1.241+ | +++ | 15.0 | 1.700 | 981,340 | 36,139 |
| **SMA Smooth-Undercut** | | | | | | | |
| 2AM2 | 29.0 | I*** | 319,100 | - | - | - | - |
| 4AM2 | 27.0 | 0.559 | 165,980 | 27.0 | 0.572 | 110 | - |
| 8AM1 | 23.0 | 1.011 | 174,790 | - | - | - | - |
| **SAW Smooth-Undercut** | | | | | | | |
| 4AS1 | 27.0 | I*** | 761,520 | - | - | - | - |
| 7AS3 | 25.0 | Runout | 1,000,000 | - | - | - | - |
| **SAW Smooth** | | | | | | | |
| 1AS2 | 40.0 | B*** | 24,840 | - | - | - | - |
| 1AS1 | 40.0 | I*** | 16,790 | - | - | - | - |
| 5AS2 | 38.0 | I*** | 13,260 | - | - | - | - |
| 7AS4 | 36.0 | G*** | 230,880 | - | - | - | - |
| 1AS4 | 36.1 | G*** | 257,630 | - | - | - | - |
| 7AS2 | 33.0 | 0.866 | 261,080 | - | - | - | - |
| 4AS3 | 29.0 | I*** | 347,570 | - | - | - | - |
| 7AS1 | 29.0 | G*** | 739,870 | - | - | - | - |
| 6AS1 | 25.0 | Runout | 1,000,000 | - | - | - | - |
| 4AS4 | 23.0 | Runout | 1,000,000 | - | - | - | - |

\* From rearrangement and integration of Equation 1, Reference 15.

\*\* Corner crack. Length on face listed.

\*\*\* Total failure: T-from weld toe, I-from internal imperfection at bond line, B-in base plate, G-in grip.

\+ Discontinuous crack.

\++ Very shallow cracks.

\+++ Existing crack from previous cycling.

## Appendix B

## Acceleration in Growth Rate of an Internally Initiated
## Fatigue Crack Upon Reaching the Surface of a Plate

It has been noted that fatigue-crack growth accelerates rapidly after an internally initiated fatigue crack breaks through to the surface of a plate. This behavior would be expected, on the basis of a fracture-mechanics analysis of elliptical internal cracks under tension-fatigue loading. For normal internal cracks (the major axis parallel to the plate surface), the maximum calculated stress-intensity factor along the crack front, K, which is related to the fatigue-crack-growth rate, increases by a factor of about 1.25 to 1.60 after breakthrough to the surface occurs.

The maximum K value along the front of an internal elliptical crack subjected to tension loading, $K_1$, occurs at the end of the minor axis and, for gross stresses small compared with the yield stress, can be calculated by using an equation developed by Irwin[B-1]

$$K_1 = \sigma \frac{(\pi a_1)^{1/2}}{\Phi_1} \qquad (B-1)$$

where

$\sigma$ = the applied gross stress,

$a_1$ = the length of the semi-minor axis of the elliptical crack (half the internal crack width),

and $\Phi_1$ = a function of the aspect ratio of the ellipse, $2a_1/2C_1$ (Figure B-1), where $2C_1$ is the crack length.

From Paris and Sih[B-2] $\Phi_1$ (an elliptic integral of the second kind) can be expressed as:

---

B-1) G. R. Irwin, "Crack Extension Force for a Part Through Crack in a Plate," Journal of Applied Mechanics, Vol. 29, No. 4, 1962, pp. 651-654.

B-2) P. C. Paris and G. C. Sih, "Stress Analysis of Cracks," Fracture Toughness Testing and its Applications, ASTM STP 381, American Society for Testing and Materials, Philadelphia, PA, April 1965, pp. 30-81.

$$\Psi_l = I_o^{\pi/2} \left\{ 1 - \left[ 1 - \left( \frac{a_l}{C_l} \right)^2 \right] \sin^2 \emptyset \right\}^{1/2} d\emptyset \qquad (B-2)$$

where I denotes an intergral. By setting

$$\left[ 1 - \left( \frac{a_l}{C_l} \right)^2 \right]^{1/2} = k, \qquad (B-3)$$

where k is called the modulus, the value of $\Psi_l$ can be found in tables of elliptic integrals.

Similarly, the maximum K value along the front of a semi-elliptical surface crack subject to tension loading, $K_s$, occurs at the end of the semi-minor axis and, for gross stresses small compared with the yield stress, can be calculated from Irwin[B-1] by using the following equation:

$$K_s = \sigma \frac{1.12 \ (\pi a_s)^{1/2}}{\Psi_s} \qquad (B-4)$$

where

$\sigma$ = the applied gross stress,

$a_s$ = the length of the semi-minor axis of the semi-ellipse (surface-crack depth for a crack shallower than its surface length and half the surface-crack length for a crack having a depth exceeding its surface length.

$\Psi_s$ is obtained from Equation B-2, substituting $a_s$ for $a_l$ and $C_s$ for $C_l$.

When internal elliptical cracks (Figure B-1) narrower than half their length, $2a_l/2C_l < 0.5$, break through to the surface, they become cracks which have depths less than half their surface length (less than semicircular), $a_s/2C_s < 0.5$. The depth of the surface crack formed will be about the same as the total width of the prior internal crack just before breakthrough, Figure B-1, and the length of the surface crack can be taken as approximately equal to the length of the prior internal crack. Therefore, dividing Equation B-4 by Equation B-1, the ratio of the maximum K levels along the crack front for the surface versus the internal crack, $K_s/K_l$, can be related to the proportions of the internal crack and is given by

$$\frac{K_s}{K_i} = \frac{1.12\sigma[\pi(2a_i)]^{1/2}\phi_i}{\sigma(\pi a_i)^{1/2}\phi_s} = 1.58\left(\frac{\phi_i}{\phi_s}\right) \qquad (B-5)$$

The numerical value of $\phi_i/\phi_s$ depends on the ratio of the internal-crack width to crack length, $2a_i/2C_i$, and varies from 1.00 for long, narrow internal cracks, $2a_i/2C_i$ approaching zero, to 0.77 for internal cracks as wide as half their length, $2a_i/2C_i = 0.5$ (these become semicircular surface cracks). Thus, from Equation B-5, for internal elliptical cracks with a width of up to half their length which break through and become surface cracks, the maximum K level along the crack front increases up to 58 percent for long, narrow internal cracks and about 22 percent for internal cracks which become semicircular surface cracks, Figure B-1.

For internal elliptical cracks wider than half their length, $2a_i/2C_i > 0.5$, but still having the major axis parallel to the plate surface, the depth of the semi-elliptical surface crack formed will be greater than its surface length, so that the minor axis of the surface crack will now lie along the surface of the plate. Thus, the location of the maximum K value along the front of the surface crack will also be at the surface of the plate. (The location of the maximum K value was at the deepest point for the earlier case of surface cracks which had a depth of less than half their surface length.) The width of the surface crack formed (which is now the length seen on the surface) will equal the length of the internal crack, $2a_s = 2C_i$, and the depth of the surface crack will be approximately equal to the width of the internal crack, $C_s = 2a_i$.

The ratio of the maximum K level along the crack front of such a surface crack (having a depth greater than its surface length) to the maximum K level for a prior internal crack still having its major axis parallel to the plate surface can be related, as before, to the proportions of the internal crack. The ratio can be calculated from an expression (similar to Equation B-5) obtained by using Equation B-1 and setting $a_s = C_i$ and $C_s = 2a_i$ in Equation B-4:

$$\frac{K_s}{K_i} = \frac{1.12\sigma(\pi C_i)^{1/2}\phi_i}{\sigma(\pi a_i)^{1/2}\phi_s} = .792\left(\frac{\phi_i}{\phi_s}\right)\left(\frac{a_i}{2C_i}\right)^{-1/2} \qquad (B-6)$$

The numerical value of $\phi_i/\phi_\sigma$ again depends on the proportions of the internal crack before break through and varies from 0.77 for

B-3

internal cracks half as wide as their length, $2a_1/2C_1 = 0.5$, to
1.30 for circular internal cracks, $2a_1 = 2C_1$.  Thus, from Equa-
tion B-6, for internal elliptical cracks with a width between one
half and their full length (a circular crack) which break through
and become surface cracks, the maximum K level along the crack
front increases as much as 22 to 45 percent, Figure B-1.

Summarizing, Figure B-1 shows that for normal internally
initiated elliptical cracks (the major axis parallel to the plate
surface) which break through to the surface, the maximum stress-
intensity factor, K, along the crack front increases a minimum of
about 22 percent for the case of internal cracks having a width
equal to half their length.  For internal cracks either longer
and narrower or more circular, the increase in the maximum K level
when the crack breaks through to the surface is greater and
ranges up to about 58 percent for long narrow internal cracks and
up to about 45 percent for circular internal cracks.  Because the
fatigue-crack-growth rate increases with the maximum K value
along the crack front, from the preceeding analysis a signi-
ficant acceleration in growth rate would be expected when an
internal elliptical crack breaks through to the surface of a
plate.

## References

B-1. G. R. Irwin, "Crack Extension Force for a Part Through Crack
     in a Plate," Journal of Applied Mechanics, Vol. 29, No. 4,
     1962, pp 651-654.

B-2. P. C. Paris and G. C. Sih, "Stress Analysis of Cracks,"
     Fracture Toughness Testing and its Applications, ASTM STP 381,
     American Society For Testing and Materials, Philadelphia, Pa.,
     April 1965, pp 30-81.

FOR THE INTERNAL CRACK:

$$K_{Ii} = \frac{\sigma\sqrt{\pi a_i}}{\phi} \qquad \phi = \int_0^{\pi/2}\left\{1 - \left[1 - \left(\frac{a_i}{c_i}\right)^2\right]\sin^2\phi\right\}^{1/2} d\phi$$

FOR A SURFACE CRACK WITH THE SAME DEPTH/SPECIMEN THICKNESS & LENGTH/SPECIMEN WIDTH RATIO AS THE INTERNAL CRACK:

$$K_{Is} = \frac{1.12\sigma\sqrt{\pi a_s}}{\phi} \qquad \begin{cases} a_s = 2a_i, \text{ FOR } 2a_i/2c_i < 0.50 \\ a_s = c_i, \text{ FOR } 0.50 < 2a_i/2c_i < 1.00 \end{cases}$$

CIRCULAR INTERNAL CRACK WHICH BECOMES A SURFACE CRACK WITH THE SAME SURFACE LENGTH AS DEPTH

SURFACE CRACKS OF DECREASING SURFACE LENGTH TO DEPTH RATIOS

SURFACE CRACKS OF INCREASING SURFACE LENGTH TO DEPTH RATIOS

INTERNAL CRACK WITH A LENGTH/WIDTH RATIO OF 2.0 WHICH BECOMES A SEMI-CIRCULAR SURFACE CRACK

W, t, $2a_i$, $2c_i$

x-axis: $2a_i/2c_i$
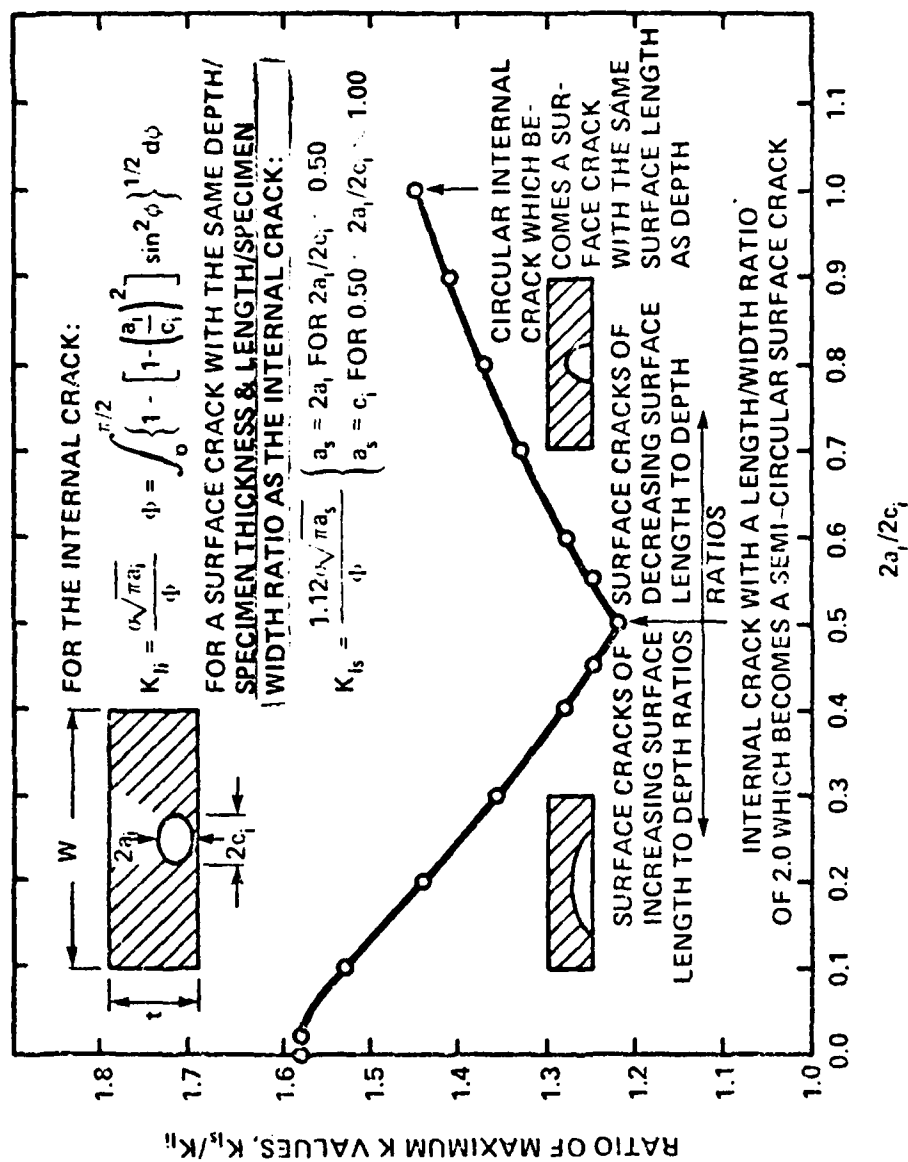
y-axis: RATIO OF MAXIMUM K VALUES, $K_{Is}/K_{Ii}$

Figure B-1   Maximum Stress Intensity Factor for a Surface Crack vs. an Internal Crack with the Same Proportions Relative to the Specimen Cross Section

## Appendix C

### Stress-Intensity Factors for Surface Cracks

The threshold stress amplitude for the case of a sharp elliptical crack was calculated by setting $K = 2.75$ ksi$\sqrt{\text{inch}}$ (3.05 MPa) in an equation developed by Irwin (text Ref. 19) for the case of an elliptical crack in an infinite solid which, for the location on the crack front at which K is highest, can be expressed as

$$K = \sigma \left( \frac{\pi a}{\phi^2} \right)^{1/2} \qquad\qquad (C-1)$$

where

$\sigma$ = the applied gross stress,
a = the length of the semi-minor axis of the ellipse,
and $\phi$ = a function of the ratio of the semi-minor to semi-major axis of the ellipse (a/c).

$$\phi = I \int_0^{\pi/2} [\sin^2\phi + (a/c)^2 \cos^2\phi]^{1/2} \, d\phi, \qquad (C-2)$$

where I denotes that an integral follows.

Similarly, the threshold stress amplitude for the case of a rounded notch was calculated by using Equation C-1 with an equation developed by Barsom (text Ref. 12) which predicts the fatigue-crack-initiation threshold for a specimen containing a notch rather than a crack:

$$\frac{\Delta K_{th}}{\rho^{1/2}} = 0.9\sigma_{ts} \qquad\qquad (C-3)$$

where

$\Delta K_{th}$ = the total range of the cyclic stress-intensity factor calculated by setting a in Equation 3 equal to the notch depth,
$\rho$ = the root radius of the notch,
and $\sigma_{ts}$ = the tensile strength of the material.

For the present case both the notch depth, a, and the root radius of the notch, $\rho$, were set equal to half the narrowest dimension of the imperfection. The effective tensile strength in the plane of the imperfections was estimated (text Ref. 21) from the hardness readings as 100 and 95 ksi (690 and 655 MPa), respectively, for the SMA and SAW weldments.

C-1

Appendix D
Table D-1

## CVN Energy Absorption and Percent Fibrous Fracture for 1-Inch A537 Class 1 SMA Weldments

| Distance from Bond Line, mm | +125 ft-lb | +125 Shear % | +100 ft-lb | +100 Shear % | RT ft-lb | RT Shear % | +50 ft-lb | +50 Shear % | +25 ft-lb | +25 Shear % | 0 ft-lb | 0 Shear % | -25 ft-lb | -25 Shear % |
|---|---|---|---|---|---|---|---|---|---|---|---|---|---|---|
| Weld Metal | | | | | 113 | 100 | 111 | 100 | 110 | 95 | 100 | 98 | 91 | 85 |
|  | | | | | 100 | 100 | 106 | 99 | 105 | 95 | 91 | 95 | 98 | 80 |
| Bond Line | | | 120 | 100 | 110 | 100 | 147 | 100 | 155 | 100 | 110 | 55 | 105 | 65 |
|  | | | 133 | 100 | 101 | 99 | 120 | 90 | 132 | 75 | 98 | 50 | 66 | 50 |
| 1 | 135 | 100 | 142 | 90 | 107 | 70 | | | | | 102 | 40 | 61 | 40 |
|  | 135 | 100 | 125 | 98 | 95 | 80 | | | | | 41 | 35 | 98 | 55 |
| 3 | 136 | 100 | 125 | 90 | 117 | 70 | 118 | 65 | 60 | 50 | 53 | 30 | 95 | 35 |
|  | 135 | 100 | 137 | 100 | 70 | 60 | 101 | 50 | 110 | 60 | 88 | 40 | 40 | 25 |
| 5 | 132 | 100 | 125 | 100 | 113 | 75 | 118 | 70 | 161 | 55 | 65 | 30 | 84 | 35 |
|  | 134 | 100 | 135 | 100 | 114 | 75 | 113 | 60 | 47 | 35 | 85 | 35 | 60 | 25 |

Temperature, °F

(Continued)

D-1

Appendix D
Table D-1 (Continued)

| Distance from Bond Line, mm | -50 ft-lb | -50 % Shear | -60* ft-lb | -60* % Shear | -75 ft-lb | -75 % Shear | -100 ft-lb | -100 % Shear | -125 ft-lb | -125 % Shear | -150 ft-lb | -150 % Shear |
|---|---|---|---|---|---|---|---|---|---|---|---|---|
| Weld Metal | 69 | 65 | 60 | 45 | 57 | 45 | 52 | 35 | 15 | 20 | 8 | 10 |
|  | 71 | 55 | 83 | 60 | 53 | 40 | 53 | 35 | 21 | 20 | 8 | 10 |
| Bond Line | 86 | 50 | 37 | 35 | 47 | 45 | 23 | 10 | 6 | 10 |  |  |
|  | 85 | 60 | 32 | 35 | 33 | 20 | 26 | 15 | 5 | 5 |  |  |
| 1 | 26 | 20 | 61 | 30 | 34 | 20 | 15 | 15 | 11 | 15 | 6 | 6 |
|  | 82 | 35 | 25 | 20 | 14 | 20 | 12 | 15 | 9 | 15 | 5 | 5 |
| 3 | 15 | 15 | 74 | 25 | 13 | 15 | 5 | 5 |  |  |  |  |
|  | 28 | 20 | 70 | 25 | 8 | 10 | 5 | 5 |  |  |  |  |
|  | 43 |  | 16 |  | 21 |  |  |  |  |  |  |  |
|  | 21 |  |  |  | 11 |  |  |  |  |  |  |  |
| 5 | 57 | 20 | 15 | 10 | 11 | 10 | 7 | 10 |  |  |  |  |
|  | 73 | 25 | 13 | 5 | 12 | 10 | 6 | 10 |  |  |  |  |

*Specimens from a separate weldment.

For average @ -60°F; take average of averages at -50 and -75 + Subtract 40% from -50 value

For min. @ -60°F; Take average of min. @ -50 and -75 + Subtract 40% from -50 value

D-2

Appendix D
Table D-2

CVN Energy Absorption and Percent Fibrous Fracture for 1-Inch A537 Class 1 SAW Weldments

| Distance from Bond Line, mm | +150 | | +100 | | RT | | +50 | | +25 | | 0 | | −25 | |
|---|---|---|---|---|---|---|---|---|---|---|---|---|---|---|
| | ft-lb | Shear % | ft-lb | Shear % | ft-lb | Shear % | ft-lb | Shear % | ft-lb | Shear % | ft-lb | Shear % | ft-lb | Shear % |
| Weld Metal | 121 | 100 | 119 | 99 | 137 | 100 | 134 | 98 | 120 | 85 | 101 | 70 | 94 | 60 |
| | 122 | 100 | 110 | 99 | 138 | 100 | 128 | 98 | 118 | 80 | 103 | 70 | 81 | 60 |
| Bond Line | | | | | 121 | 90 | | | | | 82 | 50 | 68 | 50 |
| | | | | | 103 | 80 | | | | | 77 | 60 | 71 | 50 |
| 1 | 131 | 100 | 133 | 99 | 118 | 95 | | | | | 100 | 70 | 66 | 50 |
| | 123 | 100 | 127 | 99 | 121 | 98 | | | | | 88 | 50 | 41 | 40 |
| 3 | | | 127 | 100 | 103 | 90 | 98 | 45 | 88 | 40 | 64 | 20 | 27 | 15 |
| | | | 124 | 95 | 121 | 85 | 105 | 50 | 72 | 35 | 66 | 30 | 65 | 25 |
| 5 | | | 133 | 100 | 105 | 75 | 108 | 60 | 95 | 60 | 80 | 50 | 75 | 35 |
| | | | 128 | 100 | 107 | 75 | 115 | 70 | 89 | 50 | 85 | 40 | 47 | 30 |

(Continued)

D-3

Appendix D
Table D-2 (Continued)

| Distance from Bond Line, mm | -30* ft-lb | Shear % | -50 ft-lb | Shear % | -60* ft-lb | Shear % | -75 ft-lb | Shear % | -100 ft-lb | Shear % | -125 ft-lb | Shear % | -150 ft-lb | Shear % |
|---|---|---|---|---|---|---|---|---|---|---|---|---|---|---|
| Weld Metal | 74 | 60 | 77 | 55 | 51 | 60 | 54 | 40 | 26 | 20 | 12 | 10 | 6 | 5 |
|  | 104 | 75 | 59 | 50 | 70 | 50 | 27 | 25 | 40 | 25 | 15 | 15 | 6 | 5 |
| Bond Line | 58 | 40 | 65 | 40 | 32 | 30 | 30 | 30 | 15 | 20 | 14 | 20 | 10 | 15 |
|  | 49 | 35 | 28 | 30 | 36 | 35 | 33 | 30 | 25 | 20 | 12 | 15 | 10 | 15 |
| 1 | 94 | 55 | 33 | 30 | 20 | 25 | 24 | 30 | 13 | 20 | 16 | 20 | 7 | 5 |
|  | 29 | 30 | 62 | 40 | 17 | 20 | 55 | 35 | 20 | 20 | 13 | 20 | 9 | 10 |
| 3 | 54 | 20 | 41 | 20 | 17 | 15 | 18 | 15 | 10 | 10 | 6 | 5 |  |  |
|  | 28 | 25 | 28 | 15 | 14 | 10 | 15 | 10 | 8 | 10 | 4 | 5 |  |  |
| 5 | 30 | 10 | 25 | 10 | 25 | 10 | 15 | 10 | 6 | 5 | 5 | 5 |  |  |
|  | 42 | 15 | 70 | 25 | 15 | 10 | 15 | 10 | 8 | 5 | 4 | 5 |  |  |

\* Specimens from a separate weldment.

CVN Energy Absorption and Percent Fibrous Fracture for 1/2-Inch A357 Class 1 SMA Weldments

| Distance from Bond Line, mm | +125 | | RT | | +40 | | +25 | | +20 | | 0 | |
|---|---|---|---|---|---|---|---|---|---|---|---|---|
| | ft-lb | Shear % | ft-lb | Shear % | ft-lb | Shear % | ft-lb | Shear % | ft-lb | Shear % | ft-lb | Shear % |
| Weld Metal | | | 121 | 100 | | | 104 | 70 | | | 109 | 95 |
| | | | 115 | 100 | | | 93 | 70 | | | 120 | 98 |
| Bond Line | | | 165 | 100 | 158 | 100 | | | | | 135 | 98 |
| | | | 167 | 100 | 126 | 90 | | | | | 135 | 98 |
| 1 | | | 141 | 100 | 124 | 70 | | | | | 85 | 45 |
| | | | 169 | 100 | 140 | 75 | | | | | 124 | 65 |
| 3 | | | 157 | 100 | 127 | 70 | | | 119 | 60 | 118 | 50 |
| | | | 149 | 100 | 120 | 60 | | | 115 | 60 | 111 | 50 |
| 5 | 142 | 100 | 132 | 80 | 109 | 55 | | | | | 107 | 40 |
| | 137 | 100 | 114 | 80 | 111 | 60 | | | | | 94 | 40 |

Temperature, °F

(Continued)

Appendix D
Table D-3 (Continued)

| Distance from Bond Line, mm | Temperature, °F | | | | | | | | | | | |
|---|---|---|---|---|---|---|---|---|---|---|---|---|
| | -10 | | -25 | | -35 | | -40 | | -50 | | -60 | |
| | ft-lb | Shear % | ft-lb | Shear % | ft-lb | Shear % | ft-lb | Shear % | ft-lb | Shear % | ft-lb | Shear % |
| Weld Metal | 120 | 80 | 117 | 70 | | | | | 84 | 60 | | |
| | 118 | 80 | 99 | 70 | | | | | 100 | 65 | | |
| Bond Line | | | 91 | 60 | | | | | 57 | 45 | | |
| | | | 84 | 45 | | | | | 121 | 75 | | |
| 1 | 113 | 45 | 54 | 30 | | | | | 40 | 50 | 21 | 20 |
| | 107 | 40 | 90 | 40 | | | | | 34 | 30 | 47 | 35 |
| 3 | | | | | | | 76 | 30 | 28 | 25 | | |
| | | | | | | | 12 | 5 | 7 | 10 | | |
| 5 | | | 94 | 35 | 81 | 35 | | | 38 | 10 | 16 | 5 |
| | | | 80 | 35 | 12 | 10 | | | 75 | 25 | 75 | 20 |

(Continued)

D-6

| Distance from Bond Line, mm | -75 ft-lb | -75 Shear % | -100 ft-lb | -100 Shear % | -125 ft-lb | -125 Shear % | -150 ft-lb | -150 Shear % | -175 ft-lb | -175 Shear % | -200 ft-lb | -200 Shear % |
|---|---|---|---|---|---|---|---|---|---|---|---|---|
| Weld Metal | 75 | 50 | 71 | 40 | 48 | 25 | 56 | 20 | 26 | 10 | 6 | 5 |
|  | 79 | 55 | 57 | 35 | 70 | 30 | 39 | 20 | 10 | 5 | 5 | 5 |
| Bond Line | 21 | 20 | 16 | 15 | 21 | 10 | 5 | 5 |  |  |  |  |
|  | 87 | 45 | 51 | 25 | 8 | 5 | 14 | 5 |  |  |  |  |
| 1 | 21 | 20 | 10 | 15 | 8 | 10 | 8 | 5 |  |  |  |  |
|  | 41 | 25 | 12 | 15 | 10 | 10 | 6 | 5 |  |  |  |  |
| 3 | 16 | 10 | 3 | 5 |  |  |  |  |  |  |  |  |
|  | 8 | 5 | 7 | 5 |  |  |  |  |  |  |  |  |
| 5 | 36 | 10 | 6 | 5 |  |  |  |  |  |  |  |  |
|  | 10 | 5 | 5 | 5 |  |  |  |  |  |  |  |  |

Appendix D
Table D-4

CVN Energy Absorption and Percent Fibrous Fracture for 1/2-Inch A537 Class 1 SAW Weldments

| Distance from Bond Line, mm | +125 | | +85 | | RT | | +40 | | +20 | | 0 | | -25 | | -40 | |
|---|---|---|---|---|---|---|---|---|---|---|---|---|---|---|---|---|
| | ft-lb | Shear % | ft-lb | Shear % | ft-lb | Shear % | ft-lb | Shear % | ft-lb | Shear % | ft-lb | Shear % | ft-lb | Shear % | ft-lb | Shear % |
| Weld Metal | 152 | 99 | | | 111 | 80 | 106 | 60 | | | 95 | 40 | 24 | 30 | 62 | 35 |
| | 144 | 100 | | | 140 | 85 | 86 | 50 | | | 44 | 40 | 44 | 35 | 25 | 25 |
| | | | | | | | | | | | 62 | 40 | | | | |
| Bond Line | 123 | 100 | | | 135 | 80 | 112 | 55 | | | 80 | 40 | 63 | 35 | | |
| | 142 | 100 | | | 110 | 60 | 92 | 50 | | | 76 | 40 | 21 | 25 | | |
| 1 | 149 | 100 | 128 | 100 | 108 | 60 | 121 | 75 | 66 | 40 | 118 | 65 | 100 | 45 | | |
| | 147 | 100 | 117 | 90 | 119 | 100 | 112 | 70 | 116 | 70 | 75 | 30 | 41 | 40 | | |
| 3 | | | | | 137 | 100 | 126 | 80 | 116 | 65 | 103 | 50 | 86 | 30 | | |
| | | | | | 135 | 100 | 113 | 90 | 109 | 80 | 107 | 50 | 95 | 35 | | |
| 5 | 138 | 100 | | | 125 | 100 | 101 | 85 | | | 86 | 40 | 77 | 40 | 78 | 40 |
| | 119 | 100 | | | 112 | 75 | 145 | 100 | | | 80 | 45 | 75 | 30 | 62 | 30 |

(Continued)

Appendix D
Table D-4 (Continued)

| Distance from Bond Line, mm | Temperature, °F | | | | | | | | | | | | | |
|---|---|---|---|---|---|---|---|---|---|---|---|---|---|---|
| | -50 | | -70 | | -75 | | -80 | | -90 | | -100 | | -125 | |
| | ft-lb | Shear % | ft-lb | Shear % | ft-lb | Shear % | ft-lb | Shear % | ft-lb | Shear % | ft-lb | Shear % | ft-lb | Shear % |
| Weld Metal | 29 | 20 | | | 14 | 15 | | | | | 10 | 10 | | |
| | 33 | 25 | | | 16 | 15 | | | | | 9 | 10 | | |
| Bond Line | 28 | 30 | | | 20 | 20 | 16 | 20 | | | 13 | 15 | 11 | 5 |
| | 28 | 30 | | | 24 | 20 | 18 | 20 | | | 14 | 15 | 7 | 5 |
| 1 | 15 | 15 | | | 40 | 20 | | | | | 7 | 10 | | |
| | 43 | 20 | | | 11 | 10 | | | | | 7 | 10 | | |
| 3 | 57 | 20 | 55 | 20 | 77 | 30 | | | 7 | 5 | 6 | 10 | | |
| | 77 | 35 | 20 | 10 | 54 | 20 | | | 43 | 15 | 7 | 10 | | |
| 5 | 63 | 25 | | | 42 | 15 | | | 30 | 15 | 6 | 5 | | |
| | 80 | 30 | | | 47 | 20 | | | 30 | 15 | 6 | 5 | | |

D-9

CVN Energy Absorption and Percent Fibrous Fracture for
1-Inch and 1/2-Inch A537 Class 1 Base Plate

| | Temperature, °F | | | | | | | | | | | |
|---|---|---|---|---|---|---|---|---|---|---|---|---|
| | RT | | +45 | | +30 | | 0 | | -30 | | -45 | |
| | ft-lb | Shear % | ft-lb | Shear % | ft-lb | Shear % | ft-lb | Shear % | ft-lb | Shear % | ft-lb | Shear % |
| **1-Inch Base Metal** | | | | | | | | | | | | |
| Longitudinal | DNB* | – | | | | | DNB | – | DNB | – | 216 | 100 |
| | DNB | – | | | | | 236 | 100 | 150 | 65 | 137 | 50 |
| Transverse | 134 | 80 | | | 122 | 55 | 105 | 40 | 81 | 30 | | |
| | 118 | 75 | | | 115 | 50 | 98 | 40 | 85 | 30 | | |
| **1/2-Inch Base Metal** | | | | | | | | | | | | |
| Longitudinal | 178 | 100 | 158 | 100 | DNB | | 166 | 70 | DNB | – | 224 | 100 |
| | 175 | 100 | 155 | 100 | DNB | | DNB | – | 206 | 100 | 166 | 70 |
| | | | | | | | 231 | 1 | | | 127 | 50 |
| Transverse | | | | | 120 | 70 | 116 | 50 | 103 | 35 | | |
| | | | | | 129 | 70 | 121 | 55 | 109 | 40 | | |

(Continued)

Appendix D
Table D-5 (Continued)

| | Temperature, °F | | | | | | | | | |
| | -60 | | -75 | | -90 | | -105 | | -120 | |
| Base Metal | ft-lb | Shear % | ft-lb | Shear % | ft-lb | Shear % | ft-lb | Shear % | ft-lb | Shear % |
| **1-Inch** | | | | | | | | | | |
| Longitudinal | 228 | 100 | 190 | 70 | 84 | 20 | 9 | 5 | 9 | 5 |
| | 109 | 45 | 106 | 40 | 102 | 30 | 11 | 5 | 4 | 5 |
| Transverse | 64 | 20 | 52 | 20 | 36 | 15· | 8 | 5 | 5 | 5 |
| | 74 | 25 | 60 | 20 | 30 | 15 | 9 | 5 | 5 | 5 |
| | | | | | | | 11 | 10 | | |
| **1/2-Inch** | | | | | | | | | | |
| Longitudinal | 109 | 35 | 113 | 35 | 73 | 25 | 9 | 5 | 5 | 5 |
| | 119 | 40 | 34 | 15 | 20 | 10 | 13 | 5 | 9 | 5 |
| Transverse | 93 | 30 | 89 | 25 | 78 | 20 | 52 | 15 | 15 | 5 |
| | 99 | 30 | 79 | 20 | 12 | 5 | 10 | 5 | 6 | 5 |

* DNB – Did not break.

D-11

## Appendix E

## Bending Stress Modifications to Surface-Crack K Values

The K values for the surface-cracked specimens were modified by determining the bending stress, Section 8.252, and using an equation developed by Newman (text Ref. 52) to calculate the increase in K at the crack tip due to the bending stress alone:

$$K = H\sigma_b \left(\frac{\pi a}{\phi^2}\right)^{1/2} F \qquad (E-1)$$

where

$H$ = a function of the crack depth to specimen thickness, $a/t$, and crack depth to half crack length, $a/c$, ratio given in text Ref. 52,

$\sigma_b$ = the outer fiber bending stress,

$\Phi$ = a function of the $a/c$ ratio as shown in Equation C-2,

and $F$ = a function of the $a/t$ ratio given in text Ref. 52 ($f_w$ given in text Ref. 52 was not included in F).

The increase in K due to the bending stress alone ranged from 1.0 ksi√inch (1.1 MPa√m), or 2.3 percent for a specimen having a crack depth equal to about 6 percent of the thickness to 9.3 ksi√inch (10.2 MPa√m), or 30.3 percent for a specimen having a crack depth equal to about 80 percent of the thickness. The crack-tip K levels, including the contribution from bending, are also shown in Table 13.

Because, for most of the specimens, the fracture-initiation site could be traced to a location on the crack front away from the deepest point, the K levels at these locations were also calculated. A modification of text Equation 2 was used to calculate the tension contribution to the K level,

$$K = \sigma \left(\frac{\pi a}{\Phi^2}\right)^{1/2} \left(\sin^2\emptyset + \frac{a^2}{c^2}\cos^2\emptyset\right)^{1/4} \qquad (E-2)$$

where $\sigma$, $a$, $\Phi$, and $c$ are the same as given in Equations C-1 and C-2 and $\emptyset$ is found by using the formula[E-1]

---

E-1) P. N. Randall, <u>Discussion in Plane Strain Crack Toughness Testing of High Strength Metallic Materials</u>, ASTM STP 410, American Society for Testing and Materials, Philadelphia, PA, 1967, pp. 88-126.

$$\emptyset = \sin^{-1} \frac{x}{a} \qquad\qquad (E-3)$$

where

    $x$ = the crack depth at the fracture-initiation site,

        The bending contribution to the K level was calculated by interpolating between the values of Newman's (text Ref. 52) solution for K at the crack tip and at the surface. The interpolation was linear based on the value of $\emptyset/2\pi$ where $\emptyset$ is given by Equation E-3 and is equal to zero at the surface and $\pi/2$ at the deepest point on the crack front.

Appendix Supplement

Table S-1

## CVN Energy Absorption and Percent Fibrous Fracture for 5/8- and 1-1/2-Inch ABS-CS SMA and SAW Weldments

| Distance from Bond Line, mm | Temperature, °F | | | | | | | |
| | RT | | 0 | | -30 | | -60 | |
| | ft-lb | % | ft-lb | % | ft-lb | % | ft-lb | % |

### 5/8-Inch SMA (7018 Electrode, Normal Heat Input)

| Distance from Bond Line, mm | ft-lb | % | ft-lb | % | ft-lb | % | ft-lb | % |
|---|---|---|---|---|---|---|---|---|
| Weld Metal | 112 | 80 | 75 | 35 | 23 | 15 | 10 | 5 |
| | 145 | 100 | 96 | 65 | 78 | 40 | 9 | 10 |
| | 116 | 80 | 33 | 35 | 56 | 25 | 10 | 15 |
| 1 | 54 | 95 | 40 | 50 | 29 | 35 | 23 | 25 |
| | 59 | 99 | 36 | 50 | 29 | 35 | 17 | 15 |
| | 62 | 99 | 39 | 60 | 28 | 25 | 21 | 20 |
| 3 | 45 | 70 | 29 | 25 | 15 | 10 | 17 | 15 |
| | 52 | 100 | 35 | 30 | 21 | 20 | 15 | 20 |
| | 54 | 80 | 35 | 55 | 23 | 25 | 21 | 20 |

### 5/8-Inch SMA (8018 Electrode, Normal Heat Input)

| Distance from Bond Line, mm | ft-lb | % | ft-lb | % | ft-lb | % | ft-lb | % |
|---|---|---|---|---|---|---|---|---|
| Weld Metal | 150 | 100 | 133 | 80 | 117 | 70 | 54 | 40 |
| | 153 | 90 | 135 | 80 | 122 | 70 | 82 | 55 |
| | 146 | 90 | 124 | 85 | 117 | 70 | 90 | 45 |
| 1 | 49 | 100 | 37 | 60 | 28 | 35 | 17 | 20 |
| | 53 | 99 | 38 | 60 | 20 | 25 | 16 | 20 |
| | 51 | 100 | 32 | 55 | 26 | 50 | 17 | 15 |
| 3 | 47 | 90 | 23 | 30 | 14 | 20 | 12 | 15 |
| | 41 | 90 | 29 | 30 | 34 | 40 | 12 | 15 |
| | 46 | 90 | 27 | 35 | 23 | 25 | 11 | 15 |

### 1-1/2-Inch SAW (L61 Wire/880 Flux, Normal Heat Input)

| Distance from Bond Line, mm | ft-lb | % | ft-lb | % | ft-lb | % | ft-lb | % |
|---|---|---|---|---|---|---|---|---|
| Weld Metal | 122 | 90 | 102 | 60 | 77 | 25 | 23 | 15 |
| | 134 | 100 | 118 | 70 | 70 | 35 | 41 | 15 |
| | 132 | 100 | 104 | 65 | 82 | 45 | 58 | 20 |
| 1 | 64 | 80 | 37 | 40 | 30 | 15 | 17 | 5 |
| | 62 | 85 | 40 | 60 | 23 | 10 | 19 | 10 |
| | 62 | 100 | 31 | 40 | 25 | 15 | 20 | 10 |

(Continued)

S-1

| Distance from Bond Line, mm | Temperature, °F | | | | | | | |
|---|---|---|---|---|---|---|---|---|
| | RT | | 0 | | -30 | | -60 | |
| | ft-lb | % | ft-lb | % | ft-lb | % | ft-lb | % |
| **1-1/2-Inch SAW (L61 Wire/880 Flux, Normal Heat Input) (Continued)** | | | | | | | | |
| | 53 | 80 | 26 | 20 | 21 | 10 | 20 | 5 |
| 3 | 56 | 98 | 29 | 25 | 17 | 10 | 18 | 5 |
| | 56 | 95 | 30 | 25 | 18 | 10 | 16 | 5 |
| **1-1/2-Inch SAW (L61 Wire/860 Flux, High Heat Input - 110 kJ/in.)** | | | | | | | | |
| | 108 | 85 | - | - | 38 | 25 | 7 | 10 |
| Weld Metal | 111 | 90 | - | - | 37 | 25 | 8 | 10 |
| | 108 | 90 | - | - | 61 | 30 | 48 | 20 |
| | 68 | 100 | - | - | 40 | 40 | 25 | 25 |
| 1 | 64 | 100 | - | - | 32 | 40 | 26 | 25 |
| | 64 | 100 | - | - | 36 | 40 | 25 | 25 |
| | 62 | 100 | - | - | 19 | 15 | 30 | 25 |
| 3 | 62 | 90 | - | - | 23 | 20 | 25 | 20 |
| | 58 | 95 | - | - | 35 | 35 | 31 | 20 |
| | | | | | 37 | 30 | | |
| | | | | | 42 | 35 | | |
| **1-1/2-Inch SAW (W18 Wire/880 Flux, Normal Heat Input - 75 kJ/in.)** | | | | | | | | |
| | 117 | 95 | 75 | 70 | 74 | 50 | 49 | 25 |
| Weld Metal | 120 | 100 | 75 | 70 | 80 | 60 | 64 | 35 |
| | 94 | 100 | 92 | 75 | 64 | 50 | 49 | 25 |
| | 61 | 90 | 21 | 20 | 17 | 10 | 24 | 15 |
| 1 | 67 | 100 | 23 | 25 | 21 | 15 | 20 | 10 |
| | 66 | 100 | 40 | 55 | 24 | 15 | 18 | 5 |
| | 42 | 70 | 29 | 25 | 21 | 15 | 5 | 5 |
| 3 | 57 | 90 | 23 | 20 | 21 | 20 | 20 | 10 |
| | 43 | 70 | 27 | 20 | 23 | 20 | 12 | 5 |

(Continued)

| Distance from Bond Line, mm | Temperature, °F | | | | | | | |
| | RT | | 0 | | -30 | | -60 | |
| | ft-lb | % | ft-lb | % | ft-lb | % | ft-lb | % |

1-1/2-Inch SAW (W18 Wire/880 Flux, High Heat Input - 110 kJ/in.)

| Distance from Bond Line, mm | ft-lb | % | ft-lb | % | ft-lb | % | ft-lb | % |
|---|---|---|---|---|---|---|---|---|
| | 114 | 95 | 86 | 60 | 55 | 30 | 34 | 15 |
| Weld Metal | 105 | 90 | 90 | 65 | 65 | 35 | 64 | 25 |
| | 106 | 100 | 121 | 80 | 58 | 35 | 25 | 15 |
| | 70 | 98 | 38 | 50 | 23 | 25 | 24 | 20 |
| 1 | 59 | 99 | 38 | 50 | 30 | 30 | 19 | 10 |
| | 70 | 100 | 40 | 55 | 33 | 30 | 30 | 20 |
| | 59 | 98 | 32 | 30 | 30 | 20 | 18 | 10 |
| 3 | 60 | 100 | 35 | 25 | 25 | 15 | 18 | 10 |
| | 66 | 98 | 27 | 20 | 27 | 20 | 21 | 10 |

Appendix Supplement
Table S-2

CVN Energy Absorption and Percent Fibrous Fracture for 1-1/2- and 5/8-Inch ABS-CS Base Plate

| | +100 | | RT | | +60 | | +50 | | +40 | | +20 | | 0 | | -10 | |
| | ft-lb | % | ft-lb | % | ft-lb | % | ft-lb | % | ft-lb | % | ft-lb | % | ft-lb | % | ft-lb | % |
|---|---|---|---|---|---|---|---|---|---|---|---|---|---|---|---|---|
| 1-1/2-Inch Longitudinal | | | 141 | 100 | | | | | 147 | 100 | 145 | 100 | 133 | 70 | | |
| | | | 166 | 100 | | | | | 159 | 100 | 150 | 100 | 93 | 50 | | |
| 1-1/2-Inch Transverse | 79 | 100 | 75 | 100 | 65 | 90 | | | 52 | 55 | 43 | 40 | 32 | 30 | | |
| | 75 | 100 | 59 | 98 | 65 | 90 | | | 48 | 50 | 40 | 40 | 34 | 30 | | |
| 5/8-Inch Longitudinal | | | 220 | 100 | | | | | 143 | 100 | 131 | 90 | 153 | 100 | | |
| | | | 156 | 100 | | | | | 148 | 100 | 173 | 100 | 105 | 55 | | |
| | | | | | | | | | | | 128 | 90 | 169 | 100 | | |
| 5/8-Inch Transverse | | | 57 | 100 | | | 58 | 95 | 55 | 90 | 41 | 65 | 32 | 45 | 31 | 30 |
| | | | 59 | 100 | | | 59 | 98 | 52 | 85 | 42 | 75 | 35 | 50 | 31 | 30 |

Temperature, °F

(Continued)

S-4

Appendix Supplement
Table S-2 (Continued)

| | -20 | | -30 | | -40 | | Temperature, °F -60 | | -80 | | -100 | | -130 | | -160 | |
|---|---|---|---|---|---|---|---|---|---|---|---|---|---|---|---|---|
| | ft-lb | % | ft-lb | % | ft-lb | % | ft-lb | % | ft-lb | % | ft-lb | % | ft-lb | % | ft-lb | % |
| **1-1/2 Inch Longitudinal** | 86 | 35 | 78 | 30 | 67 | 25 | 38 | 10 | 39 | 15 | 8 | 5 | | | | |
| | 93 | 35 | 93 | 35 | 70 | 25 | 35 | 10 | 23 | 5 | 12 | 5 | | | | |
| | | | 89 | 35 | 68 | 25 | 50 | 15 | 8 | 5 | | | | | | |
| | | | | | 74 | 30 | 45 | 10 | 10 | 5 | | | | | | |
| | | | | | 64 | 25 | | | 16 | 5 | | | | | | |
| | | | | | | | | | 10 | 5 | | | | | | |
| **1-1/2-Inch Transverse** | 26 | 20 | 24 | 15 | 20 | 15 | 11 | 5 | 4 | 5 | 8 | 5 | | | | |
| | 26 | 20 | 25 | 20 | 19 | 15 | 17 | 10 | 11 | 5 | 4 | 5 | | | | |
| | | | | | 20 | 15 | 14 | 5 | 10 | 5 | 14 | 5 | | | | |
| | | | | | 20 | 15 | 20 | 10 | 12 | 5 | 57 | 10 | | | | |
| **5/8-Inch Longitudinal** | 76 | 35 | | | 94 | 35 | 10 | 5 | | | 9 | 5 | 6 | 5 | 3 | 5 |
| | 122 | 60 | | | 91 | 45 | 77 | 20 | | | 25 | 10 | 3 | 5 | 3 | 5 |
| | 115 | 60 | | | 96 | 45 | 15 | 10 | | | 7 | 5 | 3 | 5 | 2 | 5 |
| **5/8-Inch Transverse** | 27 | 35 | | | 21 | 15 | 14 | 5 | 7 | 5 | 6 | 5 | 6 | 5 | 2 | 5 |
| | 29 | 40 | | | 22 | 20 | 10 | 5 | 10 | 5 | 10 | 5 | 4 | 5 | 2 | 5 |

S-5

# DATE FILME